Value of different data types for estimation of permeability
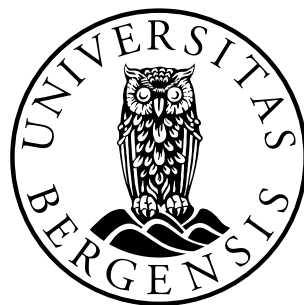
Master of Science Thesis in Reservoir Mechanics

Kristian Fossum

Center for Integrated Petroleum Research

Department of Mathematics
University of Bergen

June 2011

Acknowledgments

I would like to thank my supervisor Trond Mannseth for his help, guidance and motivation though this project. I would also like to thank Tao Feng for his help with the Eclipse simulator, and the CIPR administration for always being positive and providing a great work environment.

My fellow students deserve a lot of credit, especially Svenn and Brede for always having high spirits even through the toughest of exam periods. I would also like to thank Pål for sharing his great knowledge about mathematics and MatLab. My family and friends also deserves credit for always staying supportive. Especially Siren for always guiding, and supporting me.

Kristian Fossum,
June, 2011.

Contents

Chapter 1

Outline and Motivation

To model the fluid flow in a porous media we need information about the permeability. Unfortunately the only way to obtain measurements of the permeability is by conducting experiments on core samples. There is a high cost related to obtaining these cores, and we only get point measurements. This means that we are only able to obtain sparsely distributed data points of the permeability. The permeability field might have a simple structure making the interpolation between these points good, but most likely the permeability field has a complex structure, making the interpolation useless.
Instead of relying on measured data, there has been developed methods for estimating the permeability. These methods are based on solving an inverse problem. This procedure is inherently very complex, and it is generally hard to solve. The theory for solving these kind of problems are vast, and we can approach the problem in many ways. This means that choosing a solution procedure can be difficult. We therefore try to investigate some of the properties that exist between the given data type, and the parameter we want to estimate. If we are successful in this, we can choose estimation schemes that takes advantage of these properties.

In [13] the effect of using a multiscale basis for estimation of the diffusion coefficient in an elliptic, and parabolic equation was investigated. The authors showed that by application of a multiscale basis it was possible to obtain better estimation results. This theory was carried further in [31] where the degree of ill-posedness of the invese problem was analyzed by utilizing a multiscale basis. This showed that the model problem was more non-linear with respect to coefficients of the finer scales, but less sensitive with respect to these coefficients. The results in [31] was based on the estimation of $a(x)$ from measurements of $u(x)$ in the 1-D elliptic equation

$$-\frac{d}{dx}\left(a(x)\frac{du(x)}{dx}\right) = f(x), \quad x \in (0,1).\qquad(1.0.1)$$

In [23] the correlation between sensitivity, non-linearity and scale was investigated for a more general class of models. It was shown that there is a strong correlation between low sensitivity, high non-linearity and directions in parameter space associated with small-scale oscillations for the class of models investigated.

For the purpose of estimating the permeability in a porous media it would be of great value if there existed a relationship between sensitivity, non-linearity and scale (denoted SNS) related to the problem. This question was addressed in [33]. Here the SNS relationship for the problem of estimating the permeability from sparsely distributed time series of pressure data was considered. It was rigorously shown that this relationship does exist for one-dimensional single- and two-phase flow.
The findings in [33] motivates the use of specific methods that utilize the SNS relationship for the estimation of permeability from pressure data.

It is now reasonable to ask if there is a similar SNS relationship between permeability and other data. This will be the main issue adressed in this thesis. Motivated by the approach in [33] we try to determine if there is a SNS relationship associated with the inverse problem of permeability identification from sparsely distributed time series observations of fluid flow. This is done by rigorously analyzing the one-dimensional fluid flow equation for one- and two-phase flow. After this, we perform numerical experiments to test the theoretical results. We now look at the outline of the thesis

In Chapter 2 we give an introduction to the general inverse problem. We look at the flow equations, and define the different properties that are related to fluid flow in a porous media. We also introduce different ways of solving the inverse problem and look at some problems related to this.

In Chapter 3 we look specifically at how we can utilize the relationship between sensitivity, non-linearity and scale for solving the inverse problem.

In Chapter 4 we establish a method for deriving expressions for the sensitivity and non-linearity in different directions of parameter space.

In Chapter 5 we look at some foundations for the multiresolution analysis. We introduce a multiresolution basis, that will be used in later chapters. We also use this to illustrate some of the properties of multiresolution analysis.

In Chapter 6 we analyze the sensitivity, non-linearity and scale structure of one-dimensional single-phase flow.

In Chapter 7 we analyze the sensitivity, non-linearity and scale structure of one-dimensional two-phase flow.

In Chapter 8 we look into the effects of the simplification that was made in Chapter 5, and Chapter 6. We conduct some numerical experiments in order to analyze the reactions of these simplification.

In Chapter 9 we utilize the comercially available reservoir simulator Eclipse for the calculation of sensitivity values for a one-dimensional two-phase problem. We transform these values such that they are represented by the multiresolution basis, and compare these results to the ones obtained in Chapter 6.

In Chapter 10 we also utilize Eclipse in the same manner as for Chapter 8 but now we do the sensitivity calculations for a two-dimensional two-phase problem. We give an introduction to multidimentional multiresolution bases, and utilize a two-dimensional multiresolution basis to transform the sensitivies.

In Chapter 11 we summarize and comment on the results obtained in the thesis.

Chapter 2

Introduction

2.1 Inverse problems

In a typical mathematical problem we want to find, or estimate some unknown value. In order to do this we first have to understand which physical principles that apply. Then we have to formulate the problem into a mathematical problem. After this we can try to solve the mathematical problem either by analytical, or numerical calculations. The inverse problem is somewhat different.

For an inverse problem we have measurements of the value we found by solving the mathematical problem. This measurements can be continuous or discrete. We can have measurements at different times, or at different spatial positions. The task in an inverse problem is to use these measurements to find, or estimate, some of the parameters that characterize the mathematical model.
As an example we can consider the physical system of a beaker with water sitting over a bunsen burner. The measurements is the temperature of the water, and the parameter we want to estimate is the thermal conductivity of the water.

The problem of predicting the measurement results are called the *forward problem*. The *inverse problem* is then to use the measurement to determine the value of parameters that characterize the system. The forward problem is shown in (2.1.1). We are given a set of parameters, m, that describe the system. Assuming that we have a complete physical theory, we have a function G that relates the parameters to the measured data d

$$G(m) = d. \tag{2.1.1}$$

For an inverse problem, the task is to find m, given d. This is not a trivial task. For real observations we always have some amount of noise. This noise can

come from many different sources, we therefore look at our data as consisting of a noiseless component, plus a noise component η

$$d = G(m_{true}) + \eta. \tag{2.1.2}$$

Assuming that the forward modeling is correct, then $G(m_{true}) = d_{true}$. If we were to fit d by (2.1.1) with d described in (2.1.2) we would also fit η. This is of course undesirable, and it is often the case that measurements d with even a small η produces a m that has little or no correspondence to m_{true}. This means that the task of finding m_{true} is unstable, and because of η we might never find a model that exactly fits the data.

There is another issue that makes inverse problems hard. For many problems there is infinite numbers of m aside from m_{true} that fit the error free data d_{true}. That is the inverse problem does not have a unique solution. As an example of this we can consider the measurements of the gravity field around a planet. Given the distribution of mass inside a planet, we can uniquely predict the values of the gravity field around the planet. But there can be many distributions of mass that produce this *exact* same gravity field. Thus the inverse problem of determining the mass distribution from observations of the gravity field has many solutions.

The inverse problem is in general ill-posed. The solution might not exist, it might not be unique, and the process of computing an inverse solution can be extremely unstable. For this reason the process of finding the solution to an inverse problem can be challenging.

We typically distinguish between linear and nonlinear inverse problems. We write

- $Gm = d$ for a linear inverse problem.

- $G(m) = d$ for a nonlinear problem.

When we consider a "normal" non-linear problem the non-linearities are found in the variables like

$$y = ax^2 + b. \tag{2.1.3}$$

Considering a non-linear inverse problem, it is the parameters representation in the function that are non-linear

$$y = a^2 x + b. \tag{2.1.4}$$

More on the topic of inverse problems can be found in e.g. [5, 45].

2.2 Flow equations

Fluid flow in a porous media are governed by the same fundamental laws that govern the motion of fluids in for example; the atmosphere, pipelines and rivers. These laws are based on the conservation of mass, momentum and energy [6]. When we consider a porous media there are some problems with applying these laws. The scale of a pore is extremely small compared to the scale of a whole reservoir, and we do not know anything about the shapes, or sizes of the pores. This makes it tedious to do simulations of flow within each pore. Instead of looking at individual pores, the basic concept for porous media equations is to make averages over a volume that is big enough[1] so that local variations of parameters, like the pore size will even out. This volume is called a *Representative Elementary Volume*. Using this approach we can replace the actual porous medium with a fictive *continuum*. This is a structureless substance where at any point with spatial coordinates we can assign variables and parameters that are continuous functions of coordinates and time [8]. These variables and parameters allows us to describe the fluid flow within a porous media by means of *partial differential equations* (PDE).

We now describe the most important parameters, and the PDEs that govern the flow in a porous media.

2.2.1 Porous media

Many natural and synthetic materials are not complete solids. Inside they can have small or large voids. We refer to these voids as pores. We can find numerous examples of porous media, from a concrete slab to a sponge. The difference lies in the amount, size, and in the way the pores are connected. As an example of a porous media we can look at a sandstone. A sandstone is a sedimentary rock composed mainly of "sand-sized" minerals or rock grains. Between these grains we find pores that are interconnected and pores that are isolated. A petroleum reservoir does not have to be composed of sandstone. But it needs to be a porous media with interconnected pores in order for hydrocarbons to accumulate and be produced.

Each fluid in a porous media is called a *phase*. Oil and water are two separate phases. The phases can move through the porous media within the network of interconnected pores. We define the volume of all the connected pores as V_p, and the total volume of the porous media as V_t. Now we write the *effective*

---

[1]"Big enough" is usually very small compared to a typical reservoir, a volume of $1\,cm^3$ is normally plenty. So this is no limitation.

porosity ϕ in the following way

$$\phi = \frac{V_p}{V_t}.$$

This dimensionless quantity is usually expressed as a percentage. From now on we refer to the effective porosity as the *porosity*.

2.2.2   Fluid properties

For every phase in the porous media there are specific properties that is unique for each phase. The properties we introduce is the *density* ρ, the *viscosity* μ, and the *compressibility* c.

The density of a fluid is defined as the mass per unit volume. The units in the SI system is $[kg/m^3]$. From now on we denote the density of phase i as ρ_i.

Viscosity is a measure of a fluids internal resistance to flow and may be thought of as a measure of fluid friction. The units for viscosity in the SI system is $[N \cdot s/m^2] = [kg/m \cdot s]$. The most commonly used unit for viscosity is $Poise$ $[P]$ and *centipoise* $[cP]$. This is the unit in the the cgs (centimeter, gram, and second) system, and it is the unit we will use for viscosity. The relationship between the two is $1\,[kg/m \cdot s] = 10\,[g/cm \cdot s] = 10\,P$. From now on we denote the viscosity of phase i, as μ_i. For more on viscosity we refer the reader to e.g. [47, 8].

In fluid mechanics the *compressibility* c of a phase is the measure of the volume change of the phase due to a pressure change in the phase. This can be defined as

$$c = -\frac{1}{V}\frac{dV}{dp} = \frac{1}{\rho}\frac{d\rho}{dp}$$

where V is the total volume and p is the pressure [29].

The properties we have presented so far is independent of the number of phases there is in the porous media. There are on the other hand some quantities that only apply when there are two or more phases present.

2.2.3   Saturation

If we have more than one phase is present in the porous media, we need some kind of quantity that tells us how much of the volume that is occupied by each
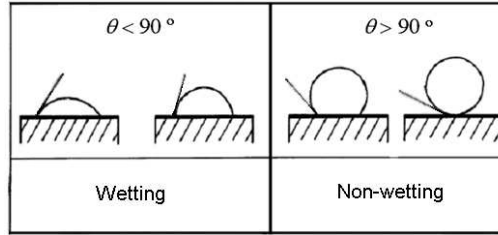
Figure 2.2.1: Wetting

phase. If a pore is occupied by oil, water and gas, we can write the total pore volume as the sum of the volume of oil, water and gas, i.e.

$$V_p = V_o + V_g + V_w.$$

The *saturation*, S, is defined as the fraction of pore volume occupied by a particular fluid

$$S_i = \frac{V_i}{V_p}, \quad i = o, w, g.$$

Since the porous media always is completely filled with fluids we have

$$\sum_{i=o,w,g} S_i = 1.$$

2.2.4   Wettability

Considering a case with more than one phase in equilibrium inside a porous media, the phases will be distributed according to each phases density. This is due to gravitational effects. When two phases (e.g. oil and water) coexist in a pore they are, because of adhesive forces on the pore wall, distributed unevenly in the pore space[47]. The force is always stronger for one of the phases. Which phase that is preferred depends on the properties of the reservoir. This property is called the *wettability* preference of the rock. We now define one of the phases as the *wetting* and the other as the *non-wetting* phase. We can decide which phase is wetting by looking at a droplet of one phase resting on the reservoir rock surrounded by the other phase. If the contact angle is small ($\phi < 90°$) the droplet is the wetting phase. If the contact angle is large ($\phi > 90°$) the droplet is the non-wetting phase, this is illustrated in figure 2.2.1.

2.2.5   Darcy's Law

Darcy's law is an empirical relationship for the flow of water through a porous media. This relationship was first discovered by Henry Darcy [14] while doing experiments on flow through a vertical column packed with sand. These

experiments demonstrated that the volumetric flow rate through the porous medium, Q , is proportional to the pressure difference over the column, $p_2 - p_1$, the cross-sectional flow area, A, and inversely proportional to the the height of the packed column, L. With a proportionality constant K, this is stated as:

$$Q = -KA\frac{p_2 - p_1}{L}.$$

Darcy's experiments has been repeated with more general conditions. Many types of fluids has been tested, and the flow direction has been varied. This has resulted in a more general way of defining Darcy's law in three dimensions:

$$\mathbf{u} = -\frac{1}{\mu}\mathbf{K}\left(\nabla p + \rho\mathbf{g}\right), \qquad (2.2.1)$$

where $\mathbf{u}$ is the Darcy velocity, ∇ is the differential operator, $\mathbf{g}$ represents the gravity vector. $\mathbf{K}$ is the proportionality constant called permeability, this is the same used in Darcy's original version of the law.

Even though equation (2.2.1) is the foundation for most theory on fluid flow in porous media, it is important to remember that this is an empirical law that in no way represents the actual fluid flow within the porous media. Darcy's law only contain data collected at points external to the porous media [22]. It has been shown that Darcy's law is valid for any *Newtonian fluid* [20], and by using theory from continuum mechanics the validity of Darcy's law is confirmed, under the assumptions that the experimental apparatus is similar to the one Darcy used in his experiments [22].

The permeability $\mathbf{K}$ is of great importance since it tell us how easily the fluid flows through the porous medium. Hence the form of $\mathbf{K}$ depends somewhat on the possible flow directions. We now describe this important parameter in more detail.

2.2.6   Permeability

Darcy noted that the flow rate was dependent on some constant that accounted for the properties of the porous media, this constant is known as the permeability. The value only depends on the rock. In Darcy's original equation the permeability was a scalar value. This is only valid if the media is *homogeneous* and *isotropic*, i.e. the media is spatially uniform, and the permeability does not change value when we look in other directions. If the media is not spatially uniform, we say that it is *heterogeneous*. And if the permeability changes value depending on the direction, the media is *anisotropic*.

When the media is anisotropic, the permeability must be represented by a second order tensor. If the media in addition is heterogeneous, the permeability

is dependent on the position in the medium. Permeability can thus be written in a general form, with x, y, z equal to the spatial coordinate directions:

$$\mathbf{K}(x, y, z) = \left\{ \begin{array}{ccc} K_{11}(x,y,z) & K_{12}(x,y,z) & K_{13}(x,y,z) \\ K_{21}(x,y,z) & K_{22}(x,y,z) & K_{23}(x,y,z) \\ K_{31}(x,y,z) & K_{32}(x,y,z) & K_{33}(x,y,z) \end{array} \right\}. \qquad (2.2.2)$$

Using units from the SI system in (2.2.1) we get $[K] = m^2$. A problem arises when we apply this unit for fluid flow, the unit is to big, hence we must use very small numbers for permeability. Another unit is much more suited, and is widely used in all fields related to flow in porous media. Hence we make an exception from the SI system when we define the unit for permeability as *Darcy*. It is commonly defined (see e.g. [29]) as follows:

Definition 1. The permeability of a porous medium is 1 *Darcy* if a fluid with viscosity of 1 cp and a pressure difference of 1 *atm/cm* is flowing through the mediums cross-section of 1 cm^2 at a rate of 1 cm^3/s.

Inserted in (2.2.1) gives $1\, Darcy \approx 0.987 \cdot 10^{-12}\, m^2$.

2.2.7   Multiphase extension of Darcy's Law

Darcy's law was introduced to model flow of one fluid through a porous media, it can be expanded to n phases.

$$\mathbf{u}_i = -\mathbf{K}\frac{k_{ri}(S_i)}{\mu_i}(\nabla p_i + \rho_i \mathbf{g}), \quad i = 1, \ldots, n. \qquad (2.2.3)$$

This expansion of Darcy's law looks similar to the original version. The only difference is the factor $k_{ri}(S_i)$ which is called the *relative permeability*. This factor accounts for the reduction of permeability as a result of the other phases. The idea is to think of each phase individually and pretend that the other phases are just a part of the rock matrix. Hence it is obvious that the relative permeability is dependent on the fluid saturation. The form of this functional relationship is dependent on the rocks properties, but in general the relative permeability is taken to be a nonlinear function of saturation.

In order to simplify the equation, we introduce *mobility* as

$$\lambda_i = \frac{k_{ri}}{\mu_i}, \quad i = 1, \ldots, n.$$

For a case where water is displacing oil, we define the *mobility ratio* as the ratio between the displacing and the displaced fluids mobility. For this case we write

$$M_{wo} = \frac{\lambda_w}{\lambda_o} = \frac{k_{rw}}{k_{ro}}\frac{\mu_o}{\mu_w}.$$

By performing an analysis of the fronts stability we distinguish between two types of displacements [34].

$$\mu_w > \mu_o = subcritical\ displacement,$$
$$\mu_w < \mu_o = supercritial\ displacement.$$

We do not perform this analysis but we can summarize by concluding that a subcritical displacement leads to a stable fluid front, and a supercritical displacement leads to an unstable fluid front.

2.3 Solving the Inverse Problem

In section 2.1 we introduced the general inverse problem and explained some of the reasons why it is so hard to solve. In this section we look into some of the techniques used to solve the inverse problem.

2.3.1 Least squares

Given a discrete linear inverse problem, we have a data vector, $\mathbf{d}$, of k observations, and a vector $\mathbf{m}$ consisting of n model parameters. We let $rank(\mathbf{G}) = n$ so the matrix $\mathbf{G}$ has full column rank. The inverse problem can then be written as a linear system of equations

$$\mathbf{Gm} = \mathbf{d}.$$

Since $k \neq n$ we have an inconsistent system of equations, but we still want to find an approximate solution. We therefore introduce the residual to measure the misfit between the actual data and $\mathbf{Gm}$. The residual is defined as

$$\mathbf{r} = \mathbf{d} - \mathbf{Gm}.$$

A natural measure for the quality of any approximate solution is the 2-norm of the residual $\|\mathbf{r}\|_2 = \|\mathbf{d} - \mathbf{Gm}\|_2$. The approximate solution that minimizes this norm is called a *least squares solution*. This solution can be obtained by projecting $\mathbf{d}$ onto the range of $\mathbf{G}$. Let

$$\begin{aligned} \mathbf{G(m)} &= \mathbf{p} \\ &= proj_{R(\mathbf{G})}\mathbf{d} \end{aligned} \qquad (2.3.1)$$

then $\mathbf{Gm} - \mathbf{d}$ is perpendicular to the range of $\mathbf{G}$. In particular each of the columns of $\mathbf{G}$ is orthogonal to $\mathbf{G(m)} - \mathbf{d}$. Thus

$$\mathbf{G}^T \left(\mathbf{Gm} - \mathbf{d} \right) = \mathbf{0} \qquad (2.3.2)$$

this is called the *normal equations* and the least squares solution is from this

$$\mathbf{m}_{L_2} = \left(\mathbf{G}^T\mathbf{G}\right)^{-1}\mathbf{G}^T\mathbf{d}. \tag{2.3.3}$$

It can be shown that if $\mathbf{G}$ is of full column rank then $\left(\mathbf{G}^T\mathbf{G}\right)^{-1}$ exists.

A typical problem that can be solved by the least squares method is finding the parameters m_1 and m_2 for a line $y = m_1 + m_2 x$, that best fits a set of $k > 2$ data points.

2.3.2   Continuous Inverse Problems

When we want to describe a physical system in the best possible way the parameters m, and the data d can be functions of time and space. When this is the case, the problem of estimating m from d is called a continuous inverse problem. One example of such a problem is the Fourier transform

$$\Phi(f) = \int_{-\infty}^{\infty} e^{-2\pi i f x}\phi(x)\,dx \tag{2.3.4}$$

where we want to obtain the continuous $\phi(x)$ from the continuous $\Phi(f)$. This is solved by deconvolution.

In many cases a continuous inverse problem can be well approximated by a discrete inverse problem. The way we perform this discretization is important for the solution procedure.

2.3.2.1   Discretization with Basis Functions

One way to discretize the continuous inverse problem is to represent the model $m(x)$ as a linear combination of p representers. With suitable functions $h_1(x), h_2(x), \ldots, h_p(x)$ that form a basis for a function space H. We can write our continuous inverse problem like

$$d(s) = \int_a^b g(s, x)m(x)\,dx,$$

we approximate $m(x)$ by

$$m(x) = \sum_{j=1}^{p} \alpha_j h_j(x).$$

When this approximation is substituted into the inverse problem we get

$$d(s_i) = \int_a^b g_i(x) \sum_{j=1}^p \alpha_j h_j(x)\, dx$$

$$= \sum_{j=1}^p \alpha_j \int_a^b g_i(x) h_j(x)\, dx, \qquad i = 1, \ldots, k.$$

Now the continuous inverse problem is reduced to a k by p linear system

$$\mathbf{G}\boldsymbol{\alpha} = \mathbf{d},$$

where

$$G_{i,j} = \int_a^b g_i(x) h_j(x)\, dx,$$

and

$$\boldsymbol{\alpha} = \sum_{j=1}^p \alpha_j,$$

This is one way to discretize our continuous inverse problem. We can now solve the linear system for $\boldsymbol{\alpha}$, and then find the model $m(x)$. For this approach we must make an intelligent choice of basis functions $h_j(x)$ in order to make the solution process as easy as possible.

2.3.3 Regularization

It can be shown that the general inverse problem is ill-posed by utilizing the SVD (Singular Value Decomposition). The generalized inverse solution can be written as (see e.g. [5])

$$\mathbf{m}_\dagger = \mathbf{V}_p \mathbf{S}_p^{-1} \mathbf{U}_p^T \mathbf{d} = \sum_{i=1}^p \frac{\mathbf{U}_{\cdot,i}^T \mathbf{d}}{s_i} \mathbf{V}_{\cdot,i} \qquad (2.3.5)$$

here the *Moore-Penrose pseudo inverse* [36, 40] is utilized. The $\mathbf{U}$ is an k by k orthogonal matrix with columns that are unit basis vectors spanning the *data space*. $\mathbf{V}$ is an n by n orthogonal matrix with columns that are basis vectors spanning the *model space*. The *Moore-Penrose pseudo inverse* is defined as

$$\mathbf{G}^\dagger = \mathbf{V}_p \mathbf{S}_p^{-1} \mathbf{U}_p^T$$

where the pseudo inverse is denoted by a dagger. The elements of $\mathbf{S}$ are called the *singular values* of the matix. Some of the singular values might be zero. We choose to arrange them by decreasing size, and only use the first p positive

singular values. This is denoted by the subscript p. Both $\mathbf{U}$ and $\mathbf{V}$ is truncated so that p columns of $\mathbf{U}$ and $\mathbf{V}$ are included. This is denoted by the subscript p.

From (2.3.5) we see that in presence of a noisy data vector, small singular values can act as a noise amplifier making the resulting answer practically useless. To solve the problem we need to introduce some remedies called *regularization*. There are many ways of performing regularization. To obtain good results we often utilize some information about the problem. This can be the relationship between sensitivity, non-linearity and scale associated with estimation of a given parameter from a given data-type. We can obtain good results by reparametrization of the parameters. This type of regularization is the main subject in our thesis and will hence be treated in a separate chapter. To illustrate some general properties of regularization we introduce three well known types of regularization:

- Truncated Singular Value Decomposition

- Zeroth-order Tikhonov Regularization

- Higher-order Tikhonov Regularization

2.3.3.1 Truncated Singular Value Decomposition

The truncated singular value decomposition (TSVD) is the simplest regularization method we introduce. From (2.3.5) we saw that small singular values combined with a noisy data vector could destroy our answer. One way to fix this problem is to remove the smallest singular values. We remember that the singular values was arranged in decreasing order down to the smallest positive value with index p. For the TSVD method we truncate at some $p' < p$. With this we can eliminate the smallest singular values but we also remove some of the model space basis vectors since $V_{.j}$ is also truncated. The resulting solution will not match the data as good as solutions based on all the model space basis vectors. This is a typical dilemma of regularization, there is always a trade-off between fitting the data and solution stability.

2.3.3.2 Zeroth-order Tikhonov Regularization

The Tikhonov regularization is perhaps the most widely used regularization technique. We will see that the Tikhonov solution effectively gives greater weight to large singular values in the SVD solution, and less weight to small singular values.

Considering an ill-posed problem $\mathbf{Gm} = \mathbf{d}$ with noisy data. To solve this, we would try to minimize the residual

$$\min \|\mathbf{r}\|_2^2 = \min \|\mathbf{Gm} - \mathbf{d}\|_2^2. \tag{2.3.6}$$

Solving this does not always produce a useful answer. We therefore introduce a regularization term α. The solution will now minimize

$$\min \|\mathbf{Gm} - \mathbf{d}\|_2^2 + \alpha^2 \|\mathbf{m}\|_2^2. \tag{2.3.7}$$

This is also called the *damped least squares problem*. Augmenting this we get an equivalent formulation as for the ordinary least squares problem

$$\min \left\| \begin{bmatrix} \mathbf{G} \\ \alpha\mathbf{I} \end{bmatrix} \mathbf{m} - \begin{bmatrix} \mathbf{d} \\ \mathbf{0} \end{bmatrix} \right\|_2^2. \tag{2.3.8}$$

This is solved by the normal equations which gives

$$\begin{bmatrix} \mathbf{G}^T & \alpha\mathbf{I} \end{bmatrix} \begin{bmatrix} \mathbf{G} \\ \alpha\mathbf{I} \end{bmatrix} \mathbf{m} = \begin{bmatrix} \mathbf{G}^T & \alpha\mathbf{I} \end{bmatrix} \begin{bmatrix} \mathbf{d} \\ \mathbf{0} \end{bmatrix}, \tag{2.3.9}$$

or simplified as

$$\left(\mathbf{G}^T\mathbf{G} + \alpha^2\mathbf{I} \right) \mathbf{m} = \mathbf{G}^T\mathbf{d}. \tag{2.3.10}$$

It can be shown (see e.g. [5]) that the solution to this is

$$\mathbf{m}_\alpha = \sum_{i=1}^{j} \frac{s_i^2}{s_i^2 + \alpha^2} \frac{(\mathbf{U}_{\cdot,i})^T \mathbf{d}}{s_i} \mathbf{V}_{\cdot,i} \tag{2.3.11}$$

recall that $\mathbf{U}$ is k by k, and $\mathbf{V}$ is n by n, we let $j = \min(k, n)$. This way all the singular values are included in this representation. By comparing (2.3.5) and (2.3.11) we see that the only difference is the factor

$$f_i = \frac{s_i^2}{s_i^2 + \alpha^2}. \tag{2.3.12}$$

This is called the *filter factors*. The advantage of Tikhonov regularization is clear when we look at how the filter factors behave. For $s_i \gg \alpha$, $f_i \approx 1$, and for $s_i \ll \alpha$, $f_i \approx 0$. For singular values between these extremes the filter factors decrease monotonically as the singular values decrease. It is now up to us to choose correct values of α.

2.3.3.3   Higher-order Tikhonov Regularization

In many situation we have some prior knowledge about the solution model. This information can be used in Tikhonov regularization. We introduce a new factor $\mathbf{L}$, in the damped least squared problem.

$$\min \|\mathbf{Gm} - \mathbf{d}\|_2^2 + \alpha^2 \|\mathbf{Lm}\|_2^2 \tag{2.3.13}$$

The factor $\mathbf{L}$ can be any suitable matrix. If we know that the solution is relatively flat, we might prefer to favor solutions with a small first derivative. Then $\mathbf{L}$ can be some finite-difference approximation to the first derivative. This is called a *first-order Tikhonov regularization*. If we prefer solutions with small second derivatives, we have to find a matix $\mathbf{L}$ that is some finite-difference approximation to the second derivative. This is called the a *second-order Tikhonov regularization*.

2.3.4   Non-linear Problems

The process of solving a non-linear inverse problem $\mathbf{G(m)} = \mathbf{d}$ is more complex than for the linear case. To be able to solve the non-linear problem we need to introduce some new methods.

Considering a system of k equations in k unknowns

$$\mathbf{F(x)} = \mathbf{0} \tag{2.3.14}$$

to solve this problem we construct a sequence of vectors, $\mathbf{x}^0, \mathbf{x}^1, \ldots$, that converges to a solution $\mathbf{x}^\star$. If $\mathbf{F}$ is continuously differentiable, we can construct a Taylor series approximation around $\mathbf{x}^0$

$$\mathbf{F(x}^0 + \Delta\mathbf{x}) \approx \mathbf{F(x}^0) + \nabla\mathbf{F(x}^0)\Delta\mathbf{x} \tag{2.3.15}$$

where $\nabla\mathbf{F(x}^0)$ is the Jacobian. To obtain an approximate equation for the difference between $\mathbf{x}^0$ and the unknown $\mathbf{x}^\star$

$$\mathbf{F(x}^\star) = \mathbf{0} \approx \mathbf{F(x}^0) + \nabla\mathbf{F(x}^0)\Delta\mathbf{x} \tag{2.3.16}$$

with $\Delta\mathbf{x} = \mathbf{x}^\star - \mathbf{x}^0$. We can now state *Newton's method*.

Algorithm 2.1 : Newton's method

Given a system of equations $\mathbf{F(x)} = \mathbf{0}$ and an initial solution $\mathbf{x}^0$, repeat the following steps to compute a sequence of solutions $\mathbf{x}^1, \mathbf{x}^2, \ldots$ Stop if and when the sequence converges to a solution with $\mathbf{F(x)} = \mathbf{0}$.

1. Use Gaussian elimination to solve

$$\nabla\mathbf{F(x}^p)\Delta\mathbf{x} = -\mathbf{F(x}^p)$$

2. Let $\mathbf{x}^{p+1} = \mathbf{x}^p + \Delta\mathbf{x}$.

3. Let $p = p + 1$.

If the initial solution $\mathbf{x}^0$ is close enough to $\mathbf{x}^\star$, $\mathbf{F}(\mathbf{x})$ is continuously differentiable in a neighborhood of $\mathbf{x}^\star$, and $\nabla\mathbf{F}(\mathbf{x}^\star)$ is non-singular, then Newton's method will converge to $\mathbf{x}^\star$.

Newton's method for systems of equations can not always be used for nonlinear inverse problems. There are many cases where the number of data points and number of model parameters are not similar. For these problems we might not have an exact solution. For linear problems we solved this by minimizing the residual function. This can be done for nonlinear problems as well. To do this we introduce Newton's method for minimizing $f(\mathbf{x})$.

If we wish to minimize a function, we remember from calculus that the derivative needs to be zero. In order to minimize a scalar-valued function $f(\mathbf{x})$ a necessary condition is $\nabla f(\mathbf{x}) = 0$. Solving this for a nonlinear function is a non-trivial task. A remedy is to approximate $f(\mathbf{x})$ by a second order Taylor expansion

$$f(\mathbf{x}^0 + \Delta\mathbf{x}) = f(\mathbf{x}^0) + \nabla f(\mathbf{x}^0)^T \Delta\mathbf{x} + \frac{1}{2}\Delta\mathbf{x}^T \nabla^2 f(\mathbf{x}^0)\Delta\mathbf{x}. \qquad (2.3.17)$$

Now we want to find a $\Delta\mathbf{x}$ such that the gradient of this approximation is zero. Keeping $\mathbf{x}^0$ constant, we take the gradient of (2.3.17) with respect to $\Delta\mathbf{x}$;

$$\nabla f(\mathbf{x}^0 + \Delta\mathbf{x}) \approx \nabla f(\mathbf{x}^0) + \nabla^2 f(\mathbf{x}^0)\Delta\mathbf{x}. \qquad (2.3.18)$$

Setting the approximate gradient equal to zero we get

$$\nabla^2 f(\mathbf{x}^0)\Delta\mathbf{x} = -\nabla f(\mathbf{x}^0) \qquad (2.3.19)$$

where $\nabla f(\mathbf{x}^0)$ is the gradient, $\nabla^2 f(\mathbf{x}^0)$ is the Hessian and $\Delta\mathbf{x} = \mathbf{x}^1 - \mathbf{x}^0$. We now state the *Newton's method for minimizing $f(\mathbf{x})$*.

Algorithm 2.2 : Newton's method for minimizing $f(\mathbf{x})$

Given a twice continuously differentiable function $f(\mathbf{x})$ and an initial solution $\mathbf{x}^0$, repeat the following steps to compute a sequence of solutions $\mathbf{x}^1, \mathbf{x}^2, \ldots$ Stop if and when the sequence converges to a solution with $\nabla f(\mathbf{x}) = \mathbf{0}$.

1. Solve $\nabla^2 f(\mathbf{x}^p)\Delta\mathbf{x} = -\nabla f(\mathbf{x}^p)$.

2. Let $\mathbf{x}^{p+1} = \mathbf{x}^p + \Delta\mathbf{x}$.

3. Let $p = p + 1$.

When the initial solution $\mathbf{x}^0$ is close enough to the minimum $\mathbf{x}^\star$, $f(\mathbf{x})$ is twice continuously differentiable, and $\nabla^2 f(\mathbf{x})$ is positive definite, then the method converge to $\mathbf{x}^\star$.

In the case of solving a nonlinear inverse problem we want to find values of the parameters that minimizes the 2-norm of the residuals. The residuals can be stated like $\mathbf{r} = \mathbf{G}(\mathbf{m}) - \mathbf{d}$. We want to minimize

$$r(\mathbf{m}) = \sum_{i=1}^{k} \left(G(\mathbf{m})_i - d_i \right)^2 . \tag{2.3.20}$$

We denote

$$r_i(\mathbf{m}) = G(\mathbf{m})_i - d_i \qquad i = 1, 2, 3, \ldots, k \tag{2.3.21}$$

and

$$\mathbf{R}(\mathbf{m}) = \begin{bmatrix} r_i(\mathbf{m}) \\ \vdots \\ r_k(\mathbf{m}) \end{bmatrix} . \tag{2.3.22}$$

With this we state our residual as:

$$r(\mathbf{m}) = \sum_{i=1}^{k} r_i(\mathbf{m})^2. \tag{2.3.23}$$

We want to use Newton's method for minimizing scalar valued functions. From algorithm 2.2 we see that we need to find both the gradient and the Hessian of $r(\mathbf{m})$. The gradient can be written as the sum of the gradients of each individual term:

$$\nabla r(\mathbf{m}) = \sum_{i=1}^{k} \nabla \left(r_i(\mathbf{m})^2 \right) . \tag{2.3.24}$$

This gives the following elements of the gradient:

$$\begin{aligned} \frac{\partial r(\mathbf{m})}{\partial m_j} &= \sum_{i=1}^{k} \frac{\partial}{\partial m_j} \left(r_i(\mathbf{m})^2 \right) \\ &= \sum_{i=1}^{k} 2 r_i(\mathbf{m}) \frac{\partial r_i(\mathbf{m})}{\partial m_j}, \end{aligned} \tag{2.3.25}$$

or in matrix notation

$$\nabla r(\mathbf{m}) = 2\mathbf{R}(\mathbf{m})\mathbf{J}(\mathbf{m})^T \tag{2.3.26}$$

where $\mathbf{J}(\mathbf{m})$ is the jacobian matrix

$$\mathbf{J}(\mathbf{m}) = \begin{bmatrix} \frac{\partial r_1(\mathbf{m})}{\partial m_1} & \cdots & \frac{\partial r_1(\mathbf{m})}{\partial m_n} \\ \vdots & \ddots & \vdots \\ \frac{\partial r_k(\mathbf{m})}{\partial m_1} & \cdots & \frac{\partial r_k(\mathbf{m})}{\partial m_n} \end{bmatrix} . \tag{2.3.27}$$

We find an expression for the Hessian of $r(\mathbf{m})$ in the same manner . Writing the sum of each individual term

$$\nabla^2 r(\mathbf{m}) = \sum_{i=1}^{k} \nabla^2 \left(r_i(\mathbf{m})^2 \right)$$
$$= \sum_{i=1}^{k} H^i(\mathbf{m}), \tag{2.3.28}$$

where $H^i(\mathbf{m})$ is the Hessian of $r_i(\mathbf{m})^2$. We write one element of the Hessian to clarify

$$H_{j,l}^i(\mathbf{m}) = \frac{\partial^2 (r_i(\mathbf{m})^2)}{\partial m_j \partial m_l}$$
$$= \frac{\partial}{\partial m_j} 2 \left(r_i(\mathbf{m}) \frac{\partial r_i(\mathbf{m})}{\partial m_l} \right) \tag{2.3.29}$$
$$= 2 \left(\frac{\partial r_i(\mathbf{m})}{\partial m_j} \frac{\partial r_i(\mathbf{m})}{\partial m_l} + r_i(\mathbf{m}) \frac{\partial^2 r_i(\mathbf{m})}{\partial m_j \partial m_l} \right),$$

in matrix notation

$$\mathbf{H}(\mathbf{m}) = 2\mathbf{J}(\mathbf{m})^T \mathbf{J}(\mathbf{m}) + \mathbf{Q}(\mathbf{m}), \tag{2.3.30}$$

where

$$\mathbf{Q}(\mathbf{m}) = 2\sum_{i=1}^{k} r_i(\mathbf{m}) \nabla^2 r_i(\mathbf{m}). \tag{2.3.31}$$

2.3.4.1   Gauss-Newton Method

In the Gauss-Newton method we ignore the $\mathbf{Q}(\mathbf{m})$ term in (2.3.30) so that the Hessian becomes

$$\mathbf{H}(\mathbf{m}) \approx 2\mathbf{J}(\mathbf{m})\mathbf{J}^T(\mathbf{m}). \tag{2.3.32}$$

To solve the non linear inverse problem by the Gauss-Newton method we use this expression for the Hessian in the Newton's method for minimizing. The iteration becomes

$$\mathbf{J}(\mathbf{m}^p)^T \mathbf{J}(\mathbf{m}^p)\Delta\mathbf{m} = -\mathbf{J}(\mathbf{m}^p)^T \mathbf{F}(\mathbf{m}^p) \tag{2.3.33}$$

The Gauss-Newton method often works well, but can fail. This is partly because the method is based on Newton's method, and can fail for the same reasons as Newton's method. The method will also fail if the matrix $\mathbf{J}(\mathbf{m}^k)^T \mathbf{J}(\mathbf{m}^k)$ is singular.

2.3.4.2   Levenberg-Marquardt Method

The Levenberg-Marquardt Method is introduced in order to fix some of the flaws in the Gauss-Newton method.

$$\left(\mathbf{J}(\mathbf{m}^p)^T\mathbf{J}(\mathbf{m}^p) + \lambda\mathbf{I}\right)\Delta\mathbf{m} = -\mathbf{J}(\mathbf{m}^p)^T\mathbf{F}(\mathbf{m}^p). \qquad (2.3.34)$$

Here the $\lambda\mathbf{I}$ term has been introduced to ensure convergence. By adjusting λ during the iterations we can ensure that the matrix always is non-singular. For large values of λ we get:

$$\mathbf{J}(\mathbf{m}^p)^T\mathbf{J}(\mathbf{m}^p) + \lambda\mathbf{I} \approx \lambda\mathbf{I}, \qquad (2.3.35)$$

which gives

$$\Delta\mathbf{m} \approx -\frac{1}{\lambda}\nabla r(\mathbf{m}). \qquad (2.3.36)$$

This is called the *steepest-descent* step. This means that the algorithm moves in direction of the gradient to most rapidly reduce $r(\mathbf{m})$. This approach assures convergence but is very slow. On the other hand if λ is very small the Levenberg-Marquardt method reverts to the Gauss-Newton method, which is fast but does not guarantee convergence.

λ is adjusted during the iterations, and one challenge is how to determine an optimal value of λ. We want a small value of λ when the Gauss-Newton method is working well, and we want a higher value of λ in situations where the Gauss-Newton method is failing. There are many different ways of determining λ and robust implementations uses sophisticated strategies for adjustment. For more on this we refer the reader to [37].

It is important to note that even though the $\lambda\mathbf{I}$ term in the Levenberg-Marquardt method resembles a Tikhonov regularization term it does nothing to regularize the solution. The $\lambda\mathbf{I}$ term is only used as way to stabilize the solution of the linear system and improve the convergence of the method. We observe that $\lambda\mathbf{I}$ does *not* enter in the objective function.

For more information on the Gauss-Newton or Levenberg-Marquardt method we refer the readers to e.g. [11, 38, 39].

2.3.5   Statistical approach

In the previous sections we began with a mathematical model of a given problem $\mathbf{Gm} = \mathbf{d}$. We assumed that there exists some true model $\mathbf{m}_{true}$ which corresponds to a true data set $\mathbf{d}_{true}$ is such a way that $\mathbf{Gm}_{true} = \mathbf{d}_{true}$. In a typical inverse problem we are given some data $\mathbf{d}$ which are a combination

of $\mathbf{d}_{true}$ and some noise. Our task is then to find the model $\mathbf{m}_{true}$. Since the inverse problem is ill-posed we need to implement regularization. This means that we are making a choice about which solutions we want. This works for many cases but it is not the only way of obtaining a solution. We now look at some fundamentally different ways of solving the inverse problem.

2.3.5.1   Bayesian methods

The Bayesian approach is based on completely different ideas than the classical approach. Instead of looking for the specific unknown model $\mathbf{m}_{true}$ we express the model as an random variable. In this mind frame the solution is a probability distribution for the model parameters. With the Bayesian approach we naturally incorporate prior information about the solution that comes from the data or from experience based intuition. The factors in the Bayesian method are

- $p(\mathbf{m})$:   The *prior distribution* of the model parameters, $\mathbf{m}$, based on knowledge available.

- $f(\mathbf{d}|\mathbf{m})$:   The *conditional distribution* of the measurements $\mathbf{d}$, given parameters $\mathbf{m}$.

- $q(\mathbf{m}|\mathbf{d})$:   The *posterior distribution* of the model parameters.

Bayes theorem is named after the 18-century mathematician Thomas Bayes. It is the foundations for the Bayesian methods and it allows us to combine the prior and the conditional distribution to form a posterior distribution.

Theorem 2. *Bayes Theorem*

$$q(\mathbf{m}|\mathbf{d}) = \frac{f(\mathbf{d}|\mathbf{m})p(\mathbf{m})}{\int_{all\,models} f(\mathbf{d}|\mathbf{m})p(\mathbf{m})\,d\mathbf{m}}. \tag{2.3.37}$$

A controversy concerning the Bayesian approach is the fact that we need to choose a prior distribution. Our choice here colors the final result. The method is therefore said to be "unscientific". As a response to this we can choose a *uninformative* prior distribution. Here all the models $\mathbf{m}$ are equally probable.

When we are using the Bayesian approach it is important to remember that the solution we obtain is a probability distribution. We can however obtain a single model, $\mathbf{m}$, as our solution. This is done by simply picking the model that maximizes $q(\mathbf{m}|\mathbf{d})$. This is called the *Maximum a posteriori* (MAP) model. Another way of getting a single model would be to use the mean of the posterior

distribution. In situations where the posterior distribution is normal, the MAP model and the posterior mean model would be identical [5].

For a general problem the computation of the integral $\int_{all\,models} f(\mathbf{d}|\mathbf{m})p(\mathbf{m})\,d\mathbf{m}$ can be very expensive. Fortunately we can perform some simplifications if the prior distribution is uninformative, or if the noise in the measured data is independent and normally distributed with standard deviation σ. For more information on Bayesian methods we refer the reader to e.g. [44, 45].

2.3.5.2   Data assimilation methods

The value of data assimilation methods can be illustrated by an example. If we have information of the temperature at som points in space, is it then possible to use this measurements to say something about how the temperature is at other points? An intelligent way is to use these measurements combined with a mathematical model. We assume that our mathematical model is not correct, we need to make better estimations of the parameters. If we make our mathematical model predict the measured temperatures, it is natural to believe that it will do a better job in estimating future temperatures. This is the idea of *Data assimilation* methods. There are many methods based on data assimilation, especially weather forecasting has applied these methods. In the field of fluid flow in porous media, the Ensemble Kalman filter has been used. This is based on the Kalman filter [28]. For readers who want more information about the Ensemble Kalman filter we refer to e.g. [2, 18, 19, 17].

Chapter 3

Multiscale approach to the inverse problem

In section 2.3 we looked into different ways of regularizing the problem. It was briefly mentioned that information about the problem could be important when chosing a regularization method. If there exists an interrelation between *sensitivity, non-linearity* and *scale,* denoted *SNS,* we can obtain good results by reparameterization of the parameters. We devote this chapter to this method of regularization because it is central to our thesis. Before we describe how to use this for solving an inverse problem we look into what we mean by sensitivity, non-linearity and scale.

3.1   Sensitivity

The objective of all inverse problems is to determine a set of parameters, m, based on a set of data, $d = G(m) + \eta$. When we define sensitivity we always mean the sensitivity of data to the parameters that define the problem. This is an important property of any inverse problem. We use the following measure for sensitivity

$$S_{i,j} = \frac{\partial d_i}{\partial m_j} = \frac{\partial G(m_j)_i}{\partial m_j},$$
(3.1.1)

where $G(m)$ is the forward model, and m is the true parameters that define the system. If a given sensitivity value, $S_{i,j}$, is low it means that big changes in the parameter, m_j, will correspond to small changes in the data ,d_i. We will then have a hard time to estimate the parameter m_j by measurements of the data vector $d_i = G(m_j)_i + \eta_i$ where we also have an error term η_i.

To obtain a good result for any inverse problem it is hence important to have knowledge about how the sensitivity values behave. We will have much higher sucess in finding correct values of the parameters if the sensitivity values are high.

3.2   Non-linearity

The inverse problem is often a non-linear problem. It is normally solved by some gradient based algorithm like the Gauss-Newton method, where we perform a linearization. If the problem is to non-linear the linearization may cause big problems for the algorithm. It may not converge, or it converges at some local minima instead of the global minima giving a useless answer. We therefore want the non-linearity to be as small as possible, to ensure that our method converges and to the correct solution. A good measure for non-linearity is thus important to ensure the stability of the numerical solution.

3.3   Scale

A typical petroleum reservoir is often characterized on many different scales. The geological model is very detailed and contains many small scale features. In order to perform sensible numerical calculations we perform an upscaling of the geological model to a reservoir model. This model does not have as many grid cells as the geological model and is more suited for numerical calculations.

We want to solve the inverse problem for some parameter in every grid block of the reservoir model, to do this we need a dense grid of data points. In real life we have measurement points in the wells of petroleum reservoirs. Because of the costs related to drilling wells we get sparsely distributed data points. This means that even though the reservoir model is coarser than the geological model we still have problems solving the inverse problem. One solution procedure would be to regularize the inverse problem in a classical Tikhonov way. We do not look further into this, but instead consider reparameterizing the inverse problem.

For the method of reparameterization to work we need an interrelation between sensitivity, non-linearity and scale. This interrelation must be such that there is large sensitivity, and small non-linearity associated with perturbations on a coarse scale. And correspondingly low sensitivity, and high non-linearity associated with perturbations on a fine scale.

γ_1	γ_2	γ_3	γ_4	γ_5	γ_6
γ_7	γ_8	γ_9	γ_{10}	γ_{11}	γ_{12}
γ_{13}	γ_{14}	γ_{15}	γ_{16}	γ_{17}	γ_{18}
γ_{19}	γ_{20}	γ_{21}	γ_{22}	γ_{23}	γ_{24}
γ_{25}	γ_{26}	γ_{27}	γ_{28}	γ_{29}	γ_{30}
γ_{31}	γ_{32}	γ_{33}	γ_{34}	γ_{35}	γ_{36}

ψ_1	ψ_2
ψ_3	ψ_4

Figure 3.3.1: Support of basis function γ_j and ψ_j

As an example of how regularization by reparameterization would work we consider a numerical grid with 36 grid cells. The parameter we want to estimate can be written as:

$$m = \sum_{j=1}^{36} \alpha_j \gamma_j(x). \tag{3.3.1}$$

We now assume that there exists an SNS interrelation for this example, and that the parameter can not be determined for all 36 grid cells. When we reparameterize the parameter so that we only need to determine the value for 4 grid cells, hence making the problem more coarse scaled

$$m = \sum_{j=1}^{4} \beta_j \psi_j(x). \tag{3.3.2}$$

Because of the SNS interrelation we expect the sensitivity of each parameter to be high, and the non-linearity to be low. This means that we should be more successful in solving the inverse problem. The support of the basis functions ψ_j and γ_j can be seen in figure 3.3.1

3.4   Applications

There has been done considerable work on this topic, and many different algorithms has been proposed. They all try to solve the inverse problem by reparametrizing the sought-after parameters so that it is represented on a different way than the grid of the reservoir model. In the following we give a short introduction to some different ways of achieving this.

3.4.1   Zonation

When we conduct zonation, the reservoir is partitioned into a gradually finer predefined set of zoned with constant but unknown permeability. In figure
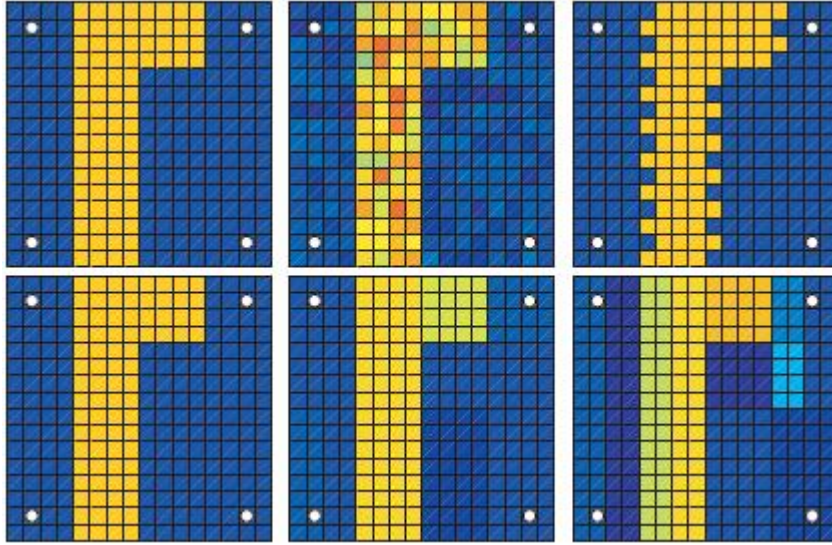
Figure 3.4.1: True permeability (upper row) and corresponding estimates (lower row) estimated by adaptive refinement. White dots show well location

3.3.1 we observed an example of zonation. We start by a low number of basis functions, and gradually refine the parameter space. In figure 3.3.1 we started with 4 grid cells and ended up with 36 grid cells. The problem with this method is that you need to know the structure of the zones prior to the estimation, and there is low flexibility for matching the real permeability field. More on zonation can be found e.g. [27].

3.4.2 Adaptive refinement

A more advanced way to solve the problem is multi-level, adaptive refinement strategies. Here the zonation structure is gradually refined, based on some measure of how much the objective function is reduced by a new refinement of the zonation structure. This means that the refinement is much more flexible with regards to matching the real permeability field. More on this strategy can be found in e.g. [3, 24, 26, 1] . A few estimation results from [24] are shown in figure 3.4.1, we see that even though we have a more flexible way of representing the different zones we still have some limitations. The shape of each zone is rectangular and hence the zones are not very flexible for representing complex shaped permeability zones, for this reason we still risk over-parameterization of the problem. To this end the theory of level-set has been applied to generate more smooth transitions between the refinement zones. For more on adaptive refinement methods that utilize this we refer the reader to e.g. [10, 30]. For more on the general theory of level-set we refer the reader to [16].

Chapter 4

Measures for sensitivity and non-linearity

In this chapter we introduce quantities that we use in the following chapters. We start by establishing some notation. The superscript T denotes the matix or vector transpose. Other superscripts on variable quantities are indexes. Exceptions from this is of course when the superscript is a fixed number ($x^2 = x \cdot x$), and when we have a superscript on a fixed number $10^k = 10 \cdot 10 \cdots 10$ (k-times).

4.1   Directional Derivatives in Parameter Space

We want to investigate the Sensitivity and non-linearity associated with scale (denoted SNS) for an inverse problem. We are given some data-vector $\mathbf{m}$, and a unit vector in parameter space $\mathbf{h}$. In order to say something about the sensitivity of $\mathbf{m}$ in direction of $\mathbf{h}$ we look at the first-order derivatives in parameter space

$$S_h = \|(\mathbf{m})_h\|. \tag{4.1.1}$$

To obtain a measure for the model non-linearities we turn to the second-order derivatives. Bates and Watts [7] introduced a relative curvature measure of non-linearity in direction of $\mathbf{h}$.

$$\kappa_h = \frac{\|(\mathbf{m})_{hh}\|}{\|(\mathbf{m})_h\|^2}. \tag{4.1.2}$$

We now give a introduction into how we can calculate S_h and κ_h.

In our case we want to estimate the spatially variable permeability k. We let the permeability be parametrized by

$$k(\mathbf{x}; \mathbf{c}) = \sum_{i=1}^{N} c_i \psi_i(\mathbf{x}) = \mathbf{c}^T \boldsymbol{\psi}(\mathbf{x}), \tag{4.1.3}$$

29

where $\boldsymbol{\psi}$ is an N-vector of piecewise constant basis functions, $\mathbf{c}$ is the associated parameter vector, and $\mathbf{x}$ is the spatial coordinate vector. The semicolon is used to separate between variables and parameters. We have variables on the left, and parameters on the right.

We define a function u by

$$u(\mathbf{x}; \mathbf{c}) = f(k(\mathbf{x}; \mathbf{c})), \qquad (4.1.4)$$

and assume that we have a sequence of model data $\{m_i\}_{i=0}^{i=M-1}$. We can define one of the elements as

$$m_i(\mathbf{c}) = \mathcal{F}(u(\mathbf{x}; \mathbf{c}); \zeta_i), \qquad (4.1.5)$$

where $\mathcal{F}$ is a linear functional acting on $u(\mathbf{x}; \mathbf{c})$.

When we let $\mathbf{h}$ be a unit vector in the parameter space. We then find the first-order directional derivative by

$$(m_i)_h = \frac{\partial m_i}{\partial \mathbf{h}}. \qquad (4.1.6)$$

All $\mathbf{h}$-directional derivatives of the model data vector then becomes

$$\begin{aligned} \left(\mathbf{m}^T\right)_h &= \frac{\partial m_0}{\partial \mathbf{h}}, \frac{\partial m_1}{\partial \mathbf{h}}, \dots, \frac{\partial m_{M-1}}{\partial \mathbf{h}} \\ &= \left((m_0)_h, (m_1)_h, \dots, (m_{M-1})_h\right). \end{aligned} \qquad (4.1.7)$$

The second-order directional derivative of m_i in $\mathbf{h}$-direction is then given by

$$(m_i)_{hh} = \frac{\partial^2 m_i}{\partial \mathbf{h}^2}, \qquad (4.1.8)$$

and all second-order $\mathbf{h}$-directional derivatives of the model data vector can then be written as

$$\begin{aligned} \left(\mathbf{m}^T\right) &= \frac{\partial^2 m_0}{\partial \mathbf{h}^2}, \frac{\partial^2 m_1}{\partial \mathbf{h}^2}, \dots, \frac{\partial^2 m_{M-1}}{\partial \mathbf{h}^2} \\ &= \left((m_0)_{hh}, (m_1)_{hh}, \dots, (m_{M-1})_{hh}\right). \end{aligned} \qquad (4.1.9)$$

4.2   Calculating the directional derivatives

A general expression for elements of the data-vector is found in (4.1.5). Using this we can show how to calculate the directional derivatives. The first-order directional derivative can be written as

$$(m_i)_h = \frac{\partial m_i}{\partial \mathbf{h}} = \mathbf{h}^T \nabla m_i(\mathbf{c}), \qquad (4.2.1)$$

where ∇ is the N-dimensional gradient vector in parameter space:

$$\nabla m_i = \frac{\partial m_i}{\partial c_1}\mathbf{e}_1 + \frac{\partial m_i}{\partial c_2}\mathbf{e}_2 + \cdots + \frac{\partial m_1}{\partial c_N}\mathbf{e}_N, \qquad (4.2.2)$$

with $\mathbf{e}_i$ being the i-th unit vector in parameter space. When we apply the general expression for the data-vector we get:

$$\nabla m_i(\mathbf{c}) = \nabla \mathcal{F}(u(\mathbf{x};\mathbf{c});\zeta_i), \qquad (4.2.3)$$

as noted earlier $\mathcal{F}$ is a linear operator working on $k(\mathbf{x};\mathbf{c})$ this means that the gradient can be moved inside $\mathcal{F}$

$$\nabla m_i(\mathbf{c}) = \mathcal{F}(\nabla u(\mathbf{x};\mathbf{c});\zeta_i). \qquad (4.2.4)$$

Using (4.1.4) and the chain rule we get

$$\nabla u(\mathbf{x};\mathbf{c}) = \nabla f(k(\mathbf{x};\mathbf{c})) = f'(k(\mathbf{x};\mathbf{c}))\nabla k(\mathbf{x};\mathbf{c}). \qquad (4.2.5)$$

Since we parametrized $k(\mathbf{x};\mathbf{c})$ in (4.1.3) we have

$$\nabla k(\mathbf{x};\mathbf{c}) = \nabla \mathbf{c}^T \boldsymbol{\psi}(\mathbf{x}) = \sum_{i=1}^{N} \frac{\partial}{\partial c_i} c_i \psi_i(x)\mathbf{e}_i = \boldsymbol{\psi}(\mathbf{x}), \qquad (4.2.6)$$

since $\mathbf{c}$ is the parameter vector associated with $k(\mathbf{x};\mathbf{c})$. Using this we get the following expression for the first-order $\mathbf{h}$-directional derivative of one element in the model data vector.

$$(m_i)_h = \mathbf{h}^T \nabla m_i(\mathbf{c}) = \mathbf{h}^T \mathcal{F}(f'(k(\mathbf{x};\mathbf{c}))\boldsymbol{\psi}(\mathbf{x});\zeta_i) \qquad (4.2.7)$$

$\mathbf{h}^T$ can be moved inside equation (4.2.7), and using

$$\mathbf{h}^T \boldsymbol{\psi}(\mathbf{x}) = k(\mathbf{x};\mathbf{h}) \qquad (4.2.8)$$

we can write

$$\boxed{(m_i)_h = \mathcal{F}(f'(k(\mathbf{x};\mathbf{c}))k(\mathbf{x};\mathbf{h});\zeta_i)} \qquad (4.2.9)$$

The second-order $\mathbf{h}$-directional derivative can be found in a similar manner. Writing

$$(m_i)_{hh} = \frac{\partial}{\partial \mathbf{h}}\left(\frac{\partial m_i}{\partial \mathbf{h}}\right) = \mathbf{h}^T \nabla \left((m_i)_h\right) \qquad (4.2.10)$$

Using (4.2.9) and still noting that $\mathcal{F}$ is a linear functional we get

$$\boxed{(m_i)_{hh} = \mathcal{F}(\nabla(f'(k(\mathbf{x};\mathbf{c}))k(\mathbf{x};\mathbf{h}));\zeta_i),} \qquad (4.2.11)$$

using the product rule we get

$$\nabla(f'(k(\mathbf{x};\mathbf{c}))k(\mathbf{x};\mathbf{h})) = \nabla f'(k(\mathbf{x};\mathbf{c}))k(\mathbf{x};\mathbf{h}) + f'(k(\mathbf{x};\mathbf{c}))\nabla k(\mathbf{x};\mathbf{h}). \quad (4.2.12)$$

Since $\mathbf{h}$ is a constant vector in parameter space we get

$$\nabla k(\mathbf{x};\mathbf{h}) = 0. \quad (4.2.13)$$

Applying the chain rule we get

$$\nabla(f'(k(\mathbf{x};\mathbf{c}))) = f''(k(\mathbf{x};\mathbf{c}))\nabla k(\mathbf{x};\mathbf{c}) \quad (4.2.14)$$

using (4.2.6), and (4.2.8) while remembering that $\mathbf{h}^T$ can be moved inside equation (4.2.10) we get the following expression for the second order $\mathbf{h}$-directional derivative of one element in the model data vector:

$$(m_i)_{hh} = \mathcal{F}(f''(k(\mathbf{x};\mathbf{c}))k^2(\mathbf{x};\mathbf{h});\zeta_i). \quad (4.2.15)$$

Our approach to finding expressions for sensitivity and non-linearity can then be summarized in a few steps:

- Find an expression for the sequence of data $\{m_i\}_{i=0}^{i=M-1}$.

- Calculate the first-order $\mathbf{h}$-directional derivatives $(\mathbf{m}^T)_h$.

- Calculate the second-order $\mathbf{h}$-directional derivatives $(\mathbf{m}^T)_{hh}$.

- Find expression for the sensitivity by equation (4.1.1).

- Find expression for the non-linearity by equation (4.1.2).

Chapter 5

Foundations for multiresolution analysis, and the Haar basis

5.1 Multiresolution analysis

Multiresolution analysis was first formulated by Meyer [35] and Mallat [32]. In this part we go through some of the basic concepts that characterize multiresolution analysis, and we use the Haar-basis as an example of an multiresolution basis. Most of the theory in this chapter is from [15, 41]. Corresponding theory can be found in other literature as well (see e.g. [42, 9, 12]). The basic idea of mulitresolution analysis is to create a sequence of successive approximation spaces, V_j, for representing functions from the space L^2. This can be formulated in the following way

$$\cdots \subset \mathcal{V}_2 \subset \mathcal{V}_1 \subset \mathcal{V}_0 \subset \mathcal{V}_{-1} \subset \mathcal{V}_{-2} \subset \cdots, \qquad (5.1.1)$$

$$\cap_{j \in \mathbb{Z}} \mathcal{V}_j = \{0\}, \qquad (5.1.2)$$

$$\overline{\cup_{j \in \mathbb{Z}} \mathcal{V}_j} = L^2(\mathbb{R}). \qquad (5.1.3)$$

Here, and for the rest of this thesis, $\mathbb{Z}$ is the set of all integers, and the overbar in (5.1.3) denotes closure. Denoting the P_j as the orthogonal projection operator onto $\mathcal{V}_j$. Then (5.1.3) guarantees that when $j \to -\infty$, $P_j f = f$ for all $f \in L^2(\mathbb{R})$. There are many ladders that fulfill (5.1.1)-(5.1.3). They do not necessary have anything to do with multiresolution. The multiresolution is a consequence of the additional requirements

$$\forall f \in L^2(\mathbb{R}) \text{ and } \forall j \in \mathbb{Z}, \qquad f(x) \in \mathcal{V}_j \Longleftrightarrow f(2^j x) \in \mathcal{V}_0, \qquad (5.1.4)$$

$$\forall f \in L^2(\mathbb{R}) \text{ and } \forall l \in \mathbb{Z}, \qquad f(x) \in \mathcal{V}_0 \Longleftrightarrow f(x - l) \in \mathcal{V}_0, \qquad (5.1.5)$$

$\exists \phi \in \mathcal{V}_0$ such that $\{\phi(x-k)\}_{k \in \mathbb{Z}}$ is a Riesz basis of the subspace $\mathcal{V}_0$. (5.1.6)

This means that every approximation space $\mathcal{V}_j$, $j \in \mathbb{Z}$, is a scaled version of the basic space $\mathcal{V}_0$. This is obtained by dyadic scaling (by a factor of 2^j) of the space $\mathcal{V}_0$. We achieve contraction or expansion depending on the sign of j. In this manner the space $\mathcal{V}_j$ has a resolution of 2^{-j}, and contains details twice as fine as those contained by the space $\mathcal{V}_{j+1}$. We see in (5.1.5) that $\mathcal{V}_0$ is invariant under integer translations. This is a feature that we require from multiresolution analysis. According to (5.1.6), the space $\mathcal{V}_0$ is generated by the function $\phi(x) \in L^2(\mathbb{R})$, and its translations. This function is called the scaling function:

$$\phi_l^j(x) = 2^{-j/2}\phi(2^{-j}x - l), \qquad j, l \in \mathbb{Z}, \qquad (5.1.7)$$

scaled j times and translated by l. The Riesz basis of the space $\mathcal{V}_j$ is the set of functions $\left\{\phi_l^j(x)\right\}$, $l \in \mathbb{Z}$.

The basic principle of multiresolution analysis is that whenever a collection of closed subspaces satisfies (5.1.1)-(5.1.6), there exists an orthonormal wavelet basis $\{\psi_l^j; j, l \in \mathbb{Z}\}$ of $L^2(\mathbb{R})$, where $\psi_l^j(x) = 2^{-j/2}\psi(2^{-j}x - l)$. This is called the "mother" wavelet, and it is a basis for the wavelet spaces $\mathcal{W}_j$. This space retains the details that are lost when we move from the space $\mathcal{V}_{j-1}$ to the space $\mathcal{V}_j$ since $\mathcal{V}_j \subset \mathcal{V}_{j-1}$. The space $\mathcal{W}_j$ is the orthogonal compliment of the subspace $\mathcal{V}_j$ related to the space $\mathcal{V}_{j-1}$

$$\mathcal{V}_{j-1} = \mathcal{V}_j \oplus \mathcal{W}_j. \qquad (5.1.8)$$

Where $\oplus$ denotes the orthogonal sum. This relationship gives us that for an arbitrary J

$$\mathcal{V}_J \oplus \mathcal{W}_J \oplus \mathcal{W}_{J-1} \oplus \cdots \oplus \mathcal{W}_j = \mathcal{V}_{j-1}, \quad J > j, \qquad (5.1.9)$$

that is, all spaces $\mathcal{W}_k$, $k \geq j$, are orthogonal to the space $\mathcal{W}_{j-1}$, because it is orthogonal to the space $\mathcal{V}_{j-1}$ which contains them. Thus we see the orthogonality of the spaces $\mathcal{W}_j$. When we apply the completeness conditions (5.1.2), (5.1.3), the equation (5.1.9) gives in the limit $j \to -\infty$

$$L^2(\mathbb{R}) = \mathcal{V}_J \oplus \sum_{j=J}^{-\infty} \mathcal{W}_j, \qquad (5.1.10)$$

and when $J \to \infty$

$$L^2(\mathbb{R}) = \sum_{j=-\infty}^{\infty} \mathcal{W}_j, \qquad (5.1.11)$$

Similar to $\mathcal{V}_j$ the wavelet spaces $\mathcal{W}_j$ can also be constructed by scaling and dyadic translations of a "mother" wavelet

$$\mathcal{W}_j = \overline{\left\{\psi_l^j \in L^2 \mid l \in \mathbb{Z}\right\}}, \qquad \psi_l^j(x) = 2^{-j/2}\psi(2^{-j}x - l), \quad j \in \mathbb{Z}. \qquad (5.1.12)$$

Because of the scaling properties $f(x) \in \mathcal{W}_j \iff f(2^j x) \in \mathcal{W}_0$ we see that our task is reduced to finding $\psi \in \mathcal{W}_0$ such that the $\psi(x - l)$ constitute an orthonormal basis for $\mathcal{W}_0$. But if we look at equation (5.1.8) it is clear that the subspaces $\mathcal{W}_0$ and $\mathcal{V}_0$ are both contained in the space $\mathcal{V}_{-1}$. That means that functions $\phi(x) \in \mathcal{V}_0$, and $\psi(x) \in \mathcal{W}_0$ belong to the space $\mathcal{V}_{-1}$. Thus they can be represented by the basis functions $\phi_l^{-1}(x) = \sqrt{2}\phi(2x - l)$. The matching representations can be written.

$$\phi(x) = \sum_l c(l)\sqrt{2}\phi(2x - l), \tag{5.1.13}$$

$$\psi(x) = \sum_l d(l)\sqrt{2}\psi(2x - l). \tag{5.1.14}$$

We see that (5.1.13) contains two scales, the function value at x, and at $2x$. Thus it has an infinite number of solutions. In order to define a unique solution, we require a normalisation

$$\int_{-\infty}^{\infty} \phi(x)dx = 1, \tag{5.1.15}$$

when we integrate (5.1.13) we get

$$1 = \int_{-\infty}^{\infty} \phi(x)\,dx = \sqrt{2}\sum_l c(l)\int_{-\infty}^{\infty} \phi(2x - l)\,dx. \tag{5.1.16}$$

Here we have required $\phi \in L^1$ to allow interchange of sum and integral. Now we perform a change of variables so that $y = 2x$, and note that the integral is independent of translation

$$1 = \sqrt{2}\sum_l c(l)\frac{1}{2}\int_{-\infty}^{\infty} \phi(y - l)\,dy, \tag{5.1.17}$$

thus we get the following condition on the coefficients $c(l)$ of equation (5.1.13).

$$\sum_l c(l) = \sqrt{2}. \tag{5.1.18}$$

5.2   The Haar basis

We now construct one of the simplest multiresolution basis functions. This basis was first introduced by Haar [25] long before the concept of wavelets was introduced. We construct, and use the basis to illustrate some of the concepts defined in section 5.1.

$$\phi\left(2^{-j}x - k\right)$$
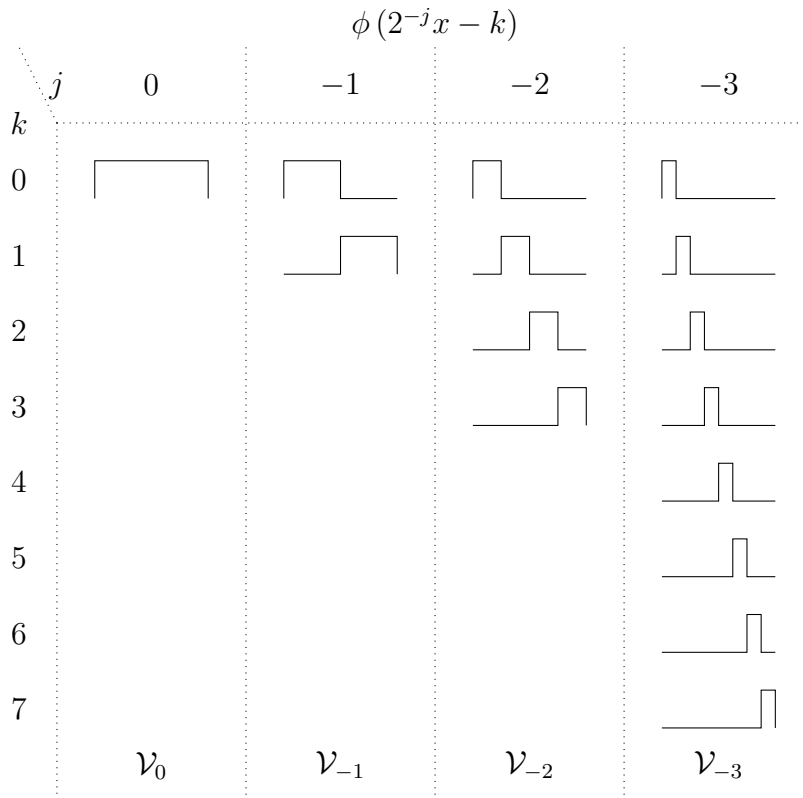
Figure 5.2.1: Haar scaling functions adopted from [12]

For the Haar basis system we want the scaling function to span the space of piecewise constant functions, on the unit interval $n \leq x < n+1$. Those functions are uniquely determined by their values $f(n)$ in all integer points $x = n$. We see that the function $f(2x) \in \mathcal{V}_{-1}$ is constant at the interval halves, and in general $f(2^{-j}x) \in \mathcal{V}_j$ is constant in intervals 2^j in length. As j decreases the space $\mathcal{V}_j$ is more able to approximate arbitrary functions by finer and finer piecewise constant functions. Since translation of a piecewise constant function, is still a piecewise constant function the spaces $\mathcal{V}_j$ is invariant relative to translation. The simplest way of defining this type of function is the Haar basis defined on the interval $[0, 1]$

$$\phi(x) = \begin{cases} 1, & x \in [0, 1], \\ 0, & \text{otherwise.} \end{cases} \tag{5.2.1}$$

The coefficients of (5.1.13) is obviously $c(0) = c(1) = 1/\sqrt{2}$. In figure 5.2.1 the spaces $\mathcal{V}_0, \mathcal{V}_{-1}, \mathcal{V}_{-2}$, and $\mathcal{V}_{-3}$ are illustrated.

We are interested in representing the L^2 space. From (5.1.10) and (5.1.11) we see that we either need all the wavelet spaces $\mathcal{W}_j$ from $j = \infty$, to $j = -\infty$ or start with from a scaling space $\mathcal{V}_j$ and use the wavelet spaces $\mathcal{W}_{j-1}$ with $j \to -\infty$. We choose the representation from 5.1.10, and start with the scaling space $\mathcal{V}_0$.

To find the corresponding wavelet we look at the wavelet space $\mathcal{W}_j$. When the space $\mathcal{V}_0$ contains functions that are constant on the unit interval, the space $\mathcal{V}_{-1}$ contains functions that are constant at halves of the unit intervals. According to equation (5.1.8) it is clear that $\mathcal{W}_0 \subset \mathcal{V}_{-1}$, that is functions from $\mathcal{W}_0$ are constants at half intervals, and the space $\mathcal{W}_0$ is orthogonal to $\mathcal{V}_0$. This means that for arbitrary constant functions $g \in \mathcal{V}_0$ and $f \in \mathcal{W}_0$ the following condition is met.

$$(f, g) = \sum_n \int_n^{n+1} g(x)f(x)dx = \sum_n g(n) \int_n^{n+1} f(x)dx = 0.$$

.For this to apply for an arbitrary $g(n)$, $\quad n = 0, \pm 1, \dots$ the integral over every whole interval of the function in $\mathcal{W}_0$ must be zero.

$$\int_n^{n+1} f(x)dx = 0, \quad n = 0, \pm 1, \dots$$

Now the wavelet space can be summarized in the following way

$\mathcal{W}_0 = \{constant\ at\ half\ intervals\ with\ the\ condition\colon\ f(n) + f(n + 1/2) = 0\}.$

The basis is then defined by the Haar wavelet

$$\psi(x) = \begin{cases} 1, & x \in \left[0, \frac{1}{2}\right], \\ -1, & x \in \left[\frac{1}{2}, 1\right], \\ 0, & \text{otherwise.} \end{cases} \tag{5.2.2}$$

Translations $\psi(x - l)$, $l \in \mathbb{Z}$ generate the space $\mathcal{W}_0$. The more general space $\mathcal{W}_j$ is created by translations of the function $\psi(2^{-j}x)$, from (5.1.2), and (5.1.3) it follows that

$$\psi_l^j(x) = 2^{-j/2}\psi(2^{-j}x - l) \quad j, l \in \mathbb{Z} \tag{5.2.3}$$

is a basis in L^2, where the index j defines the resolution of the system. In figure 5.2.2 we see an example of how the space $\mathcal{V}_{-3}$ can be decomposed by the Haar scaling function and the Haar Wavelets.

Due to the discontinuity of the basis functions the Haar basis has small approximation smoothness. This has been the drawback of the Haar wavelets. For our analysis we assume that the permeability is made up of piecewise constant functions, in that sense the Haar-basis works excellent. It is also in the essence of the SNS study to chose a hierarchical basis. Some elements of the Haar basis are shown in the figure 5.2.3.

$$\mathcal{V}_{-3} = \mathcal{V}_0 \oplus \mathcal{W}_0 \oplus \mathcal{W}_{-1} \oplus \mathcal{W}_{-2}$$
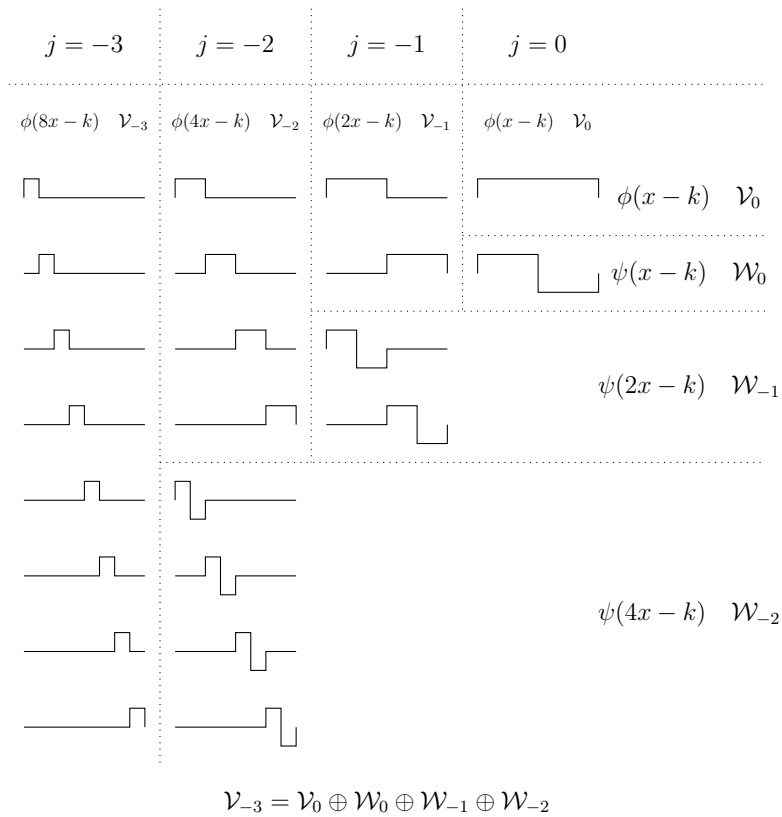
Figure 5.2.2: Decomposition of $\mathcal{V}_{-3}$ adopted from [12]
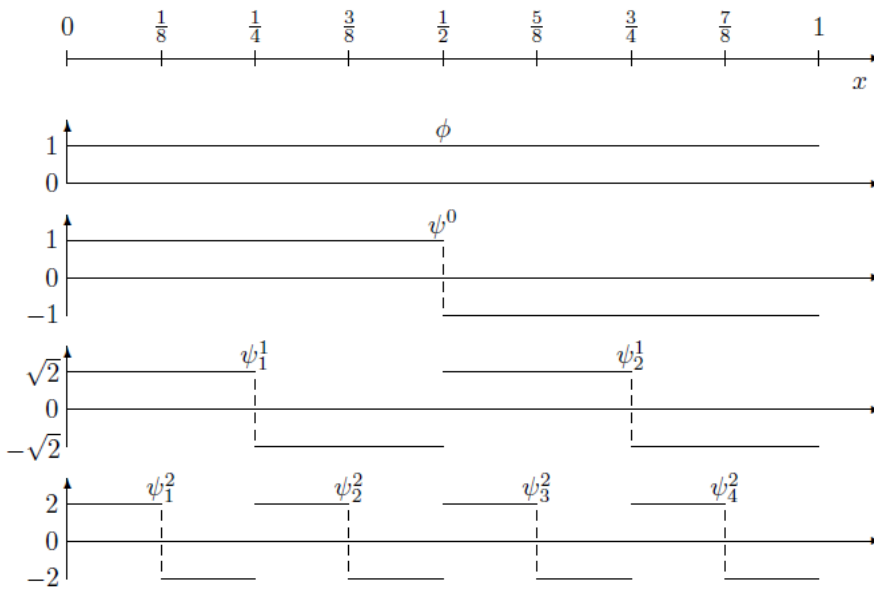
Figure 5.2.3: Haar basis

Chapter 6

SNS structure of single-phase flow

Single-phase flow occurs in many settings. Groundwater flow or oil flow in a naturally driven petroleum reservoir with no connecting aquifer is both examples of single-phase flow. In [33] the SNS structure associated with the inverse problem of identifying permeability from fluid pressure measurements was investigated. We now analyse the SNS structure associated with permeability identification from measurements of the fluid flow.

6.1 Equations

From chapter 2 we saw that 1-D single-phase flow can be modeled using Darcy's law:

$$u = -\mu^{-1}k(x;\mathbf{c})\frac{dp}{dx},\qquad(6.1.1)$$

where u denotes the Darcy velocity, μ the viscosity, and p pressure. We assume that the Darcy velocity can be observed at different time steps t_i. We let μ and u be constant in space, and we assume that the pressure is known at each end of the interval $[0,1]$. Integrating (6.1.1) from 0 to 1 gives

$$p(0,i) - p(1,i) = u\mu \int_0^1 k^{-1}(x;\mathbf{c})\, dx.\qquad(6.1.2)$$

By denoting $\Delta_x p(t_i) = p(0,i) - p(1,i)$ we get an expression of the Darcy velocity at time i

$$u(t_i) = \frac{\Delta_x p(t_i)}{\mu \int_0^1 k^{-1}(x;\mathbf{c})\, dx},\qquad(6.1.3)$$

we also denote $\Delta_t \Delta_x p = \Delta_x p(t_{i+1}) - \Delta_x p(t_i)$ and arive at an expression for the difference in flow rates between two time steps

$$u(t_{i+1}; \mathbf{c}) - u(t_i; \mathbf{c}) = \frac{\Delta_t \Delta_x p}{\mu \int_0^1 k^{-1}(x; \mathbf{c}) \, dx}. \tag{6.1.4}$$

We have now obtained a sequence of data we use to analyse the SNS structure. By the approach we derived in section 4.2 and letting $\zeta_i = t_i$

$$m_i(\mathbf{c}) = u(t_{i+1}; \mathbf{c}) - u(t_i; \mathbf{c}), \tag{6.1.5}$$

$$f(\mathbf{c}) = \frac{1}{I(g(\star; \mathbf{c}))}, \tag{6.1.6}$$

$$I(g(\star; \mathbf{c})) = \int_0^1 g(x; \mathbf{c}) \, dx, \tag{6.1.7}$$

$$g(x; \mathbf{c}) = r(k(x; \mathbf{c})), \tag{6.1.8}$$

$$r(k) = k^{-1}, \tag{6.1.9}$$

$$\mathcal{F}(f; t_i) = \frac{\Delta_t \Delta_x p}{\mu} f. \tag{6.1.10}$$

Now we find an expression for $(m_i)_h$ by using

$$(m_i)_h = \mathcal{F}(f'(k(\mathbf{x}; \mathbf{c})) k(\mathbf{x}; \mathbf{h})), \tag{6.1.11}$$

where f' is the derivative of f with respect to its argument. This gives

$$f'(k(\mathbf{x}; \mathbf{c})) = -\frac{1}{I^2(g(\star; \mathbf{c}))} I(g'(\star; \mathbf{c})), \tag{6.1.12}$$

written out we get the following expression

$$(m_i)_h = \frac{\Delta_t \Delta_x p}{\mu} \frac{\int_0^1 k^{-2}(\mathbf{x}; \mathbf{c}) k(\mathbf{x}; \mathbf{h}) dx}{\left[\int_0^1 k^{-1}(\mathbf{x}; \mathbf{c}) dx \right]^2}. \tag{6.1.13}$$

We can also get an expression for $(m_i)_{hh}$ by using

$$(m_i)_{hh} = \mathcal{F}(f''(k(\mathbf{x}; \mathbf{c})) k^2(\mathbf{x}; \mathbf{h}); \zeta_i), \tag{6.1.14}$$

with

$$f'' = \frac{2 \{ I(g'(\star; \mathbf{c})) \}^2}{I^3(g(\star; \mathbf{c}))} - \frac{I(g''(\star; \mathbf{c}))}{I^2(g(\star; \mathbf{c}))}, \tag{6.1.15}$$

and $\zeta_i = t_i$. Written out this gives the following expression

$$(m_i)_{hh} = \frac{2 \Delta_t \Delta_x p}{\mu} \left[\frac{\left\{ \int_0^1 k^{-2}(\mathbf{x}; \mathbf{c}) k(\mathbf{x}; \mathbf{h}) dx \right\}^2}{\left\{ \int_0^1 k^{-1}(\mathbf{x}; \mathbf{c}) dx \right\}^3} \right.$$
$$\left. + \frac{\int_0^1 k^{-3}(\mathbf{x}; \mathbf{c}) k^2(\mathbf{x}; \mathbf{h}) dx}{\left\{ \int_0^1 k^{-1}(\mathbf{x}; \mathbf{c}) dx \right\}^2} \right]. \tag{6.1.16}$$

6.2 Analysis of sensitivity and non-linearity

The expressions derived for $(m_i)_h$ and $(m_i)_{hh}$ enables us to analyze the value of sensitivity and non-linearity in direction of $\mathbf{h}$. By letting $\mathbf{h}$ take values corresponding to different Haar-basis elements, and then calculating S_h and κ_h for each Haar element, we get insight into how sensitivity and non-linearity changes with scale. Before we proceed we make some simplifications.

We assume that the permeability $k(\mathbf{x}; \mathbf{c})$ is constant. This means that we can write $k(\mathbf{x}; \mathbf{c}) = k(\mathbf{c})$, and this allows us to simplify (6.1.13) and (6.1.16) such that we get

$$(m_i)_h = \frac{\Delta_t \Delta_x p}{\mu} \frac{k^{-2}(\mathbf{c}) \int_0^1 k(\mathbf{x}; \mathbf{h}) \, dx}{k^{-2}(\mathbf{c})} = \frac{\Delta_t \Delta_x p}{\mu} \int_0^1 k(\mathbf{x}; \mathbf{h}) \, dx. \qquad (6.2.1)$$

and

$$(m_i)_{hh} = \frac{2\Delta_t \Delta_x p}{\mu} \left\{ \frac{\left[k^{-2}(\mathbf{c}) \int_0^1 k(x; \mathbf{h}) dx \right]^2}{k^{-3}(\mathbf{c})} + \frac{k^{-3}(\mathbf{c}) \int_0^1 k^2(x; \mathbf{h}) dx}{k^{-2}(\mathbf{c})} \right\}$$
$$= \frac{2\Delta_t \Delta_x p}{\mu} k^{-1}(\mathbf{c}) \left\{ \left[\int_0^1 k(x; \mathbf{h}) dx \right]^2 + \int_0^1 k^2(x; \mathbf{h}) dx \right\}. \qquad (6.2.2)$$

We are now able to analyze what happens in different directions of $\mathbf{h}$. First letting $\mathbf{h}^T = (1, 0, \ldots, 0)$ this corresponding to the direction of ϕ, (6.2.1) gives

$$(m_i)_\phi = \frac{\Delta_t \Delta_x p}{\mu}, \qquad (6.2.3)$$

and (6.2.2) gives us

$$(m_i)_{\phi\phi} = \frac{4\Delta_t \Delta_x p}{\mu} k^{-1}(\mathbf{c}). \qquad (6.2.4)$$

We apply (4.1.1), and (4.1.2) and get the following expressions for sensitivity and non-linearity

$$S_\phi = \left\| \frac{\Delta_t \Delta_x p}{\mu} \right\|, \qquad (6.2.5)$$

$$\kappa_\phi = \left\| \frac{4\Delta_t \Delta_x p}{\mu} k^{-1}(\mathbf{c}) \right\|. \qquad (6.2.6)$$

In similar fashion we let $\mathbf{h}$ be in direction of a basis element ψ_l^j. This gives

$$(m_i)_{\psi_l^j} = 0, \qquad (6.2.7)$$

$$(m_i)_{\psi_l^j \psi_l^j} = \frac{2\Delta_t \Delta_x p}{\mu} k^{-1}(\mathbf{c}). \qquad (6.2.8)$$

We apply (4.1.1) and (4.1.2) and get the following result

$$S_{\psi_l^j} = 0, \tag{6.2.9}$$

$$\kappa_{\psi_l^j} = \infty. \tag{6.2.10}$$

This means that only perturbations that change the average value of k on [0,1], can be observed in $\mathbf{m}$ when $k(x; \mathbf{c})$ is a constant function of x. This result is not surprising, taking into account that we have single-phase flow and with our knowledge of how Darcy's law was derived. It is also similar to the results obtained for pressure measurements in [33].

Chapter 7

SNS Structure of Two-Phase Flow

In this chapter we investigate SNS in the case of two-phase flow. We perform the analysis on a 1-D porous medium. The medium is initially filled with oil, and water is injected at one end, causing the oil to be produced at the other end. This is continued until the water has displaced all the oil (in real life there would be a residual water saturation before the water is injected, and a residual oil saturation will remain. For the sake of simplicity we assume that the medium is totally filled with oil initially, and that all the oil is displaced). During this process there is three different zones in the porous medium: One where the water has displaced the oil (this is closest to the injection point), one zone where the water has yet to reach (this is closest to the production point). The last zone is between these two containing both oil and water, denoted the two-phase region. The position and extent of these zones changes as the water displaces the oil, we can define the position of the interfaces seperating the zones in the following way:

$$z_w(t) = \text{position of water/two-pase interface at time } t,$$
$$z_o(t) = \text{position of two-phase/oil interface at time } t.$$

We model the fluid rates by the 1-D version of Darcy's law, which is written as we introduced it in section 2.2.7. Neglecting the gravitational effects, we have

$$u = -\lambda k(x; \mathbf{c})\frac{dp}{dx}, \tag{7.0.1}$$

where u is the total Darcy velocity, λ the total mobility, and p the pressure. u and λ can be given in terms of the corresponding phase quantities by

$$u = u_o + u_w,$$
$$\lambda = \lambda_o + \lambda_w. \tag{7.0.2}$$

We assume for the rest of this analysis, that the pressure is known at the end-points of the interval $[0, 1]$ at all times.

As we described earlier, the process of flooding a porous media generates three different regions. In this analysis we consider two different scenarios. One where the zone between oil and water has zero extension, and one where it has nonzero extension.

7.1   Equations

We start by looking at how some of the factors in Darcy's law depend on the fluid saturation. During the water injection process we get three different saturation zones. Using the definition of saturation introduced in section 2.2.3 we can write these three zones as

$$S(x, t) = \begin{cases} 1 & x < z_w(t), \\ \theta(x, t) & x \in [z_w(t), z_o(t)], \\ 0 & x > z_o(t). \end{cases} \tag{7.1.1}$$

Where $\theta(x, t)$ is a function describing the saturation inside the two-phase zone. From section 2.2.7 we learned that mobility is dependent on the relative permeability. This again is dependent on the saturation. In our three defined zones, this can be written as

$$k_{r,o}(S(x, t)) = \begin{cases} 0 & x < z_w(t), \\ k_{r,o}(\theta(x, t)) & x \in [z_w(t), z_o(t)], \\ 1 & x > z_o(t), \end{cases} \tag{7.1.2}$$

$$k_{r,w}(S(x, t)) = \begin{cases} 1 & x < z_w(t), \\ k_{r,w}(\theta(x, t)) & x \in [z_w(t), z_o(t)], \\ 0 & x > z_o(t). \end{cases} \tag{7.1.3}$$

Now we can define the mobility for the different regions

$$\lambda(S(x, t)) = \begin{cases} \mu_w^{-1} & x < z_w(t), \\ \lambda(\theta(x, t)) & x \in [z_w(t), z_o(t)], \\ \mu_o^{-1} & x > z_o(t). \end{cases} \tag{7.1.4}$$

We follow the approach developed in section 4.2 and start out by finding an expression for the sequence of data. This is done from equation (7.0.1). Rewriting and integrating from $x = 0$ to $x = 1$ gives

$$u(t_i; \mathbf{c}) = \frac{p(0, t_i) - p(1, t_i)}{\int_0^1 \lambda^{-1}(S(x, t_i)) k^{-1}(x; \mathbf{c}) \, dx} \tag{7.1.5}$$

inserting the definitions for the different regions, and using the notation $\Delta_x p(t_i) = p(0, t_i) - p(1, t_i)$ gives

$$u(t_i; \mathbf{c}) = \frac{\Delta_x p(t_i)}{\mu_w J_1(t_i) + \mu_o J_2(t_i) + J_3(t_i)} \qquad (7.1.6)$$

where

$$J_1(t_i) = \int_0^{z_w(t_i)} k^{-1}(x; \mathbf{c}) \, dx$$

$$J_2(t_i) = \int_{z_o(t_i)}^1 k^{-1}(x; \mathbf{c}) \, dx \qquad (7.1.7)$$

$$J_3(t_i) = \int_{z_w(t_i)}^{z_o(t_i)} \lambda^{-1}(S(x, t_i)) k^{-1}(x; \mathbf{c}) \, dx$$

in order to further simplify the equation we must make some assumptions about how the water displaces the oil. During this analysis we will derive several integrals, the superscipt p or np denotes if the integral belongs to the piston, or non-piston section.

7.1.1   Piston displacement

We assume that the water displaces the oil in the same manner as a piston would push a fluid out of a tube. For this scenario the two-phase zone have zero extent, and the fluid interfaces $z_w(t_i)$ and $z_o(t_i)$ merge into one surface $z(t_i)$ separating the two fluids. This means that in equation (7.1.6) $J_3(t_i) = 0$, and we get

$$u(t_i, \mathbf{c}) \frac{\Delta_x p(t_i)}{\mu_w \int_0^{z(t_i)} k^{-1}(x; \mathbf{c}) \, dx + \mu_o \int_{z(t_i)}^1 k^{-1}(x; \mathbf{c}) \, dx}, \qquad (7.1.8)$$

using that

$$\mu_w \int_0^{z(t_i)} k^{-1}(x; \mathbf{c}) \, dx = \mu_w \int_0^1 k^{-1}(x; \mathbf{c}) \, dx - \mu_w \int_{z(t_i)}^1 k^{-1}(x; \mathbf{c}) \, dx, \quad (7.1.9)$$

we arrive at the following expression for the sequence of data $m_i(\mathbf{c}) = u(t_{i+1}; \mathbf{c}) - u(t_i; \mathbf{c})$

$$m_i(\mathbf{c}) = \frac{\Delta_x p(t_{i+1})}{\mu_w \int_0^1 k^{-1}(x; \mathbf{c}) \, dx + (\mu_o - \mu_w) \int_{z(t_{i+1})}^1 k^{-1}(x; \mathbf{c}) \, dx}$$
$$- \frac{\Delta_x p(t_i)}{\mu_w \int_0^1 k^{-1}(x; \mathbf{c}) \, dx + (\mu_o - \mu_w) \int_{z(t_i)}^1 k^{-1}(x; \mathbf{c}) \, dx}. \qquad (7.1.10)$$

To obtain the second step in the approach from section 4.2 we find an expression for $(m_i)_h$ by employing equation (4.2.9). We define

$$f(\mathbf{c}) = q\left(K_1\left(I_1^p(g(\star, \mathbf{c})), I_2^p(g(\star, \mathbf{c}))\right), K_2\left(I_1^p(g(\star, \mathbf{c})), I_3^p(g(\star, \mathbf{c}))\right)\right), \quad (7.1.11)$$

with

$$q = \frac{\Delta_x p(t_{i+1})}{K_1} - \frac{\Delta_x p(t_i)}{K_2}, \tag{7.1.12}$$

$$K_1 = I_1^P + I_2^p, \tag{7.1.13}$$

$$I_1^P = \mu_w \int_0^1 g(x; \mathbf{c})\, dx, \tag{7.1.14}$$

$$I_2^P = (\mu_o - \mu_w) \int_{z(t_{i+1})}^1 g(x; \mathbf{c})\, dx, \tag{7.1.15}$$

$$K_2 = I_1^p + I_3^p, \tag{7.1.16}$$

$$I_3^p = (\mu_o - \mu_w) \int_{z(t_i)}^1 g(x; \mathbf{c})\, dx, \tag{7.1.17}$$

$$g(x; \mathbf{c}) = r(k(x; \mathbf{c})), \tag{7.1.18}$$

$$r(k) = k^{-1}, \tag{7.1.19}$$

$$\mathcal{F}(f; t_i) = f. \tag{7.1.20}$$

This gives the following expression for $f'(\mathbf{c})$

$$
\begin{aligned}
f'(\mathbf{c}) = & \frac{\partial q_1}{\partial K_1}\left\{\frac{\partial K_1}{\partial I_1^p}\frac{\partial I_1^p}{\partial g} + \frac{\partial K_1}{\partial I_2^p}\frac{\partial I_2^p}{\partial g}\right\} \\
& - \frac{\partial q_2}{\partial K_2}\left\{\frac{\partial K_2}{\partial I_1^p}\frac{\partial I_1^p}{\partial g} + \frac{\partial K_2}{\partial I_3^p}\frac{\partial I_3^p}{\partial g}\right\}.
\end{aligned}
\tag{7.1.21}
$$

This gives the following expression for $(m_i)_h$ assuming that we have constant permeability. The calculations for this is found in appendix A.1.1

$$
\begin{aligned}
(m_i)_h = \Bigg(& \frac{\Delta_x p(t_{i+1})}{[\mu_o + (\mu_w - \mu_o)z(t_{i+1})]^2} \\
& \times \left\{ \mu_w \int_0^1 k(x; \mathbf{h})\, dx + (\mu_w - \mu_o) \int_{z(t_{i+1})}^1 k(x; \mathbf{h})\, dx \right\} \\
& - \frac{\Delta_x p(t_i)}{[\mu_o + (\mu_w - \mu_o)z(t_i)]^2} \\
& \times \left\{ \mu_w \int_0^1 k(x; \mathbf{h})\, dx + (\mu_w - \mu_o) \int_{z(t_i)}^1 k(x; \mathbf{h})\, dx \right\} \Bigg).
\end{aligned}
\tag{7.1.22}
$$

From (4.2.15) we find the expression for $(m_i)_{hh}$, still assuming constant permeability. The calculations for this is presented in appendix A.1.1.

$$
\begin{aligned}
(m_i)_{hh} =& \frac{2k^{-1}(\mathbf{c})\Delta_x p(t_{i+1})}{[\mu_o + (\mu_w - \mu_o)z(t_{i+1})]^3} \\
& \times \left\{ \mu_w \int_0^1 k(x;\mathbf{h})\,dx + (\mu_o - \mu_w)\int_{z(t_{i+1})}^1 k(x;\mathbf{h})\,dx \right\}^2 \\
& - \frac{2k^{-1}(\mathbf{c})\Delta_x p(t_{i+1})}{[\mu_0 + (\mu_w - \mu_o)z(t_{i+1})]^2} \\
& \times \left\{ \mu_w \int_0^1 k^2(x;\mathbf{h})\,dx + (\mu_o - \mu_w)\int_{z(t_{i+1})}^1 k^2(x;\mathbf{h})\,dx \right\} \\
& - \frac{2k^{-1}(\mathbf{c})\Delta_x p(t_i)}{[\mu_o + (\mu_w - \mu_o)z(t_i)]^3} \\
& \times \left\{ \mu_w \int_0^1 k(x;\mathbf{h})\,dx + (\mu_o - \mu_w)\int_{z(t_i)}^1 k(x;\mathbf{h})\,dx \right\}^2 \\
& + \frac{2k^{-1}(\mathbf{c})\Delta_x p(t_i)}{[\mu_0 + (\mu_w - \mu_o)z(t_i)]^2} \\
& \times \left\{ \mu_w \int_0^1 k^2(x;\mathbf{h})\,dx + (\mu_o - \mu_w)\int_{z(t_i)}^1 k^2(x;\mathbf{h})\,dx \right\}.
\end{aligned}
\tag{7.1.23}
$$

7.1.2   Non-Piston displacement

We now assume that there is a two-phase zone separating the water and the oil. When this is the case $J_3(t_i)$ in (7.1.6) does not equal zero. This means that our functions need to be altered. We use the fact

$$
\begin{aligned}
\mu_w \int_0^{z_w(t_i)} k^{-1}(x;\mathbf{c})\,dx = & \; \mu_w \int_0^1 k^{-1}(x;\mathbf{c})\,dx \\
& - \mu_w \int_{z_w(t_i)}^{z_o(t_i)} k^{-1}(x;\mathbf{c})\,dx \\
& - \mu_w \int_{z_o(t_i)}^1 k^{-1}(x;\mathbf{c})\,dx,
\end{aligned}
\tag{7.1.24}
$$

we get the following expression for the fluid rate at time t_i

$$
u(t_i;\mathbf{c}) = \frac{\Delta_x p(t_i)}{\mu_w I_1^{np} + (\mu_o - \mu_w)I_2^{np}(t_i) + I_3^{np}(t_i)},
\tag{7.1.25}
$$

$$
I_1^{np} = \int_0^1 k^{-1}(x;\mathbf{c})\,dx,
\tag{7.1.26}
$$

$$I_2^{np}(t_i) = \int_{z_o(t_i)}^1 k^{-1}(x; \mathbf{c}) \, dx, \tag{7.1.27}$$

$$I_3^{np}(t_i) = \int_{z_w(t_i)}^{z_o(t_i)} (\lambda^{-1}(S(x, t_i)) - \mu_w) k^{-1}(x; \mathbf{c}) \, dx, \tag{7.1.28}$$

we now get the sequence of data $m_i(\mathbf{c}) = u(t_{i+1}; \mathbf{c}) - u(t_i; \mathbf{c})$

$$\begin{aligned}
m_i(\mathbf{c}) = & \frac{\Delta_x p(t_{i+1})}{\mu_w I_1^{np} + (\mu_o - \mu_w) I_2^{np}(t_{i+1}) + I_3^{np}(t_{i+1})} \\
& - \frac{\Delta_x p(t_i)}{\mu_w I_1^{np} + (\mu_o - \mu_w) I_2^{np}(t_i) + I_3^{np}(t_i)},
\end{aligned} \tag{7.1.29}$$

with I_1^{np}, I_2^{np} and I_3^{np} as in (7.1.26), (7.1.27), and (7.1.28).

We derive an expression for $(m_i)_h$ by employing equation (4.2.9). We define

$$\begin{aligned}
f(\mathbf{c}) = & q \left(K_1 \left(I_1^{np}(\star, \mathbf{c}), I_2^{np}(\star, \mathbf{c}), I_3^{np}(\star, \mathbf{c}) \right), \right. \\
& \left. K_2 \left(I_1^{np}(\star, \mathbf{c}), I_4^{np}(\star, \mathbf{c}), I_5^{np}(\star, \mathbf{c}) \right) \right),
\end{aligned} \tag{7.1.30}$$

with

$$q = \frac{\Delta_x p(t_{i+1})}{K_1} - \frac{\Delta_x p(t_i)}{K_2}, \tag{7.1.31}$$

$$K_1 = I_1^{np} + I_2^{np} + I_3^{np}, \tag{7.1.32}$$

$$I_1^{np} = \mu_w \int_0^1 g(x; \mathbf{c}) \, dx, \tag{7.1.33}$$

$$I_2^{np} = (\mu_o - \mu_w) \int_{z_o(t_i)}^1 g(x; \mathbf{c}) \, dx, \tag{7.1.34}$$

$$I_3^{np} = \int_{z_w(t_i)}^{z_o(t_i)} (\lambda^{-1}(S(x, t_i)) - \mu_w) g(x; \mathbf{c}) \, dx, \tag{7.1.35}$$

$$K_2 = I_4^{np} + I_5^{np} + I_6^{np}, \tag{7.1.36}$$

$$I_4^{np} = \mu_w \int_0^1 g(x; \mathbf{c}) \, dx, \tag{7.1.37}$$

$$I_5^{np} = (\mu_o - \mu_w) \int_{z_o(t_{i+1})}^1 g(x; \mathbf{c}) \, dx, \tag{7.1.38}$$

$$I_6^{np} = \int_{z_w(t_{i+1})}^{z_o(t_{i+1})} (\lambda^{-1}(S(x, t_{i+1})) - \mu_w) g(x; \mathbf{c}) \, dx, \tag{7.1.39}$$

$$g(x; \mathbf{c}) = r(k(x; \mathbf{c})), \tag{7.1.40}$$

$$r(k) = k^{-1}. \tag{7.1.41}$$

This gives us

$$\mathcal{F}(f; t_i) = f. \tag{7.1.42}$$

Like the case with piston displacement we assume that the permeability is constant $k(x; \mathbf{c}) = k(\mathbf{c})$.

We would like to simplify the expression even further. The mobility $\lambda(S(x,t))$ typically varies slowly with $S(x,t)$. The saturation in $x \in [z_w, z_o]$ is given by $\theta(x,t)$, and this function is decreasing monotonically. This means that the function $\lambda^{-1}(S(x,t))$ is replaced with an average value λ^{-1}. We further assume that the two fronts z_w and z_o are traveling with the same speed, this means that the average value is the same on $(z_{w,i}, z_{o,i})$ as on $(z_{w,i+1}, z_{o,i+1})$.

The calculations to get $(m_i)_h$ are given in appendix A.1.2, but with the assumptions described above we have

$$
\begin{aligned}
(m_i)_h =& \frac{\Delta_x p(t_{i+1})}{\left[\mu_o + (\mu_w - \mu_o)\, z_{o,i+1} + \left(\lambda^{-1} - \mu_w\right) \delta_{i+1}\right]^2} \\
&\times \left\{ \mu_w \int_0^1 k(x; \mathbf{h})\, dx + (\mu_o - \mu_w) \int_{z_{o,i+1}}^1 k(x; \mathbf{h})\, dx \right. \\
&\left. + \left(\lambda^{-1} - \mu_w\right) \int_{z_{w,i+1}}^{z_{o,i+1}} k(x; \mathbf{h})\, dx \right\} \\
&- \frac{\Delta_x p(t_i)}{\left[\mu_o + (\mu_w - \mu_o)\, z_{o,i} + \left(\lambda^{-1} - \mu_w\right) \delta_i\right]^2} \\
&\times \left\{ \mu_w \int_0^1 k(x; \mathbf{h})\, dx + (\mu_o - \mu_w) \int_{z_{o,i}}^1 k(x; \mathbf{h})\, dx \right. \\
&\left. + \left(\lambda^{-1} - \mu_w\right) \int_{z_{w,i}}^{z_{o,i}} k(x; \mathbf{h})\, dx \right\}.
\end{aligned}
\tag{7.1.43}
$$

With $\delta_{i+1} = z_{o,i+1} - z_{w,i+1}$, and $\delta_i = z_{o,i} - z_{w,i}$.
The expression for $(m_i)_{hh}$ is given by (4.2.15) and the calculation to get this quantity is given in appendix A.1.2. With the same assumptions as for $(m_i)_h$

and the same definition for δ_{i+1} and δ_i we get

$$
\begin{aligned}
(m_i)_{hh} =& 2k^{-1}(\mathbf{c}) \frac{\Delta_x p(t_{i+1})}{\left[\mu_o + (\mu_w - \mu_o)\, z_{o,i+1} + (\lambda^{-1} - \mu_w)\, \delta_{i+1}\right]^3} \\
& \times \left\{ \mu_w \int_0^1 k(x;\mathbf{h})\, dx + (\mu_o - \mu_w) \int_{z_{o,i+1}}^1 k(x;\mathbf{h})\, dx \right. \\
& \left. + \left(\lambda^{-1} - \mu_w\right) \int_{z_{w,i+1}}^{z_{o,i+1}} k(x;\mathbf{h})\, dx \right\}^2 \\
& - 2k^{-1}(\mathbf{c}) \frac{\Delta_x p(t_{i+1})}{\left[\mu_o + (\mu_w - \mu_o)\, z_{o,i+1} + (\lambda^{-1} - \mu_w)\, \delta_{i+1}\right]^2} \\
& \times \left\{ \mu_w \int_0^1 k^2(x;\mathbf{h})\, dx + (\mu_o - \mu_w) \int_{z_{o,i+1}}^1 k^2(x;\mathbf{h})\, dx \right. \\
& \left. + \left(\lambda^{-1} - \mu_w\right) \int_{z_{w,i+1}}^{z_{o,i+1}} k^2(x;\mathbf{h})\, dx \right\} \\
& - 2k^{-1}(\mathbf{c}) \frac{\Delta_x p(t_i)}{\left[\mu_o + (\mu_w - \mu_o)\, z_{o,i} + (\lambda^{-1} - \mu_w)\, \delta_i\right]^3} \\
& \times \left\{ \mu_w \int_0^1 k(x;\mathbf{h})\, dx + (\mu_o - \mu_w) \int_{z_{o,i}}^1 k(x;\mathbf{h})\, dx \right. \\
& \left. + \left(\lambda^{-1} - \mu_w\right) \int_{z_{w,i}}^{z_{o,i}} k(x;\mathbf{h})\, dx \right\}^2 \\
& + 2k^{-1}(\mathbf{c}) \frac{\Delta_x p(t_i)}{\left[\mu_o + (\mu_w - \mu_o)\, z_{o,i} + (\lambda^{-1} - \mu_w)\, \delta_i\right]^2} \\
& \times \left\{ \mu_w \int_0^1 k^2(x;\mathbf{h})\, dx + (\mu_o - \mu_w) \int_{z_{o,i}}^1 k^2(x;\mathbf{h})\, dx \right. \\
& \left. + \left(\lambda^{-1} - \mu_w\right) \int_{z_{w,i}}^{z_{o,i}} k^2(x;\mathbf{h})\, dx \right\}.
\end{aligned}
\tag{7.1.44}
$$

7.2 Analysis of Sensitivity and Non-linearity for Two-Phase Flow

In section 7.1 we obtained equations for $(m_i)_h$ and $(m_i)_{hh}$ in the case of two-phase flow with piston displacement and non-piston displacement. We now use these equations to analyze the SNS structure when estimating permeability from measurements of the fluid flow rate for two-phase flow. In section 6.2 this analysis was performed for a one-phase flow example.

We analyze the SNS structure by letting $\mathbf{h}$ take values corresponding to different Haar-basis elements. Then we calculate values for sensitivity S, and non-linearity κ for the different basis elements. Because of the hierarchical structure of the Haar-basis we are able to study the sensitivity and non-linearity on different scales.

7.2.1   Piston displacement

We start by looking into the case of piston displacement. As described earlier this corresponds to the water pushing the oil like a piston. This means that the two-phase zone separating the two fluids are of zero extent, and we can imagine the separation of the fluids like a surface with position $z(t_i)$ at time equals t_i.

From equation (7.1.22) we observe that the position of $z(t_i)$ is important as it determines the integration limits, and will hence have influence on the value of the integral. Thus the way we collect our measurements plays an important role for the SNS structure. We distinguish between two types of data collection.

- Ordered measurement collection

- Non-ordered measurement collection

The ordered collection of data points means that we make measurements in such a way that the front moves the same distance between each measurement point. This can be written like:

$$z(t_{i+1}) - z(t_i) = \text{constant.} \tag{7.2.1}$$

In the non-ordered case we take measurements in a random way. This means that the front may, or may not move the same distance between each measurement.

7.2.1.1   Ordered measurements

We start the analysis by looking at the value for sensitivity. The directional derivative of $m_i(\mathbf{c})$ in direction of $\mathbf{h}$ is given by (7.1.22) . We calculate $(m_i)_\phi$ corresponding to the directional derivative in direction of a constant basis, and $(m_i)_{\psi_l^j}$ corresponding to the directional derivative in direction of different Haar wavelets. Using (4.1.1) we calculate the values of sensitivity for the two
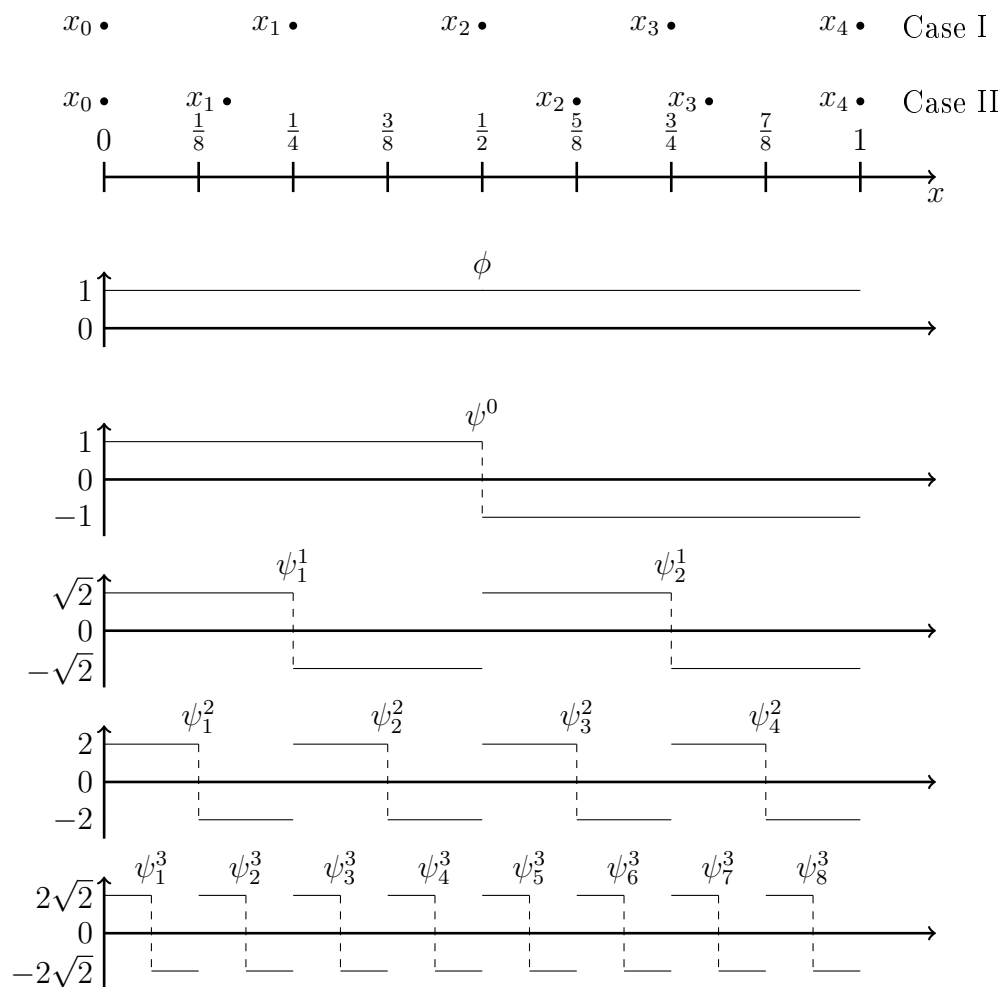
Figure 7.2.1: Elements of Haar basis, and measurement points. Case I represents ordered measurements. Case II represents non-ordered measurements.

different cases. We only look at one spatial dimension $x \in [0, 1]$ this means that we can simplify equation (7.1.22) by letting $z(t_i) = x_i$ and $z(t_{i+1}) = x_{i+1}$. This is done because $z(t_i)$ only represents the fluid fronts position at time t_i. We now calculate $(m_i)_\phi$ by observing that $k(x; \mathbf{h}) = 1$. By inserting this in (7.1.22) we get

$$(m_i)_\phi = \frac{\Delta_x p(t_{i+1})}{\left[\mu_o + (\mu_w - \mu_o)\, x_{i+1}\right]^2} \left\{\mu_o + (\mu_w - \mu_o)\, x_{i+1}\right\}$$
$$- \frac{\Delta_x p(t_i)}{\left[\mu_o + (\mu_w - \mu_o)\, x_i\right]^2} \left\{\mu_o + (\mu_w - \mu_o)\, x_i\right\}, \tag{7.2.2}$$

by cancellation this is

$$(m_i)_\phi = \frac{\Delta_x p(t_{i+1})}{\left[\mu_o + (\mu_w - \mu_o)\, x_{i+1}\right]}$$
$$- \frac{\Delta_x p(t_i)}{\left[\mu_o + (\mu_w - \mu_o)\, x_i\right]}. \tag{7.2.3}$$

To calculate $(m_i)_{\psi_l^j}$ we still look at (7.1.22), but now $k(x; \mathbf{h}) \neq 1$, hence the integrals will obtain different values. Because of the properties of the Haar-basis wavelet elements ψ_l^j it is clear that when $\mathbf{h}$ is in direction of ψ_l^j we have

$$\int_0^1 k(x; \mathbf{h})\, dx = 0. \tag{7.2.4}$$

This means that the variation with scale of the directional derivative is determined by the integral

$$\int_{x_i}^1 k(x; \mathbf{h})\, dx, \tag{7.2.5}$$

and

$$\int_{x_{i+1}}^1 k(x; \mathbf{h})\, dx, \tag{7.2.6}$$

with $\mathbf{h}$ in direction of ψ_l^j. To analyze these integrals we make use of figure 7.2.1. We assume that we have x_i observations where $i = 0, 1, 2, \ldots, 2^L$. In figure 7.2.1 Case I we see an example with $L = 2$. Depending on the value of j we get three situations:

1. $x_{i+1} - x_i < \frac{1}{2} \left[supp\, \psi_l^j\right]$

2. $x_{i+1} - x_i = \frac{1}{2} \left[supp\, \psi_l^j\right]$

3. $x_{i+1} - x_i \geq \left[supp\, \psi_l^j\right]$

There seems to be a gap between case 2, and case 3 that has been neglected. Because of the ordered measurements, our maximum amount of measurements being 2^L, and that the Haar wavelets are translated with 2^{-j} steps, there are no cases where

$$\frac{1}{2}\left[supp\,\psi_l^j\right] < (x_{i+1} - x_i) < \left[supp\,\psi_l^j\right].$$

With measurements as illustrated by Case I in figure 7.2.1 situation 1 corresponds to $\mathbf{h}$ being in direction of ψ^0 . We see that integration over ψ^0 would result in a non-zero value for both the integrals. Considering a more general case of ordered measurements, we would see that if one of the integration limits x_i/x_{i+1} lined up with the start point of a basis element the integral value is zero. But because of the distance between integration points described by situation 1 the other integral would not line up with a start point, ensuring that $(m_i)_\psi$ is always non-zero for situation 1.

To illustrate situation 2 we use figure 7.2.1 Case I. In this example Situation 2 corresponds to $\mathbf{h}$ in direction of ψ_l^1. Integration over ψ_l^1 elements with measurements as in case I would guarantee that one of the integrals becomes zero, and the other integral becomes a non-zero value. When we consider a more general situation, the results will still hold. As an simple example we consider making x_i ordered measurements with $i = 0, 1, \ldots, 2^3$. Then the analysis just conducted could be performed again with $\mathbf{h}$ in direction of ψ_l^2 to satisfy the demand from situation 2. This ensures that $(m_i)_\psi$ is always non-zero for situation 2.

Situation 3 is illustrated by $\mathbf{h}$ being in direction of both ψ_l^2 and ψ_l^3 in figure 7.2.1 Case I. We observe that both integral value becomes zero for integration over ψ_l^2 and ψ_l^3. This is also be valid for a more general situation as long as the measurements are taken in an ordered way. And we apply the demands from situation 3.

It is hard to give the exact value of the vector norm both in direction of ϕ and in direction of ψ_l^j. But by using (4.1.1) it is clear that:

$$S_\phi > 0, \tag{7.2.7}$$

$$S_{\psi_l^j} = \begin{cases} > 0, & 0 \leq j < L, \\ 0, & j \geq L. \end{cases} \tag{7.2.8}$$

To analyze the non-linearity we utilize (4.1.2). To get insight into how non-linearity depends on the scale we calculate values of $(m_i)_{hh}$ when $\mathbf{h}$ is in direction of ϕ, and ψ_l^j. To do this we analyze equation (7.1.23) for the different basis elements.

In direction of ϕ we still get that $k(x; \mathbf{h}) = 1$, so we obtain the following expression

$$
\begin{aligned}
(m_i)_{\phi\phi} =& \frac{2k^{-1}(\mathbf{c})\Delta_x p(t_{i+1})}{\left[\mu_o + (\mu_w - \mu_o)\, x_{i+1}\right]^3} \left(\mu_o + (\mu_w - \mu_o)\, x_{i+1}\right)^2 \\
&- \frac{2k^{-1}(\mathbf{c})\Delta_x p(t_{i+1})}{\left[\mu_o + (\mu_w - \mu_o)\, x_{i+1}\right]^2} \left(\mu_o + (\mu_w - \mu_o)\, x_{i+1}\right) \\
&- \frac{2k^{-1}(\mathbf{c})\Delta_x p(t_i)}{\left[\mu_o + (\mu_w - \mu_o)\, x_i\right]^3} \left(\mu_o + (\mu_w - \mu_o)\, x_i\right)^2 \\
&+ \frac{2k^{-1}(\mathbf{c})\Delta_x p(t_i)}{\left[\mu_o + (\mu_w - \mu_o)\, x_i\right]^2} \left(\mu_o + (\mu_w - \mu_o)\, x_i\right),
\end{aligned}
\tag{7.2.9}
$$

cancellation of terms and factorization gives

$$
\begin{aligned}
(m_i)_{\phi\phi} =& \frac{2k^{-1}(\mathbf{c})\Delta_x p(t_{i+1})}{\left[\mu_o + (\mu_w - \mu_o)\, x_{i+1}\right]} (1 - 1) \\
&- \frac{2k^{-1}(\mathbf{c})\Delta_x p(t_i)}{\left[\mu_o + (\mu_w - \mu_o)\, x_i\right]} (1 - 1),
\end{aligned}
\tag{7.2.10}
$$

which leads to

$$
(m_i)_{\phi\phi} = 0.
\tag{7.2.11}
$$

When evaluation (7.1.23) in direction of ψ we observe that $k(x; \mathbf{h}) \neq 1$ and thus the integrals take different values. To find an expression for $(m_i)_{\psi_l^j \psi_l^j}$ we need to analyze the integrals

$$
\int_0^1 k(x; \mathbf{h})\, dx,
\tag{7.2.12}
$$

$$
\int_0^1 k^2(x; \mathbf{h})\, dx,
\tag{7.2.13}
$$

$$
\int_{x_i}^1 k(x; \mathbf{h})\, dx,
\tag{7.2.14}
$$

$$
\int_{x_i}^1 k^2(x; \mathbf{h})\, dx,
\tag{7.2.15}
$$

$$
\int_{x_{i+1}}^1 k(x; \mathbf{h})\, dx,
\tag{7.2.16}
$$

$$
\int_{x_{i+1}}^1 k^2(x; \mathbf{h})\, dx.
\tag{7.2.17}
$$

We instantly recognize integral (7.2.12), (7.2.14) and (7.2.16) from the case with the first derivative. They act similar, and we do not need to analyze

them any further. Integral (7.2.13), (7.2.15), and (7.2.17) are new. But since
the integrand is squared it is clear that the integral value will never become
zero. We do not calculate the exact vector norm but using equation (4.1.2) we
get that

$$\kappa_\phi = 0, \tag{7.2.18}$$

$$\kappa_{\psi_l^j} = \begin{cases} > 0, & 0 \leq j < L, \\ \infty, & j \geq L. \end{cases} \tag{7.2.19}$$

7.2.1.2   Non-ordered measurements

We now investigate what happens when the measurements of flow is taken at
random intervals. The fronts positions $z(t_i)$ and $z(t_{i+1})$ can still be written
as x_i and x_{i+1}, but now these points does not have a structured placement,
as in the previous case. We still have x_i observations with $i = 0, 1, 2, \ldots, 2^L$.
In figure 7.2.1 case II we see one example of how the measurements can be
placed. The sensitivity and non-linearity is analyzed in the same manner as
for the ordered measurements. That is we analyze the equations (7.1.22) and
(7.1.23) in direction of the different basis elements ϕ and ψ_l^j.

When $\mathbf{h}$ is in direction of ϕ we have $k(x; \mathbf{h}) = 1$. We thus obtain the same
expression for $(m_i)_\phi$ as for ordered measurements. The value is on the other
hand not the same since the points x_i and x_{i+1} are different for the two cases.

To find the derivative in ψ_l^j-direction we use equation (7.1.22). For the same
reasons as for ordered measurements we simplify the equation by setting

$$\int_0^1 k(x; \mathbf{h}) \, dx = 0. \tag{7.2.20}$$

Now we must evaluate the integral

$$\int_{x_{i+1}}^1 k(x; \mathbf{h}) \, dx, \tag{7.2.21}$$

and

$$\int_{x_i}^1 k(x; \mathbf{h}) \, dx. \tag{7.2.22}$$

For ordered measurements we performed our analysis by looking at three dif-
ferent situations, each corresponding to a different relationship between the
measurement points and the support of the analyzed basis element. For non-
ordered measurements, the distance between two measurement point is not
constant, hence we need another approach to the analysis. From the example
of measurement placement in figure 7.2.1 Case II we can make some observa-
tions.

It is obvious that when we integrate over a basis element ψ_l^j and the integration limits x_{i+1} and x_i align with the start-points of $supp\,\psi_{i+1}^L$ and $supp\,\psi_i^L$ the value of the integral and, $S_{\psi_l^j}$, is zero. From figure 7.2.1 Case II we see that x_{i+1} and x_i does not align for non-ordered measurement. This scenario can be expected for any general placement of non-ordered measurement. Hence we have a value greater than zero for the case with $j = L$.

When $j < L$ the support of each basis element grows. By looking at figure 7.2.1 we can imagine a different placement of the measurements that allowed some of the measurement point to aligned with the support of a basis element. But since we have x_i measurements, and $i = 0, 1, 2, \ldots, 2^L$ it is guaranteed that some measurement point will not align with the support of the basis elements. This means that the integral values is greater than zero, for some of the measurement points.

To find the point where the integrals become zero we need to let $j > L$. If we forget the specific example given in figure 7.2.1 Case II and think of a general case of randomly placed measurements, we see that there must exists for each x_i a unique $J > L$, such that the start-point of $supp\,\psi_i^J$ aligns with x_i. This means that one of the integrals are zero, further we observe that there exists a universal $K \geq J$ such that all the x_i aligns with a start point of $supp\,\psi_i^K$. We summarize this in

$$S_\phi > 0, \tag{7.2.23}$$

$$S_{\psi_l^j} = \begin{cases} > 0, & 0 \leq j < L, \\ > 0, & L \leq j < K \,, \\ 0, & j \geq K. \end{cases} \tag{7.2.24}$$

For the analysis of non-linearity we employ equation (7.1.23). In direction of ϕ the expression is the same as for ordered measurements, that is

$$(m_i)_{\phi\phi} = 0. \tag{7.2.25}$$

To find the expression for $(m_i)_{\psi\psi}$ we need to analyze the same integrals as for the ordered measurements. Integral (7.2.12), (7.2.14) and (7.2.16) can be recognized from the expression of the first derivative, and obtains the same values for both cases. The integrals (7.2.13), (7.2.15), and (7.2.17) never becomes zero since the integrand is squared. We will not find exact values of the vector norm in this case, but by using (4.1.2) it is clear that

$$\kappa_\phi = 0, \tag{7.2.26}$$

$$\kappa_{\psi_l^j} = \begin{cases} > 0, & 0 \leq j < L, \\ > 0, & L \leq j < K, \\ \infty, & j \geq K. \end{cases} \tag{7.2.27}$$

7.2.2   Non-piston displacement

We now investigate the case of non-piston displacement. Water is still injected to displace the oil, but instead of a surface separating the two fluids we get a two-phase zone. To analyze the SNS interrelation in this case we use equations (4.1.1) as a measure of sensitivity in **h**-direction, and (4.1.2) as a measure of non-linearity in **h**-direction. In section 7.1.2 we found expressions for $(m_i)_h$ and $(m_i)_{hh}$ that were valid for a case with non-piston displacement. To analyze the effect scale has on sensitivity and non-linearity we let **h** correspond to different Haar-basis elements.

To make things simple we assume that we have measured the flow velocity in such a manner that $z_{o,i}$ is perfectly aligned with the points x_i for $i = 0, 1, 2, \ldots, 2^L$.

We start the analysis by looking at the sensitivity and non-linearity in direction of ϕ. We use equation (7.1.43) and let $k(x; \mathbf{h}) = 1$ this gives

$$
\begin{aligned}
(m_i)_\phi = & \frac{\Delta_x p(t_{i+1})}{\left[\mu_o + (\mu_w - \mu_o)\, z_{o,i+1} + \left(\lambda^{-1} - \mu_w\right) \delta_{i+1}\right]^2} \\
& \times \left\{\mu_o + (\mu_w - \mu_o)\, z_{o,i+1} + \left(\lambda^{-1} - \mu_w\right) \delta_{i+1}\right\} \\
& - \frac{\Delta_x p(t_i)}{\left[\mu_o + (\mu_w - \mu_o)\, z_{o,i} + \left(\lambda^{-1} - \mu_w\right) \delta_i\right]^2} \\
& \times \left\{\mu_o + (\mu_w - \mu_o)\, z_{o,i} + \left(\lambda^{-1} - \mu_w\right) \delta_i\right\},
\end{aligned}
\tag{7.2.28}
$$

with $\delta_i = z_{o,i} - z_{w,i}$, and $\delta_{i+1} = z_{o,i+1} - z_{w,i+1}$ being the width of the two-phase zone at two different time. This simplifies to

$$
\begin{aligned}
(m_i)_\phi = & \frac{\Delta_x p(t_{i+1})}{\left[\mu_o + (\mu_w - \mu_o)\, z_{o,i+1} + \left(\lambda^{-1} - \mu_w\right) \delta_{i+1}\right]} \\
& - \frac{\Delta_x p(t_i)}{\left[\mu_o + (\mu_w - \mu_o)\, z_{o,i} + \left(\lambda^{-1} - \mu_w\right) \delta_i\right]}.
\end{aligned}
\tag{7.2.29}
$$

Hence we can at once establish, independent of the width of the two-phase zone.

$$
S_\phi > 0.
\tag{7.2.30}
$$

For the non-linearity when **h** is in the direction of ϕ we use (7.1.44), and let

$$k(x; \mathbf{c}) = 1$$

$$
\begin{aligned}
(m_i)_{\phi\phi} =& \frac{2k^{-1}(\mathbf{c})\Delta_x p(t_{i+1})}{\left[\mu_o + (\mu_w - \mu_o)\, z_{o,i+1} + (\lambda^{-1} - \mu_w)\, \delta_{i+1}\right]^3} \\
& \times \left\{\mu_o + (\mu_w - \mu_o)\, z_{o,i+1} + \left(\lambda^{-1} - \mu_w\right)\delta_{i+1}\right\}^2 \\
& - \frac{2k^{-1}(\mathbf{c})\Delta_x p(t_{i+1})}{\left[\mu_o + (\mu_w - \mu_o)\, z_{o,i+1} + (\lambda^{-1} - \mu_w)\, \delta_{i+1}\right]^2} \\
& \times \left\{\mu_o + (\mu_w - \mu_o)\, z_{o,i+1} + \left(\lambda^{-1} - \mu_w\right)\delta_{i+1}\right\} \\
& - \frac{2k^{-1}(\mathbf{c})\Delta_x p(t_i)}{\left[\mu_o + (\mu_w - \mu_o)\, z_{o,i} + (\lambda^{-1} - \mu_w)\, \delta_i\right]^3} \\
& \times \left\{\mu_o + (\mu_w - \mu_o)\, z_{o,i} + \left(\lambda^{-1} - \mu_w\right)\delta_i\right\}^2 \\
& + \frac{2k^{-1}(\mathbf{c})\Delta_x p(t_i)}{\left[\mu_o + (\mu_w - \mu_o)\, z_{o,i} + (\lambda^{-1} - \mu_w)\, \delta_i\right]^2} \\
& \times \left\{\mu_o + (\mu_w - \mu_o)\, z_{o,i} + \left(\lambda^{-1} - \mu_w\right)\delta_i\right\}.
\end{aligned}
\tag{7.2.31}
$$

Cancellation of terms gives

$$
\begin{aligned}
(m_i)_{\phi\phi} =& \frac{2k^{-1}(\mathbf{c})\Delta_x p(t_{i+1})}{\left[\mu_o + (\mu_w - \mu_o)\, z_{o,i+1} + (\lambda^{-1} - \mu_w)\, \delta_{i+1}\right]} \times (1 - 1) \\
& - \frac{2k^{-1}(\mathbf{c})\Delta_x p(t_i)}{\left[\mu_o + (\mu_w - \mu_o)\, z_{o,i} + (\lambda^{-1} - \mu_w)\, \delta_i\right]} \times (1 - 1).
\end{aligned}
\tag{7.2.32}
$$

We see that

$$(m_i)_{\phi\phi} = 0. \tag{7.2.33}$$

This result is identical to the result obtained for piston displacement. We conclude by using (4.1.2) that

$$\kappa_\phi = 0. \tag{7.2.34}$$

Now if $\mathbf{h}$ is in direction of ψ_l^j we see that $k(x; \mathbf{h}) \neq 1$, and hence the integral values is different. Remembering that the properties of the Haar-basis wavelet gives

$$\int_0^1 k(x; \mathbf{h})\, dx = 0. \tag{7.2.35}$$

We still use (7.1.43) to get the first derivative in direction of ψ_l^j, hence we get

$$
\begin{aligned}
(m_i)_{\psi_l^j} = {} & \frac{\Delta_x p(t_{i+1}) k^{-1}(\mathbf{c})}{\left[\mu_o + (\mu_w - \mu_o) z_{o,i+1} + (\lambda^{-1} - \mu_w) f_{i+1}\right]^2} \\
& \times \left\{ (\mu_o - \mu_w) \int_{z_{o,i+1}}^1 k(x; \mathbf{h})\, dx + \left(\lambda^{-1} - \mu_w\right) \int_{z_{w,i+1}}^{z_{o,i+1}} k(x; \mathbf{h})\, dx \right\} \\
& - \frac{\Delta_x p(t_i) k^{-1}(\mathbf{c})}{\left[\mu_o + (\mu_w - \mu_o) z_{o,i} + (\lambda^{-1} - \mu_w) f_i\right]^2} \\
& \times \left\{ (\mu_o - \mu_w) \int_{z_{o,i}}^1 k(x; \mathbf{h})\, dx + \left(\lambda^{-1} - \mu_w\right) \int_{z_{w,i}}^{z_{o,i}} k(x; \mathbf{h})\, dx \right\}.
\end{aligned}
$$
(7.2.36)

To determine how this expression depends on the scale value j, we must analyze the integrals

$$
\int_{z_{o,i+1}}^1 k(x; \mathbf{h})\, dx,
\tag{7.2.37}
$$

$$
\int_{z_{o,i}}^1 k(x; \mathbf{h})\, dx,
\tag{7.2.38}
$$

$$
\int_{z_{w,i+1}}^{z_{o,i+1}} k(x; \mathbf{h})\, dx,
\tag{7.2.39}
$$

$$
\int_{z_{w,i}}^{z_{o,i}} k(x; \mathbf{h})\, dx.
\tag{7.2.40}
$$

We recognize integral (7.2.37), and integral (7.2.38) from our analysis of piston displacement. It is clear that these two integrals produces the same values for non-piston displacement, as for piston displacement. The effect of the two-phase zone are found in integral (7.2.39) and integral (7.2.40). This is explicitly shown as the integration limits of the two integrals depend on the shape and size of the two-phase zone.

Instead of analyzing the sensitivity directly we derive an equation for $(m_i)_{\psi_l^j \psi_l^j}$. This is done because we suspect that some of the integrals in this expression might also depend on the shape and size of the two-phase zone. To avoid saying thing twice, we derive all the equations before we start our analysis. Remembering that for $\mathbf{h}$ in direction of ψ_l^j we have

$$
\int_0^1 k(x; \mathbf{h})\, dx = 0.
\tag{7.2.41}
$$

This gives us

$$
\begin{aligned}
(m_i)_{\psi\psi} =& \frac{2k^{-1}(\mathbf{c})\Delta_x p(t_{i+1})}{\left[\mu_o + (\mu_w - \mu_o)\, z_{o,i+1} + \left(\lambda^{-1} - \mu_w\right) f_{i+1}\right]^3} \\
& \times \left\{ (\mu_o - \mu_w) \int_{z_{o,i+1}}^{1} k(x;\mathbf{h})\, dx + \left(\lambda^{-1} - \mu_w\right) \int_{z_{w,i+1}}^{z_{o,i+1}} k(x;\mathbf{h})\, dx \right\}^2 \\
& - \frac{2k^{-1}(\mathbf{c})\Delta_x p(t_{i+1})}{\left[\mu_o + (\mu_w - \mu_o)\, z_{o,i+1} + \left(\lambda^{-1} - \mu_w\right) f_{i+1}\right]^2} \\
& \times \left\{ (\mu_o - \mu_w) \int_{z_{o,i+1}}^{1} k^2(x;\mathbf{h})\, dx + \left(\lambda^{-1} - \mu_w\right) \int_{z_{w,i+1}}^{z_{o,i+1}} k^2(x;\mathbf{h})\, dx \right\} \\
& - \frac{2k^{-1}(\mathbf{c})\Delta_x p(t_i)}{\left[\mu_o + (\mu_w - \mu_o)\, z_{o,i} + \left(\lambda^{-1} - \mu_w\right) f_i\right]^3} \\
& \times \left\{ (\mu_o - \mu_w) \int_{z_{o,i}}^{1} k(x;\mathbf{h})\, dx + \left(\lambda^{-1} - \mu_w\right) \int_{z_{w,i}}^{z_{o,i}} k(x;\mathbf{h})\, dx \right\}^2 \\
& + \frac{2k^{-1}(\mathbf{c})\Delta_x p(t_i)}{\left[\mu_o + (\mu_w - \mu_o)\, z_{o,i} + \left(\lambda^{-1} - \mu_w\right) f_i\right]^2} \\
& \times \left\{ (\mu_o - \mu_w) \int_{z_{o,i}}^{1} k^2(x;\mathbf{h})\, dx + \left(\lambda^{-1} - \mu_w\right) \int_{z_{w,i}}^{z_{o,i}} k^2(x;\mathbf{h})\, dx \right\}.
\end{aligned}
$$
$$(7.2.42)$$

We recognize integral (7.2.37) and integral (7.2.38) which has already been analyzed. We also recognize integral (7.2.39) and integral (7.2.40) which will be analyzed soon. The remaining integrals are

$$\int_{z_{o,i+1}}^{1} k^2(x;\mathbf{h})\, dx \tag{7.2.43}$$

$$\int_{z_{w,i+1}}^{z_{o,i+1}} k^2(x;\mathbf{h})\, dx \tag{7.2.44}$$

$$\int_{z_{o,i}}^{1} k^2(x;\mathbf{h})\, dx \tag{7.2.45}$$

$$\int_{z_{w,i}}^{z_{o,i}} k^2(x;\mathbf{h})\, dx \tag{7.2.46}$$

These have all squared integrands, and is thus never zero. This means that regardless of how we analyze the integral (7.2.39) and integral (7.2.40) , we get

$$(m_i)_{\psi_l^j \psi_l^j} \neq 0 \quad \forall j. \tag{7.2.47}$$

The difference between piston displacement and non-piston displacement is now governed by how the integral

$$\int_{z_{w,i+1}}^{z_{o,i+1}} k(x;\mathbf{h})\, dx, \tag{7.2.48}$$

and

$$\int_{z_{w,i}}^{z_{o,i}} k(x; \mathbf{h}) \, dx, \tag{7.2.49}$$

will behave as $\mathbf{h}$ is in direction of ψ_l^j and the scale index j varies. To analyze the integrals we observe that the limits of integration, and hence the value of the integral depend on the shape and size of the two-phase zone. We therefore divide our analysis of these two integrals into three different cases.

1. Width of the two-phase zone is narrower than the distance the fluid fronts moves between two measurements.

2. Width of the two-phase zone is exactly the distance the fluid fronts moves between two measurements.

3. Width of the two-phase zone is greater than the distance the fluid front moves between two measurements.

These cases are illustrated in figure 7.2.2.

7.2.2.1   Case 1

We assume that the width of the two-phase zone is smaller than the distance the two-phase zone moves between two observations. For simplicity we let

$$z_{o,i+1} - z_{w,i+1} = z_{o,i} - z_{w,i} = \frac{(z_{o,i+1} - z_{o,i})}{2}.$$

We observe that integral (7.2.48) and (7.2.49) first becomes zero as $j > L$. This is because the width of the two-phase zone is less then the width between to measurement point. To ensure that the integral is zero we need to integrate over a basis element with narrower support than ψ_l^L has. This is illustrated in figure 7.2.2 Case I. We chose to make our measurements in such a way that the oil front z_o was aligned with the points x_i. As a result of this the integral (7.2.37) and (7.2.38) behave as for ordered measurements in piston displacement. We do not calculate the exact vector norm, but using (4.1.1), and keeping the results obtained for integral (7.2.37) and (7.2.38) in mind we get

$$S_{\psi_l^j} = \begin{cases} > 0, & 0 \le j < L, \\ > 0, & j = L, \\ 0, & j > L. \end{cases} \tag{7.2.50}$$

and by (4.1.2)

$$\kappa_{\psi_l^j} = \begin{cases} > 0, & 0 \le j < L, \\ > 0, & j = L, \\ \infty, & j > L. \end{cases} \tag{7.2.51}$$
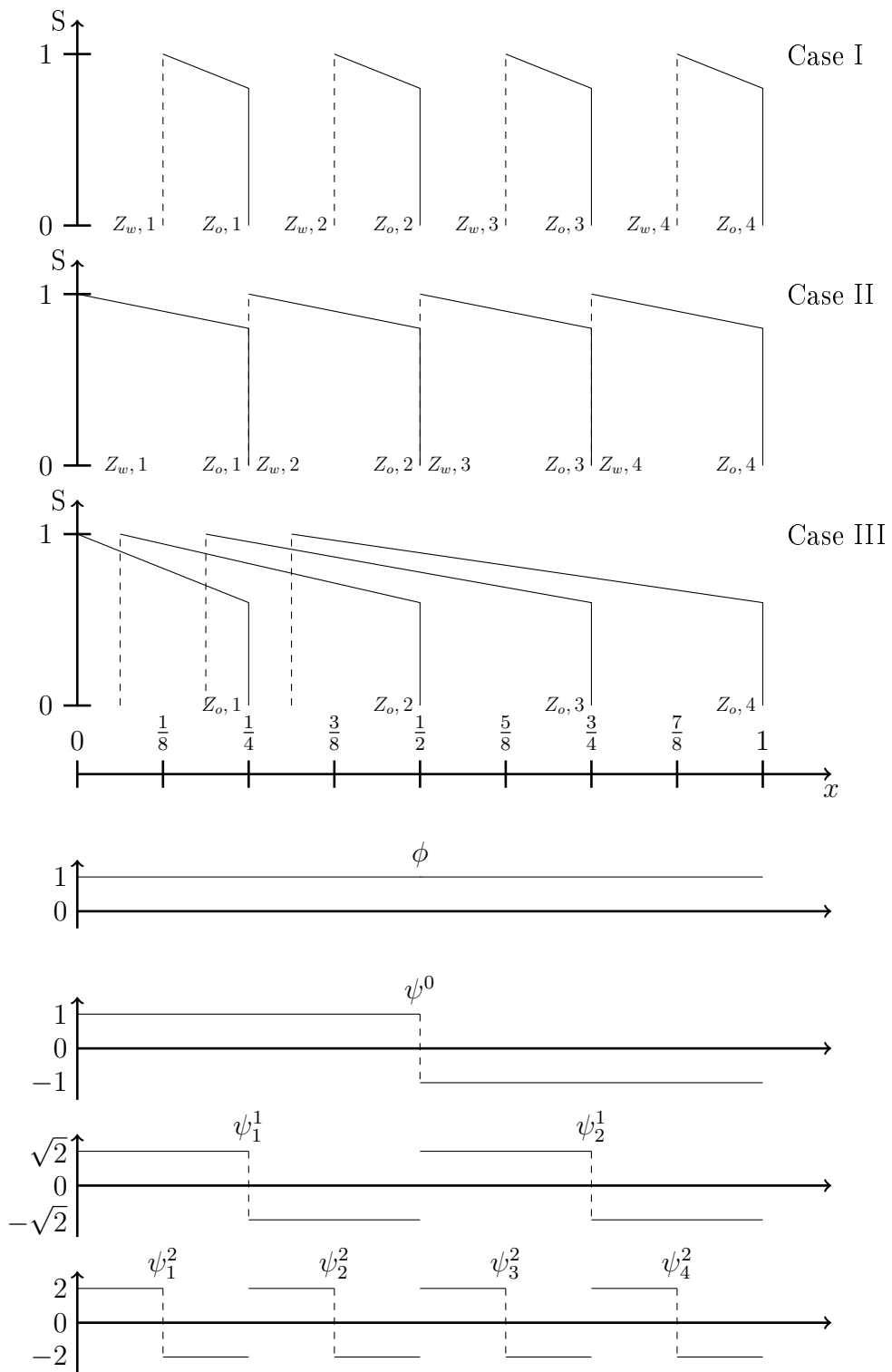
Figure 7.2.2: Elements of Haar basis, and water saturation for three different cases.

7.2.2.2 Case 2

We assume that the width of the two-phase zone is exactly the distance the two-phase zone moves between two observations. That is

$$z_{o,i+1} - z_{w,i+1} = z_{o,i} - z_{w,i} = z_{o,i+1} - z_{o,i}.$$

This is illustrated in figure 7.2.2 Case II. Now we see that integral (7.2.39) and (7.2.40) becomes zero for the same scale index as the integrals (7.2.37), and (7.2.38). This is because the width of the two phase zone in this case is just as wide as the support of basis element ψ_l^L. We still do not calculate the exact vector norm, but by (4.1.1) we get

$$S_{\psi_l^j} = \begin{cases} > 0 & 0 \le j < L \\ 0 & j \ge L \end{cases} \tag{7.2.52}$$

and by (4.1.2)

$$\kappa_{\psi_l^j} = \begin{cases} > 0 & 0 \le j < L \\ \infty & j \ge L. \end{cases} \tag{7.2.53}$$

7.2.2.3 Case 3

We now assume that the width of our two-phase zone is larger than the distance the fluid fronts move between two observations. We assumed that our measurements were taken in such a way that $z_{o,i}$ was perfectly aligned with the points x_i. Because of these assumptions we observe that the two-phase zone cannot have constant width since the maximum possible width would be the distance between the injection point x_0 and the first measurement point x_1. This case was analyzed under Case 2.

When the two-phase zone is not constant, we might have a situation like the one illustrated for Case III in figure 7.2.2. We see that $z_{w,i}$ is not aligned with the measurement point, and hence not aligned with the support of the basis functions in scale $j = L$. This situation is somewhat similar to the one analyzed for non-ordered measurement points in section 7.2.1.2 since the left limit of integration is non-ordered and the right is fixed. The result is therefore similar. We stress that the values of integral (7.2.37) and (7.2.38) is not affected by this since they depend on the position of z_o which is still positioned in an ordered fashion. As for case 1 and case 2 we do not calculate the exact vector norm, but by (4.1.1)

$$S_{\psi_l^j} = \begin{cases} > 0, & 0 \le j < L, \\ > 0, & L \le j < K, \\ 0, & j \ge K. \end{cases} \tag{7.2.54}$$

for a universal K, that ensures the alignment of $z_{w,i}$ with the start of basis element ψ_l^K. Using the expression for $(m_i)_{\psi\psi}$ and (4.1.2)

$$\kappa_{\psi_l^j} = \begin{cases} > 0, & 0 \leq j < L, \\ > 0, & L \leq j < K, \\ \infty, & j \geq K. \end{cases} \qquad (7.2.55)$$

7.3 Summary and Conclusions

In this chapter we have investigated the SNS structure of two-phase flow during water flooding of a petroleum reservoir. This was done by following the general approach presented in section 4.2. We realized that the flooding could happen in two different ways which needed to be analyzed separately.

- The surface separating intruding water and displaced oil had zero thickness.

- There exists a zone containing both water and oil separating the intruding water from the displaced oil.

For both cases we assumed that we had $i = 0, 1, 2, \ldots 2^L$ observations. And that the fluid fronts position was related to equidistantly spaced points x_i.

We first comment the results from the first scenario, that is, when the surface separating water and oil had zero thickness. In the analysis we looked at ordered and non-ordered measurement points.
For the **ordered measurements** we were able to estimate the sensitivity S given in (7.2.7) and (7.2.8) , we were also able to estimate the non-linearity κ given in (7.2.18) and (7.2.19). From this we observed that there is a change from positive values of sensitivities to zero values. There is a corresponding change from finite, to infinite values of the non-linearity. The change happens when the scale index j of the basis element ψ_l^j becomes equal or higher than the measurement index L. When this happens the support of basis elements with that scale index is equal to distance between the measurement points, and the integration values equals zero.
For **non-ordered measurement** the estimates of sensitivity S are given in (7.2.23) and (7.2.24). Estimates of κ are given by (7.2.26) and (7.2.27). For this case the sensitivity goes to zero, and the non-linearity goes to infinity at a scale index $K > L$. This is due to the ordered placement of the basis elements, and the non-ordered placement of measurements. We need to go to a higher scale index in order to ensure that the integration limits is at the intersection

between two basis elements. Even though we need to have scale index K in order to ensure that the sensitivity is zero, we would expect the vector norm in direction of basis elements with scale index between L, and K to have small values. This is because the limits of integration almost match the intersection between basis elements. In this case we do not expect a sudden drop from positive to zero values for the sensitivity, but a more gradual transition towards zero.

In the second scenario, that is when there existed a two-phase zone between the intruding water and the displaced oil. Our equations were somewhat different. This called for a separate analysis of the problem. An expression for $(m_i)_h$ and $(m_i)_{hh}$ was found. The analysis was based on letting $\mathbf{h}$ take values corresponding to different Haar-basis elements. During this we found that the shape and size of the two-phase zone was important for the results in direction of the non-constant Haar basis elements. For the constant basis estimates for sensitivity was given by (7.2.30) and estimates for κ by (7.2.34). For the non-constant basis elements we divided the analysis into three parts.

- The two-phase zone is narrower than the distance the two-phase zone moves between two measurements.

- The two-phase zone is exactly as wide as the distance it moves between two measurements.

- The two-phase zone is wider than the distance it moves between two measurements.

For the first case, sensitivity estimates were given by (7.2.50), and estimates for κ were given by (7.2.51). From this we see that when the two-phase zone is narrow, the sensitivity does not become zero at the scale index L. Instead we have to go to a scale index $j > L$ before the value becomes zero. How high of a scale index we need depends on the width of the two-phase zone. A narrow two-phase zone needs a higher scale index in order to guarantee that the sensitivity S becomes zero.

For the second case, sensitivity estimates were given by (7.2.52), and estimates for κ were given by (7.2.53). We see that this is the same structure as for piston displacement with ordered measurements. This is because such a wide two-phase zone will more easily be covered by the support of a basis-element at scale index L.

For the third case, estimates for sensitivity were given by (7.2.54), and estimates for κ were given by (7.2.55). This situation lead to a result similar to the one for non-ordered measurement points with zero two-phase zone. This

means that we need to go to a scale index $K > L$ to ensure that the sensitivity is zero.

In order to relate this to a real world scenario we must think about which of the different cases that are most realistic. In a real world petroleum reservoir we always have a two-phase zone separating the injected water and the displaced oil. Compared to the distance between wells the two phase zone will most likely be small. Assuming that measurements are taken with some time-interval we see that the case with a narrow two-phase zone will be most realistic for this case. We assume that we have no information about the position of the two-phase zone. It is therefore unlikely that we are able to align the front with any equidistantly spaced point x_i. Even though it has not been analyzed, it is obvious that our results from the analysis of non-ordered measurement points for piston displacement will carry over to this case. Based on this we do expect a SNS relationship for a real world case, but we do not expect to observe a specific scale index where the sensitivity drops to zero, and non-linearity rises to infinity. We instead expect the sensitivity to gradually decrease, and the non-linearity to gradually increase as the scale index rises. Hence indicating the existence of a SNS relationship for estimation of permeability from measurements of flow.

Chapter 8

Non-Constant Permeability

In chapter 6 and 7 we investigated the interrelation between sensitivity, non-linearity, and scale for the inverse problem of identifying the permeability in a petroleum reservoir from observations of fluid production rates. This was done by analyzing the equation for fluid flow. We assumed that the flow was constant in the spatial direction, incompressible, and with constant viscosity μ. We also assumed that we only had flow in one spatial dimension, and that the permeability field $k(x; \mathbf{c})$ was constant for the whole reservoir.

For any real petroleum reservoirs the permeability is never constant in the whole field. In this chapter we investigate some of the effects a non-constant permeability field might have on the interrelation between sensitivity and scale. We will not look into the effects on non-linearity. This is because of the way we define sensitivity S_h, non-linearity κ_h along a unit vector $\mathbf{h}$ in parameter space

$$S_h = \|(\mathbf{m})_h\|, \tag{8.0.1}$$

$$\kappa_h = \frac{\|(\mathbf{m})_{hh}\|}{\|(\mathbf{m})_h\|^2}. \tag{8.0.2}$$

Since we are interested in finding out when S_h goes to zero, we can see that this coincides with the non-linearity going to infinity as long as $(\mathbf{m})_{hh}$ is finite. The results from the analysis in chapter 6 and 7 suggest that the non-linearity is finite. Taking this into account, we only investigate the non-constant permeability fields effect on the sensitivity.

8.1   Effects of non-constant permeability

In the analysis of water-flooding a 1-D petroleum reservoir, and we found expressions for the sensitivities. We looked at how the sensitivity values changed with scale. This was done for different flooding scenarios that lead to different expressions for the sensitivities. For all these expressions $k(x; \mathbf{c})$ was included as a factor in many of the terms. This can be seen in equations (6.1.13) for one phase flow, and in equations (A.1.23) and (A.1.63) for the two-phase flow.

For chapter 6 and chapter 7 we assumed constant permeability $k(x; \mathbf{c}) = k(\mathbf{c})$, we hence put $k(\mathbf{c})$ outside the all integrals. The value of sensitivity was determined by integrals over $k(x; \mathbf{h})$ and by letting $\mathbf{h}$ be in direction of different Haar wavelets we could investigate the SNS structure. To gain understanding of the effects of a non-constant permeability field we need to investigate the integrals that were simplified by the assumption $k(x; \mathbf{c}) = k(\mathbf{c})$.

From equations (6.1.13) , (A.1.23), and (A.1.63) we find three integrals we want to investigate further:

- $I_1 = \int_0^1 k(x; \mathbf{c})^{-2} \cdot k(x; \mathbf{h}) \, dx$

- $I_2 = \int_{x_i}^1 k(x; \mathbf{c})^{-2} \cdot k(x; \mathbf{h}) \, dx$

- $I_3 = \int_{x_{w,i}}^{x_{o,i}} k(x; \mathbf{c})^{-2} \cdot k(x; \mathbf{h}) \, dx$

We observe that the integrand in these three expressions are the same. The only difference is the limits of integration.

8.1.1   Representation of $k(x; \mathbf{c})$ and $k(x; \mathbf{h})$

In section 6.2 and 7.2 we used the Haar-basis to represent $k(x; \mathbf{h})$. We would therefore like to analyze how a non-constant $k(x; \mathbf{c})$ affect a general Haar-basis element. One of the reasons for choosing the Haar basis was the belief that permeability can be expressed as piecewise constant functions. In the following we would like to keep the analysis as simples as possible, without losing important features. In order to keep things simple we only look at the influence $k(x; \mathbf{c})$ has on a single general basis element. The best way of obtaining information about the effect is to calculate the integrals I_1, I_2, and I_3. This calculation will be performed by a numerical scheme. To avoid problems with the numerical method we would like to work with a continuous integrand.

To obtain this while we avoid losing the important oscillatory features we will approximate one Haar basis element by the continuous function.

$$k(x; \mathbf{h}) = sin(2\pi x), \qquad x \in [0, 1]. \tag{8.1.1}$$

We have illustrated the similarity of the Haar basis and $sin(2\pi x)$ in figure 8.1.1.
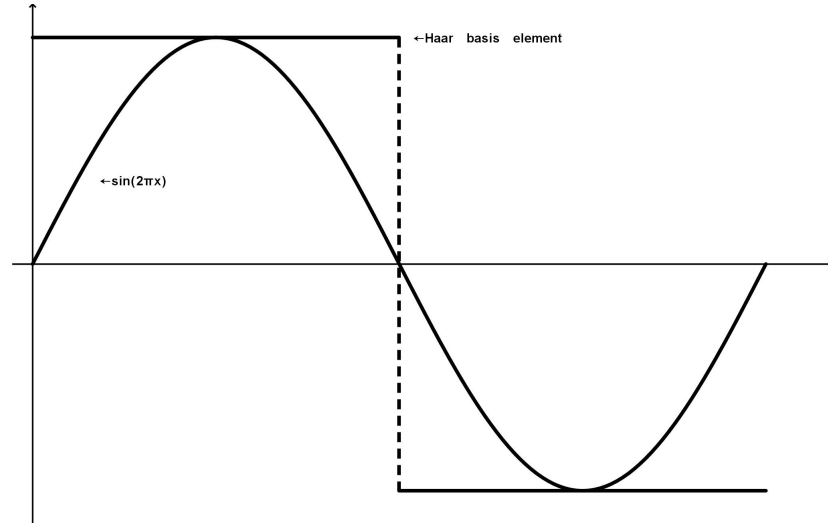
Figure 8.1.1: sin(x) as approximation of one Haar basis element

We also want to represent $k(x; \mathbf{c})$ in a flexible and continuous way. For a real petroleum reservoir the permeability varies through the whole field. This variation can have many different frequencies and amplitudes, and it is not certain that any basis element has the same phase as the permeability. To represent $k(x; \mathbf{c})$ in such a flexible way we let:

$$k(x; \mathbf{c}) = a + b\, sin(2\pi(cx + d)). \tag{8.1.2}$$

When we adjust a we can tune the mean magnitude of the permeability field. By adjusting $b, c,$ and d we vary the amplitude, frequency and phase of the permeability field. Since a real permeability field is never zero we introduce the following condition on the parameters a and b in $k(x; \mathbf{c})$

$$a > b. \tag{8.1.3}$$

With these representations of $k(x; \mathbf{c})$ and $k(x; \mathbf{h})$ the integrand becomes

$$k(x; \mathbf{c})^{-2} \cdot k(x; \mathbf{h}) = [a + b\, sin(2\pi(cx + d))]^{-2} \cdot sin(2\pi x). \tag{8.1.4}$$

8.1.2   Analysis of the integrand

In chapter 7 we saw that the scale dependence in the expressions for sensitivity was in the integrals I_1, I_2, and I_3. We saw that the scale had big impact on the sensitivity value. When the integration limits matched the support of the basis element the integral value became zero. This was done under the before-mentioned assumption that the permeability was constant. To analyze the effects of a non-constant permeability field we must analyze if the numerical value of the integral is still zero when integrating over the whole support of $k(x; \mathbf{h})$ with our new integrand (8.1.4). All three integrals have the same integrand, we thus want to investigate some of the integrands properties before we start to calculate the integrals. First we see how the different representations look like, in figure 8.1.2 we have plotted $k(x; \mathbf{h})$, $k(x; \mathbf{c})^{-2}$, and $k(x; \mathbf{c})^{-2} \cdot k(x; \mathbf{h})$ with $a = 2$, $b = 1.5$, $c = 2$, and $d = 0$.

(a) $k(x; \mathbf{h})$ (b) $k(x; \mathbf{c})^{-2}$ (c) $k(x; \mathbf{c})^{-2} \cdot k(x; \mathbf{h})$
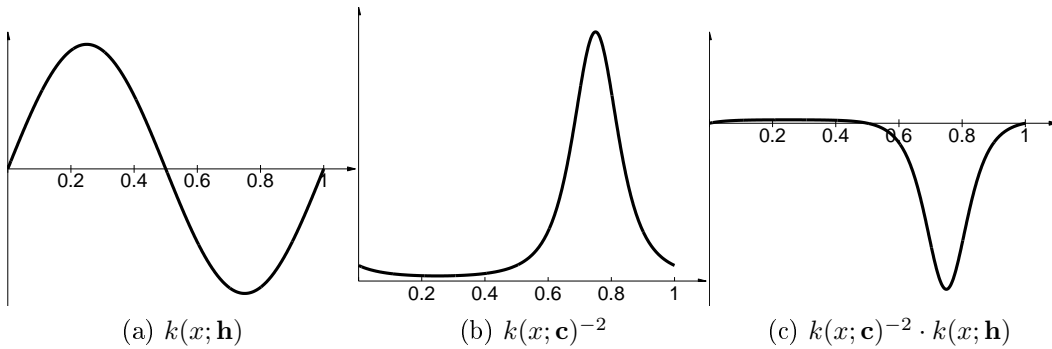
Figure 8.1.2: Approximations of the functions

In figure 8.1.2 we illustrate the two factors of the integrand, and the total integrand for some example values of a, b, c and d. This is an example to illustrate the effect from a non-constant permeability field on integral I_1. The important feature to point out is the negative spike we observe for the integrand illustrated in figure 8.1.2c. Integrating from 0 to 1, the value of that integral would differ from zero because of this negative spike. The reason for the spike is clear when we know that $k(x; \mathbf{h})$ in figure 8.1.2a is multiplied with the $k(x; \mathbf{c})^{-2}$ in figure 8.1.2b. This simple illustration shows an integral that was zero for constant permeability will not become zero in this example. This motivates us to try more cases. To get some more information about the spike in the integrand we analyze the maximum value of it. Choosing a point $x = x'$ such that $k(x'; \mathbf{h})$ is a min or max point. We then adjust c and d in such a manner that $k(x'; \mathbf{c})^{-2}$ is a maxima. Since max/min of the sin function is ± 1 we get

$$\frac{k(x'; \mathbf{h})}{[k(x; \mathbf{c})]^2} = \frac{\pm 1}{[a - b]^2} \tag{8.1.5}$$

We observe that if $a \approx b$ the spike has a high value which lead to a high value for the integral, and probably the largest effect on the SNS structure. This is what we see in fig 8.1.2 where $a = 2$ and $b = 1.5$. If $a \gg b$ the point will still be a maximum point for $k(x; \mathbf{c})^{-2} \cdot k(x; \mathbf{h})$ but the effect will not be as big.

To relate this to a real petroleum reservoir we need to look at what the parameters a, b, c, and d represents. $k(x; \mathbf{c})$ is the representation of the permeability field for the reservoir, the parameter a gives information about the mean permeability value. The parameter b gives information about the amplitude of the permeability variation. A case with $a \approx b$ can be translated to a strongly heterogeneous reservoir, while a case with $a \gg b$ can be translated to a weakly heterogeneous reservoir. The parameter c is the frequency of $k(x; \mathbf{c})$, i.e. how fast the permeability field changes. When $c = 0$ the permeability field does not change at all, thus we have a constant permeability field. By letting the value of c vary, we gain insight into how different permeability fields affect the SNS relationship. The parameter d is the phase shift of $k(x; \mathbf{c})$, that is, the displacement of $k(x; \mathbf{c})$ relative to $k(x; \mathbf{h})$ (which has zero phase shift). In a real permeability field we assume that the field might be displaced relative to the basis element $k(x; \mathbf{h})$. For that reason we test different values of d.

8.2 Numerical analysis of integrals

Now we look at the three integrals presented in section 8.1. We have seen that the integrand depends on the values of a, b, c and d. We assume that the effect of a non-constant permeability field is largest for a reservoir with $a \approx b$. To test this we devise one test with $a \approx b$, and one with $a \gg b$. For each of this we calculate the values of the integral for different values of c and d. We then plot the value of the integrals as a function of c to analyze where the effects of a non-constant $k(x; \mathbf{c})$ is largest. We let $c \in [0, 10]$, and $d \in [0, 0.9]$.

The integrals are calculated using the matlab function `quadgk`. This is the adoptive Gauss-Kronrod quadrature method. This method is the most efficient for high accuracies and oscillatory integrands. For more on this method, we refer the reader to [43].

Since we expect to see bigger effect from cases with $a \approx b$, then from $a \gg b$ we let d go from 0 to 0.9 with increments of 0.1 for the reservoir with $a \approx b$. For the reservoir with $a \gg b$ we let d go from 0 to 0.75 with increments of 0.25. For each subsection we comment on general features of each integral, and the effect a non-constant permeability field has on the SNS structure will then be thoroughly discussed in the summary and conclusion section.

Table 8.1: Parameters for test T_1 and T_2.

	T_1	T_2
a	2	10
b	1.5	1
Range c	$[0, 10]$	$[0, 10]$
Steps c	0.01	0.01
Range d	$[0, 0.9]$	$[0, 0.75]$
Steps d	0.1	0.25

8.2.1   Analysis of I_1

The first integral we analyze is

$$I_1 = \int_0^1 [a + b\,sin(2\pi(cx + d))]^{-2} \cdot sin(2\pi x)\,dx.$$

We denote the value of this integral α_{I_1}, and plot the different values of α_{I_1} as a function of the reservoirs frequency c. We present this plot for all the different values of d. In order to test the difference between a strongly and a weakly heterogeneous reservoir we conceive two tests. The first called T_1 has $a \approx b$, the second called T_2 has $a \gg b$. The parameters for the two tests are summarized in table 8.1.

The results of test T_1 and T_2 are shown in figure 8.2.1 and 8.2.2. We now comment on some features that can highlight the effect a non-constant permeability field has on the SNS structure. For both tests we observe that the integral value α_{I_1} is 0 when the reservoir frequency c is 0. That is, when we have constant permeability, the integral over one basis element equals zero. This result is not surprising when we look at the basis element, but this is the same result obtained in chapter 6 and 7. Hence it builds confidence in the method we apply.

From the graphs we see that both types of reservoirs act similar to different permeability frequencies. The difference we observe is the value of the integrals. From figure 8.2.1, we observe that for T_1 $\max \alpha_{I_1} \approx 0.9$. While we see in figure 8.2.2 that for T_2 $\max \alpha_{I_1} \approx 1 \cdot 10^{-3}$.

From figure 8.2.1 and figure 8.2.2 we observe that the greatest deviations from zero is found in the frequency area $0.5 < c < 2.5$. The exact position depends on the phase d. We note that this is around the frequency of $k(x; \mathbf{h})$ which is $c = 2$. When $c > 2.5$ we observe some small oscillatory deviation from zero, but the amplitude are much smaller. Even though the placement of these local tops depend on the value of d, the general trend is that of dampened oscillation. For the frequencies $c < 0.5$ the value goes rapidly to zero for all the different values of d.
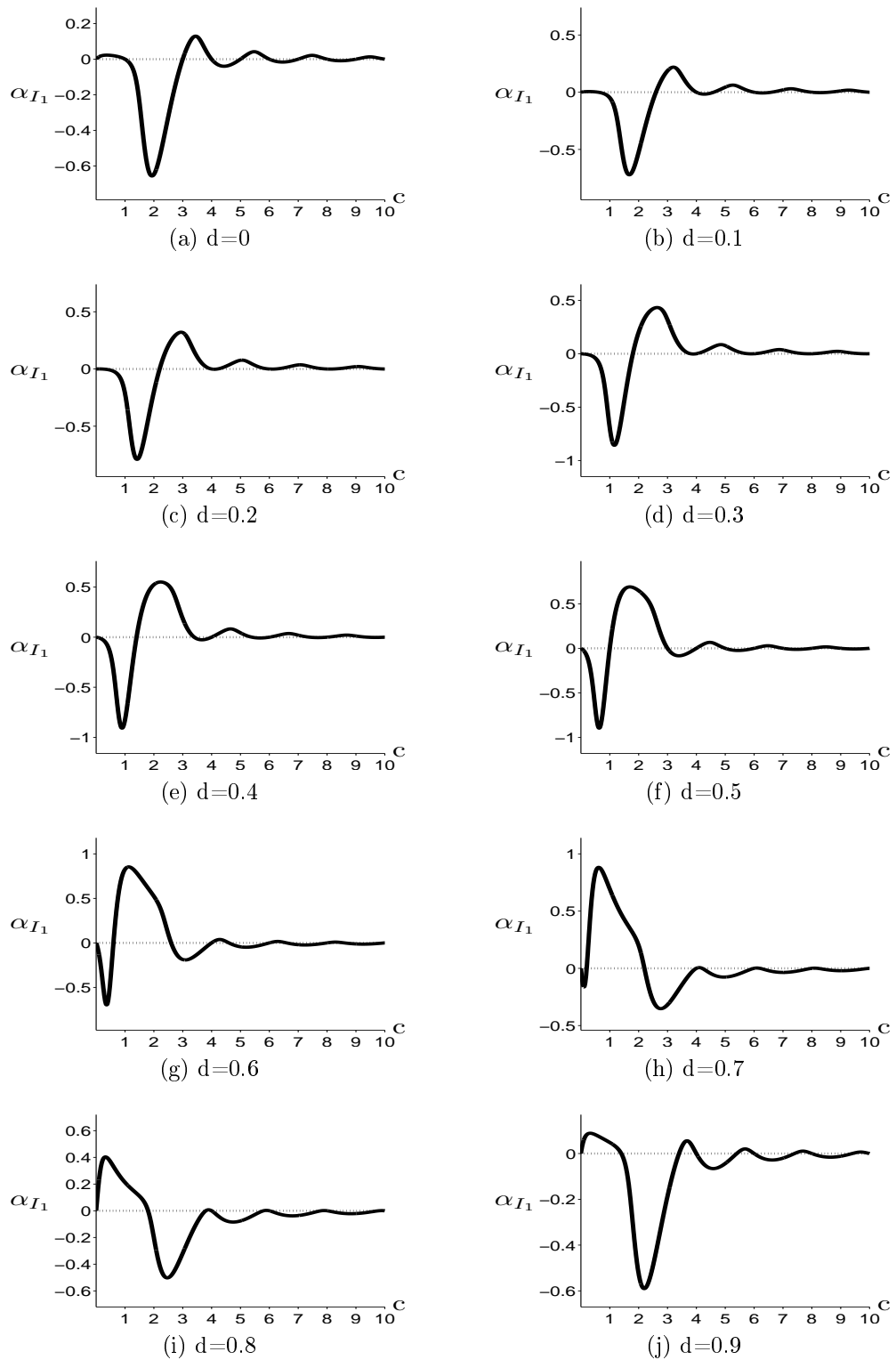
Figure 8.2.1: Test T_1 , value for constant permeability shown by stippled line

(a) d=0

(b) d=0.25

(c) d=0.5

(d) d=0.75
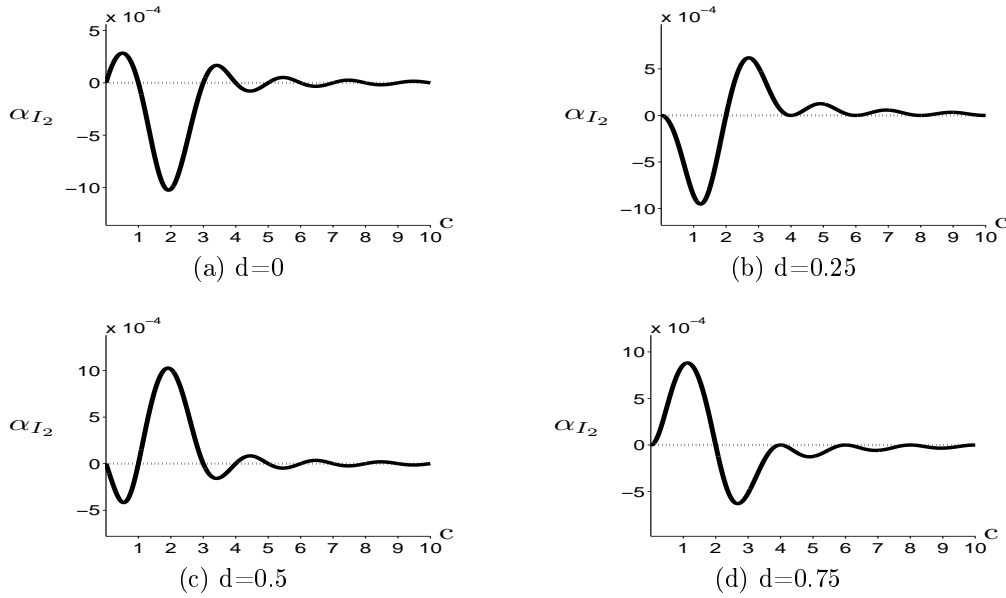
Figure 8.2.2: Test T_2, value for constant permeability shown by stippled line

8.2.2   Analysis of I_2

We now analyze the effect on the integral

$$ I_2 = \int_{x_i}^1 [a + b\,sin(2\pi(cx + d))]^{-2} \cdot sin(2\pi x)\,dx. $$

For this integral there is a dependence on the left limit of integration x_i, in addition to the dependence on $k(x; \mathbf{c})$. To analyze the effect of non-constant permeability combined with non-constant limits of integration, we try several different values for the position x_i, and for each of these we calculate the value of I_2 for all values of the frequency c. To keep the presentation of results brief we have chosen to present results for a single value of the phase shift d. We chose the value that gave the biggest deviation from zero for integral I_1. We conducted experiments for several different values of d, and the results were similar.

In order to test both the effect of $a \approx b$ and $a \gg b$ we construct two tests T_3 and T_4. The parameters for these test are summarized in table 8.2. We have plotted the values of the integral α_{I_2} as a function of the permeability frequency c. The results are presented in figure 8.2.3 and figure 8.2.4.

Figure 8.2.3a is off course the same as figure 8.2.1e since the limits of integrations are the same. As x_i goes from 0 to 0.9 we observe that for low frequencies the integral behave similar to integral I_1, for higher frequencies the behavior is somewhat different. For x_i between 0 and 0.5 the behavior for large frequencies

Table 8.2: Parameters for test T_3 and T_4

	T_3	T_4
a	2	10
b	1.5	1
d	0.4	0
$Range\ c$	$[0, 10]$	$[0, 10]$
$Step\ c$	0.01	0.01
$Range\ x_i$	$[0, 0.9]$	$[0, 0.75]$
$Step\ x_i$	0.1	0.25

are of the same nature as for I_1, that is they behave as dampened oscillations. The difference is that the value deviate from the value obtained for constant permeabilities. For x_i from 0.6 to 0.9 we see higher oscillations for the high frequencies, but the trend is still that low values of c creates the biggest deviations from zero. The same pattern is observed for the case when $a \gg b$. But as for I_1 the values we get are a lot smaller when $a \gg b$.

8.2.3   Analysis of I_3

The last integral we consider is

$$I_3 = \int_{x_{w,i}}^{x_{o,i}} [a + b\,sin(2\pi(cx + d))]^{-2} \cdot sin(2\pi x)\,dx.$$

This integral appears as a consequence of the two-phase zone that comes between the injected water and the displaced oil. The size of the two-phase zone can vary and we will thus test different sizes of the two-phase zone as well as different frequencies of the permeability field. We now the width of the two-phase zone

$$x_o - x_w = h, \qquad h \in [0, 1]. \tag{8.2.1}$$

We device two tests, one with $a \approx b$ and one with $a \gg b$. For both tests we only present one value for d but in our work we tested several, and the results were similar. The parameters for the two tests are shown in table 8.3.

It is not only the size of h that is important, it is also the position of the two-phase zone. In the analytical results we saw that a narrow two-phase altered the SNS structure, based on this we assume that the dependence on position is highest for small values of h. To test several positions we move the two-phase zone with equidistant steps

$$steps = \frac{h}{5}.$$
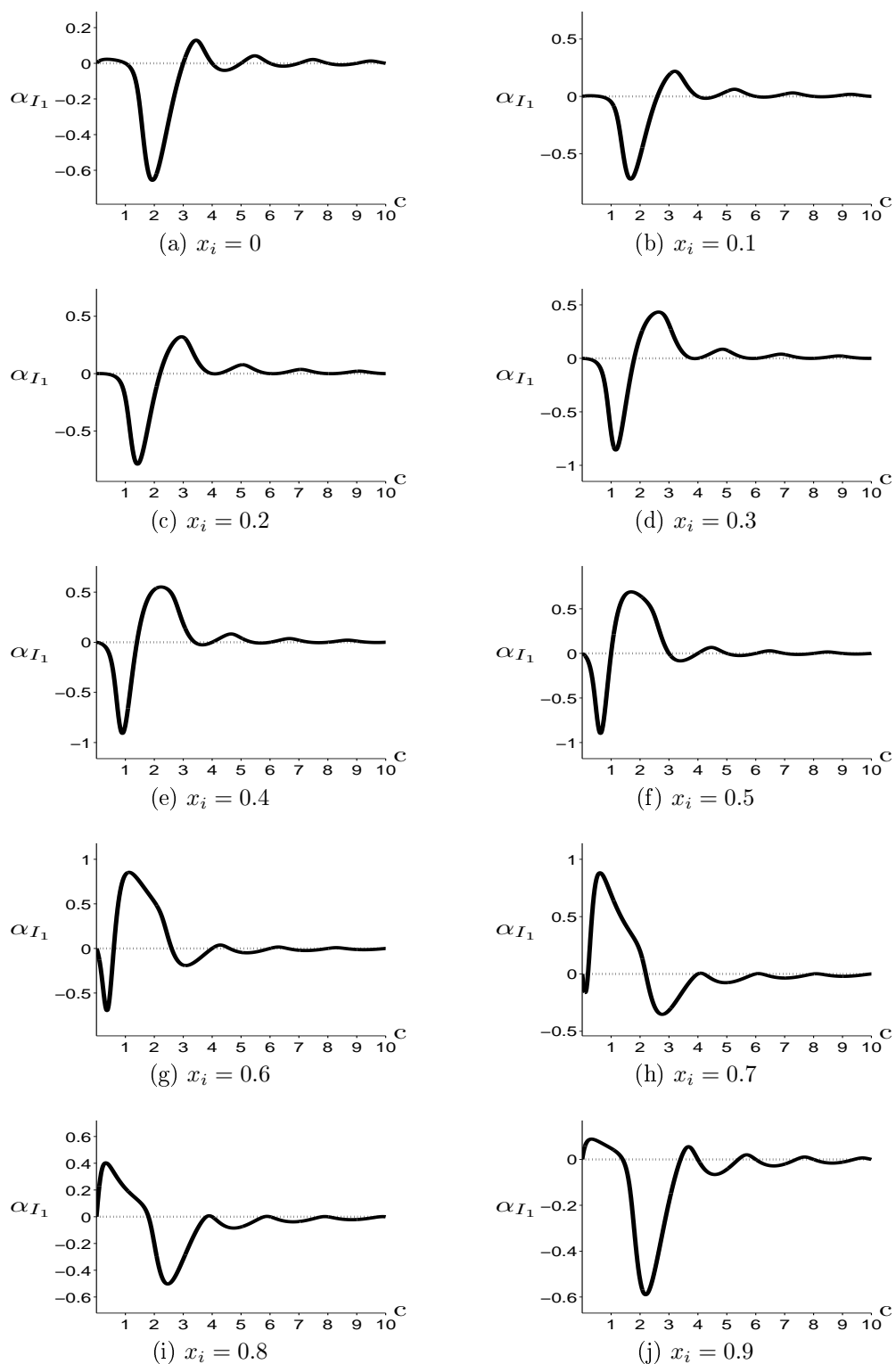
Figure 8.2.3: Test T_3, value for constant permeability shown by the stippled line

(a) $x_i = 0$

(b) $x_i = 0.25$

(c) $x_i = 0.5$

(d) $x_i = 0.75$
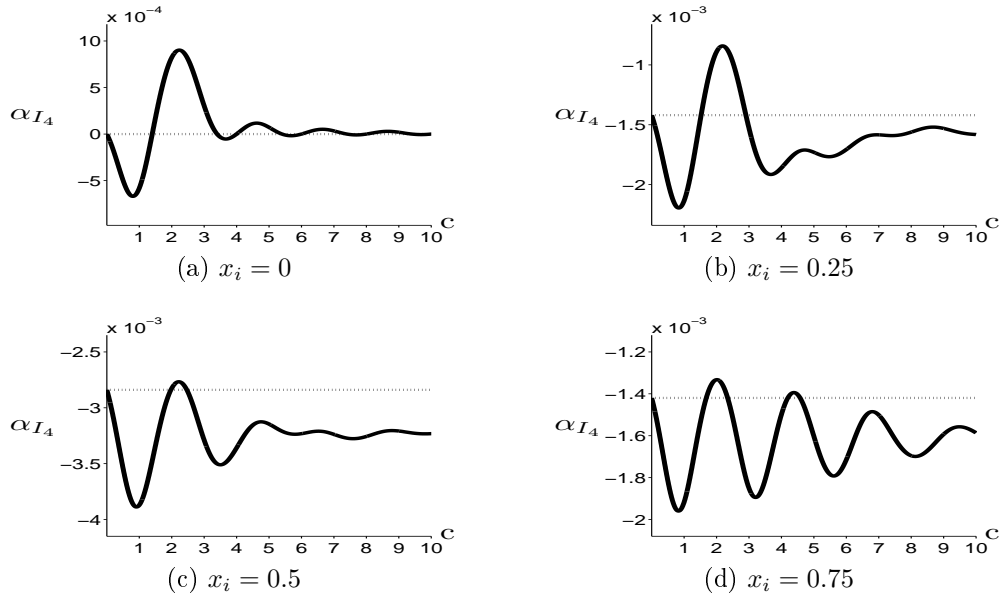
Figure 8.2.4: Test T_4, value for constant permeability shown by the stippled line

Table 8.3: Parameters for test T_5 and T_6

	T_5	T_6
a	2	10
b	1.5	1
d	0	0
$Range\ c$	$[0, 10]$	$[0, 10]$
$Step\ c$	0.01	0.01
h	$^1/_2, {}^1/_4, {}^1/_8, {}^1/_{16}, {}^1/_{32}$	$^1/_2, {}^1/_4, {}^1/_8, {}^1/_{16}, {}^1/_{32}$

After calculating the integral values α_{I_5} and α_{I_6} for the range of frequencies c, and for different positions of the two-phase zone we pick the one that has the highest mean deviation from zero. This is chosen as to get a worst case scenario. The results for the two tests are shown in figure 8.2.5, and figure 8.2.6.

In figure 8.2.5 we see the measurements from the five different two-phase zones. In figure 8.2.5a, we see that the structure is relatively similar to the one observed in figure 8.2.1a, the most obvious difference is that for high values of c the integral deviates from the constant permeability value. As the two-phase zone becomes narrow this similarity disappears. When the two-phase zones is narrower, we observe that the oscillations with larger values of c is of approximately the same amplitude as for low values of c. For $h = 1/16$, and $h = 1/32$ there is hardly any difference between the amplitude of oscillation for low and high values of frequency c. But it is worth noting that the value

(a) $h = \frac{1}{2}$

(b) $h = \frac{1}{4}$

(c) $h = \frac{1}{8}$

(d) $h = \frac{1}{16}$

(e) $h = \frac{1}{32}$
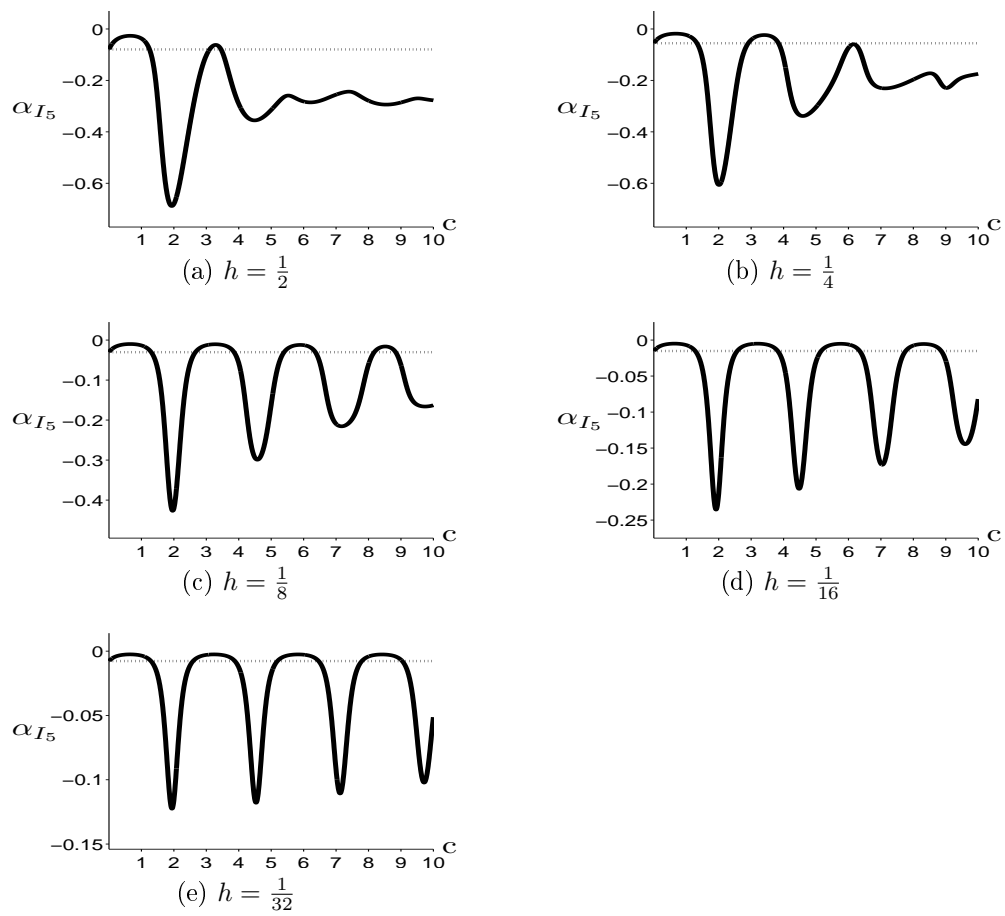
Figure 8.2.5: Test T_5, value for constant permeability shown by the stippled line

(a) $h = \frac{1}{2}$

(b) $h = \frac{1}{4}$

(c) $h = \frac{1}{8}$

(d) $h = \frac{1}{16}$

(e) $h = \frac{1}{32}$
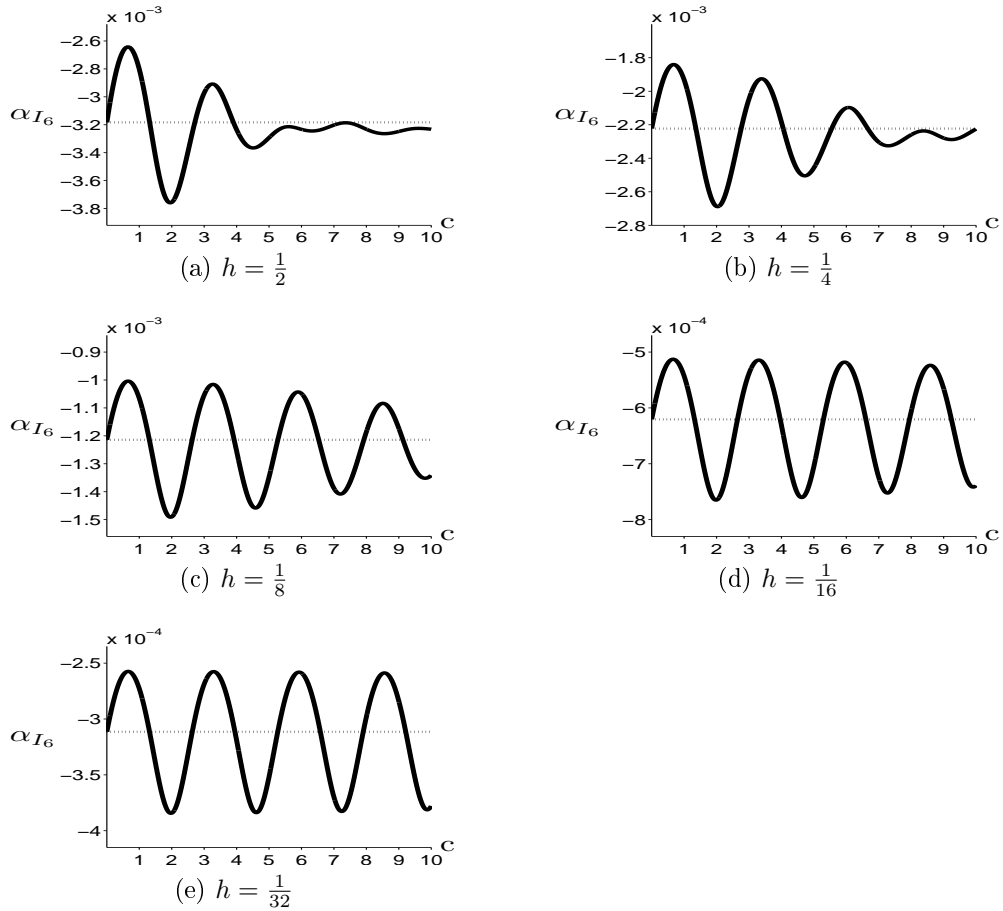
Figure 8.2.6: Test T_6, value for constant permeability shown by the stippled line

of the amplitude is much lower for narrow two-phase zones, then for wide.

Results for the case where $a \gg b$ are shown in figure 8.2.6 we observe similar characteristics as the case for $a \approx b$. The difference is, as it was for I_1 and I_2, the values of the integral α_{I_3} are much smaller. We can also observe that we observe evenly sized oscillations already at $h = 1/16$.

8.3   Numerical error

From figures 8.2.1, 8.2.2, 8.2.3, 8.2.4, 8.2.5, and figure 8.2.6 we see that the values of α_{I_1}, α_{I_2}, α_{I_3}, α_{I_4}, α_{I_5} and α_{I_6} is often very small. Therefore we need to investigate to which precision the quadrature method calculates the integrals. Fortunately the matlab function `quadgk` can output an approximate bound on the absolute error $|Q - I|$ where Q is the approximated integral, and I is the exact value of the integral.

(a) Error test T_1

(b) Error test T_2

(c) Error test T_3

(d) Error test T_4

(e) Error test $T_5(e)$

(f) Error test $T_6(e)$
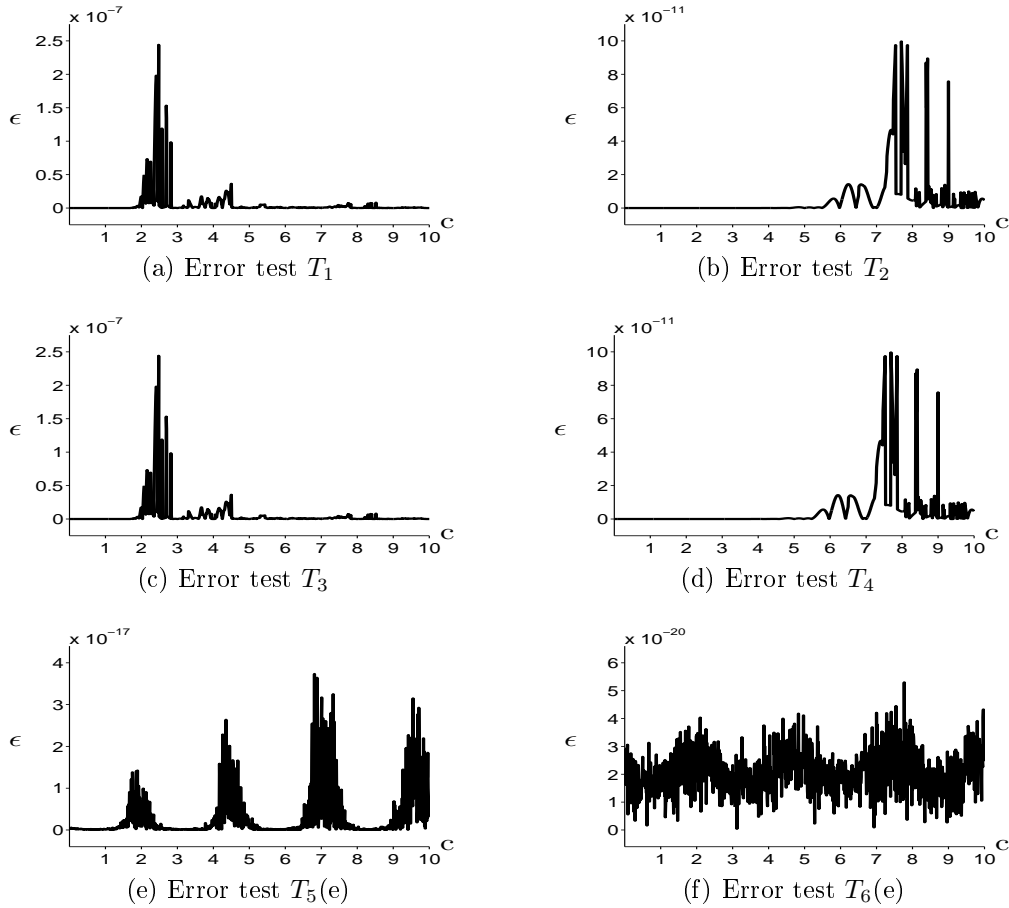
Figure 8.3.1: Error bounds for tests

In the investigation of integral I_1 we tried for many different values of d. In integral I_2 we had different values of x_i. And in integral I_3 we had different values of h combined with different positions of the two-phase zone. In all the experiments, we calculated the error. We will not present all these results.

For integral I_1 and I_2 we picked the configuration of d and x_i that produced the highest mean error. The results from test T_1 and T_2 are shown in figure 8.3.1a, and figure 8.3.1b. The results from test T_3 and T_4 are shown in figure 8.3.1c, and figure 8.3.1d.

For integral I_3 we have already made a choice with regard to the results we want to present. To present the worst case scenario, we saw that $h = 1/32$ produced the lowest values of α_{I_5} , here a high error in the quadrature has the biggest effect. That is why we calculated the error for all positions of the two-phase front in the case with $h = 1/32$. And we present the position that produced the highest mean error. The error results from test T_5 and T_6 are shown in figure 8.3.1e, and figure 8.3.1f.

When we compare figures 8.2.1, 8.2.2, 8.2.3, 8.2.4, 8.2.5, and figure 8.2.6 to

figure 8.3.1 we observe that the error in no way dominates the results.

8.4   Summary and conclusions

In chapter 6 and 7 we calculated the sensitivity in direction of different Haar-basis elements. This allowed us to calculate how the sensitivity and non-linearity values changed with the scale of the basis elements. This was done under assumption that the permeability was constant. This assumption is never valid for real world petroleum reservoirs, thus we needed to analyze the effects of a non-constant permeability field. To keep the analysis brief we chose to only analyze the effect on sensitivity. Chapter 6 and 7 told us that the sensitivity expression depended on scale through the three integrals; I_1, I_2, and I_3. These integrals was simplified with the assumption of constant permeability. To analyze the effect of a non-constant permeability field we evaluate the non-simplified integrals by a numerical quadrature scheme from matlab.

In Chapter 6 and 7 we saw that the sensitivity gradually decreased to zero as the scale went from coarse to fine. In the case of the constant basis element all the integrals produced a non-zero value, but when we looked at oscillating basis elements the integral I_1 was instantly zero. As we reduces the scale the integrals I_2, and I_3 became equal to integral I_1 and hence zero. This was for the case with constant permeability. We now analyze what effect a non-constant permeability field will have on this SNS structure.

The biggest impact of a non-constant permeability field is that the integral I_1 will have a large deviation from zero when the frequency of the permeability field equals the frequency of the basis element. The effect on integrals I_2 and I_3 is also most prominent for frequencies equal to the frequency of the basis element, but for these cases we also see deviations for higher values of c, although the effect were not as high. For a real world petroleum reservoir we have little information about the frequency. A fairly general statement would be that a real case permeability field has both high frequency elements, and low frequency elements. For elements with high frequencies relative to the basis elements the effect on integration values are minor. We might observe some deviations from a constant case for integral I_2 and I_3, but no influence on integral I_1. Elements with low frequencies relative to the basis elements could expect to see some effects on the SNS structure. In this case we would have to go to a finer scale, and hence increase the frequency of the basis elements to ensure that the sensitivity value is zero.

The objective of this chapter was to investigate whether a non-constant permeability field alter the SNS structure. We can conclude by observing that

the SNS structure is affected, but not altered in any substantial way by a non-constant permeability field. We see that depending on the frequency of the permeability field we must expect to find a more uneven decrease in sensitivity values. We can see lower or higher values than expected from the sensitivity, and we might have to go to a finer scale before the sensitivity is zero.

Chapter 9

Numerical sensitivity by Eclipse

So far in this thesis we have established the existence of a SNS relationship between estimating permeability from measurements of flow for a simplified case. We made several assumptions but the most grave simplification was that the permeability field was constant. The effects of this simplification was investigated in chapter 8, we concluded that a non-constant permeability field would not alter the SNS structure but perhaps make it more uneven. In chapter 8 we only investigated the possible effects on sensitivity, assuming that we would see something similar for the non-linearity. We did not calculate the full expression for the sensitivity. In this chapter we apply the commercially available reservoir simulator Eclipse [21]. The advantages of using a full reservoir simulator are many. Most important is that we can obtain values for the sensitivity without making simplifications. The other aspect is that a full reservoir simulator applies the full fluid flow equations, including important elements like conservation of mass and energy.

Another important issue is that we can compare the values we obtained in our somewhat simplified case with the values the reservoir simulator outputs. We are also able to test if our conclusions regarding a non-constant permeability field holds.

9.1   Introduction

Eclipse generates sensitivity calculations if requested, by the gradient option. For a in-depth description of how Eclipse calculates the derivatives we refer the reader to [21]. For a more general introduction to how computation of gradients in reservoir simulators occurred we refer the reader to [4]. We only analyze the sensitivity values, this is because the non-linearity can not be obtained in a

similar fashion from Eclipse. Our analytical experience tells us that the non-linearity will have a similar dependence on scale as the sensitivity. We now give a short overview into how Eclipse generates the sensitivity measurements, and how we can utilize these for our analysis.

The gradient option computes gradients of the solution, e.g. oil production rates, with respect to various property parameters that are predefined by the user. This can be, e.g. the X-direction permeability multipliers. When we spescify which parameters the gradients should be calculated for, we must also define which sub-region the cell belongs to. In this way Eclipse computes the gradients of the solution with respect to the gradient parameters within each user-defined sub-region possessing active cells. This means that it is possible to make Eclipse calculate gradients for a fine scale as we want, down to to size of individual grid cells. In the analytical work one of the simplifications made was that we only considered a 1-D case. This simplification is done in this chapter as well. By letting the reservoir consist of 160 grid cells placed on a line the fluids are forced to only flow in one direction.

In the analytical work we parametrized the permeability by the Haar-basis. Eclipse calculates the sensitivity using a local basis. That means that we need to perform a basis-transformation in order to compare sensitivity values. The values Eclipse provides can be written as $\partial m / \partial \alpha$ where m is the solution ,e.g. oil production rate, and α is the parameter using the local basis. We want to compare this value against $\partial m / \partial \beta$ where β is the parameters using the Haar-basis. When we assume that parameters in the local basis, α, can be transformed to the Haar-basis, $\beta(\alpha)$, by a transformation matrix A

$$\beta(\alpha) = A\alpha.$$

For a simple case using two parameters this then gives

$$\beta_1 = a_{11}\alpha_1 + a_{12}\alpha_{2,}$$
$$\beta_2 = a_{21}\alpha_1 + a_{22}\alpha_{2,}$$

we then see that

$$\frac{\partial m}{\partial \alpha_1} = \frac{\partial m}{\partial \beta_1}\frac{\partial \beta_1}{\partial \alpha_1} + \frac{\partial m}{\partial \beta_2}\frac{\partial \beta_2}{\partial \alpha_1},$$
$$\frac{\partial m}{\partial \alpha_2} = \frac{\partial m}{\partial \beta_1}\frac{\partial \beta_1}{\partial \alpha_2} + \frac{\partial m}{\partial \beta_2}\frac{\partial \beta_2}{\partial \alpha_2},$$

which gives

$$\left.\begin{aligned}\frac{\partial m}{\partial \alpha_1} = a_{11}\frac{\partial m}{\partial \beta_1} + a_{21}\frac{\partial m}{\partial \beta_2} \\ \frac{\partial m}{\partial \alpha_2} = a_{12}\frac{\partial m}{\partial \beta_1} + a_{22}\frac{\partial m}{\partial \beta_2}\end{aligned}\right\} = A^T\frac{\partial m}{\partial \beta}.$$

In order to get the value of the derivative in the Haar-basis we write

$$\frac{\partial m}{\partial \beta} = (A^T)^{-1} \frac{\partial m}{\partial \alpha}. \tag{9.1.1}$$

But since the Haar-basis elements are orthonormal we get

$$A = (A^T)^{-1}, \tag{9.1.2}$$

and

$$\frac{\partial m}{\partial \beta} = A \frac{\partial m}{\partial \alpha}, \tag{9.1.3}$$

this means that in order to get the derivative of the Haar-basis elements we need to multiply the derivative of the local-basis elements with the transform-matix A.

9.2 Transformation

We now look at how to perform the transformation from gradients calculated with local basis-functions to gradients calculated from Haar basis-functions. From (9.1.3) we see that we do not need to think about the derivatives. We only need to find the transformation matrix to go from a local basis to the Haar basis. The transformation matrix presented here is based on [46].

One way to construct the Haar functions is to define a family of N Haar functions $h_k(x)$, $(k = 0, 1, 2, \ldots, N - 1)$ that are defined on the interval $0 \le x \le 1$. We then let a specific function $h_k(x)$ depend on the parameters p and q.

$$k = 2^p + q - 1.$$

For any value of $k \ge 0$, p, and q are uniquely determined so that 2^p is the largest power of 2 contained in k, and $q - 1$ is the remainder. In this fashion we can write tables of the corresponding values of different indexes N. When $N = 8$ we get the values for p, q, and k. Shown in table 9.1. We then define the Haar function in the following way.

- $k = 0$, the Haar function is a constant.

$$h_0(x) = \frac{1}{\sqrt{N}}. \tag{9.2.1}$$

- $k > 0$, the Haar function is defined in the following way

$$h_k(x) = \frac{1}{\sqrt{N}} \begin{cases} 2^{p/2} & (q-1)/2^p \le x \le (q-0.5)/2^p, \\ -2^{p/2} & (q-0.5)/2^p \le x \le q/2^p, \\ 0 & otherwise. \end{cases} \tag{9.2.2}$$

Table 9.1: values of p, q, and k. for $N = 8$

k	0	1	2	3	4	5	6	7
p	0	0	1	1	2	2	2	2
q	0	1	1	2	1	2	3	4

Using these definitions, we can create a N by N matrix for the discrete Haar-transform. For $N = 8$ this matrix becomes

$$H_8 = \frac{1}{\sqrt{8}} \begin{bmatrix} 1 & 1 & 1 & 1 & 1 & 1 & 1 & 1 \\ 1 & 1 & 1 & 1 & -1 & -1 & -1 & -1 \\ \sqrt{2} & \sqrt{2} & -\sqrt{2} & -\sqrt{2} & 0 & 0 & 0 & 0 \\ 0 & 0 & 0 & 0 & \sqrt{2} & \sqrt{2} & -\sqrt{2} & -\sqrt{2} \\ 2 & -2 & 0 & 0 & 0 & 0 & 0 & 0 \\ 0 & 0 & 2 & -2 & 0 & 0 & 0 & 0 \\ 0 & 0 & 0 & 0 & 2 & -2 & 0 & 0 \\ 0 & 0 & 0 & 0 & 0 & 0 & 2 & -2 \end{bmatrix} \qquad (9.2.3)$$

The matrix H_8 can then be used as the transform matrix A in (9.1.3). By some simple matrix calculations we can see that H_8 is orthonormal. H_8 thus fulfills the demands for the transformation matrix A and will transform 8 discrete values of the local basis to corresponding values in the Haar-basis.

9.3 The numerical experiments

In this section we give an overview of how we conduct the numerical experiments. As mentioned we would like to test how the sensitivity change along different Haar-basis elements when we have a constant and a non-constant permeability field. To accomplish this we need to construct tests that account for the different flow structures that were analyzed in chapter 7, while also highlighting the effect of different non-constant permeability fields analyzed in chapter 8.

In the analytical study conducted in chapter 7 we divided the analysis in two parts. First we looked at a flow pattern where the injected water displaced the oil like a piston. After this we analyzed the case when there was an two-phase zone separating water and oil. We would of course like to test both these scenarios by using the Eclipse simulator. This can not be achived, because Eclipse uses a numerical scheme to do the flow calculation there is always some
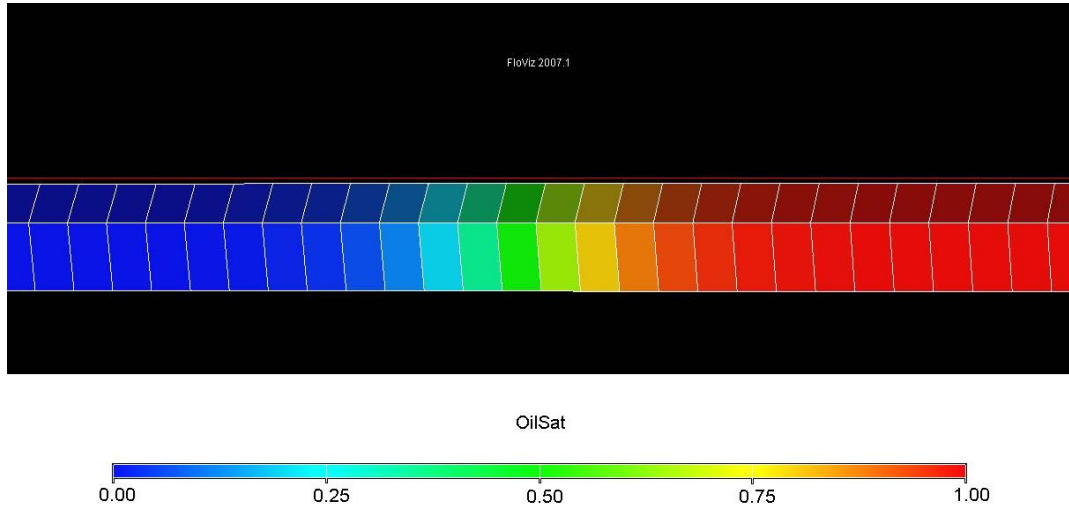
Figure 9.3.1: Narrow two-phase zone

numerical error. So even when we specify the fluid properties in such a way that we would expect a piston displacement we do not achieve a pure piston displacement.

The test we construct does not include a piston displacement, but we try to make the two-phase zone as narrow as possible in order to make the effects of the two-phase zone small. The fluid front can be seen in figure 9.3.1. In chapter 8 we analyzed the effects of a non-constant permeability field. From this we learned that the frequency of the permeability field has an effect on the sensitivity value. A strongly heterogeneous reservoir will affect the sensitivity in higher degree than a weakly heterogeneous reservoir. To test this we construct eight different permeability fields with four different frequencies. We then let four represent weakly heterogeneous reservoirs, and four represent strongly heterogeneous reservoirs. Since the front is not a piston-front, we need to define when the front moves past. In the following we say that the front passes when the oil saturation $S_o = 0.9$. We then chose the measurement times by looking at the fluid front in FloViz, a visualization program that is part of the Eclipse package[21]. This means that the measurement points are only placed in an approximately ordered fashion, and this needs to be taken into account when we analyze the results.

With this numerical setup we will in addition test some of the analytical results from [33] . As mentioned in chapter 1 the analysis in [33] was based on measurements of pressure, but numerical experiments were never conducted. In the Eclipse simulator it is the user who define which solution values to be used in the sensitivity calculations. It is therefore natural that we use the workflow described here to also investigate the results made in [33].

Table 9.2: Different viscosity's

	μ_o	0.5
Narrow two-phase zone	μ_w	1
	$p_{c,ow}$	0

9.4   Sensitivity of flow measurements

The first thing we look at is the sensitivity with regards to flow measurements. We specify Eclipse to output

$$\frac{\partial\,WOPR_i}{\partial\,permX_j} \tag{9.4.1}$$

where $i = 0, 1...$ is the different time steps, $j = 1, ...$ is the different sub-regions, and $WOPR$ is the well oil production rate. In the previous analysis we used the difference in fluid flow data as our data, we thus introduce the following expression for $\partial m/\partial\beta$

$$\frac{\partial\,m_i}{\partial\,permX_j} = \frac{\partial\,WOPR_{i+1}}{\partial\,permX_j} - \frac{\partial\,WOPR_i}{\partial\,permX_j}. \tag{9.4.2}$$

Where $i = 0, 1, ..., T$ is the timesteps and $j = 1, ..., 2^L$ is the sub-regions. For each of the timesteps T we transform the 2^L sized vector containing the sensitivity data on the local basis by

$$\frac{\partial m_i}{\partial \beta} = H_{2^L} \frac{\partial m_i}{\partial \alpha} \tag{9.4.3}$$

The resulting vector contains $(m(c)_i)_\phi$ on the first row, $(m(c)_i)_{\psi^0}$ on the second row, $(m(c)_i)_{\psi_1^1}$ on the third row and so on. Doing this for all the timesteps we produce T of these vectors. Combining these vectors into a 2^L times T matrix. Looking at the equation (4.1.1) we get the measurement for the sensitivity by simply taking the norm of each row in this matrix. Thus producing the sensitivity in the direction of each Haar basis element. Since we want to compare the numerical values to the analytical, we study the sensitivity as the scale becomes smaller. With the Haar basis we have a number of basis elements that are on the same scale, but translated relative to each other. For instance ψ_1^2 and ψ_2^2. We have sensitivity measurement for each of these elements, but as we are most interested in the value as the scale changes we select the basis element that produces the highest value, that is, $\max_l \left\| (\mathbf{m})_{\psi_l^j} \right\|$.

In the following experiments we let $T = 4$, and we divide the reservoir into 32 sub-regions. We are then able to get measures of the sensitivity down to ψ_l^4, $l = 1, \ldots, 16$, and it means that we need to use H_{32} to do the transformation.

Table 9.3: Permeability values for weakly heterogeneous reservoir

	I	II	III	IV
K_1(mD)	3843.5	4337.5	4544.6	4212.5
K_2(mD)	4831.5			
K_3(mD)	4584.4	4751.7		
K_4(mD)	4919.0			
K_5(mD)	4311.5	3691.5	4237.3	
K_6(mD)	3071.4			
K_7(mD)	4698.3	4783.1		
K_8(mD)	4868.0			
K_9(mD)	4357.5	4436.5	4285.9	
K_{10}(mD)	4515.5			
K_{11}(mD)	4486.3	4135.4		
K_{12}(mD)	3784.5			
K_{13}(mD)	4311.0	3826.7	3782.3	
K_{14}(mD)	3342.4			
K_{15}(mD)	4412.1	3737.9		
K_{16}(mD)	3063.7			

9.4.1 Weakly heterogeneous reservoir

We first conduct experiments for a weakly heterogeneous reservoirs with different frequencies. This is done by creating four different reservoirs with 16,8,4 and 1 permeability values. The first 16 values was created by using the matlab function `rand` which gives random numbers between 0 and 1. The two next was made by taking the mean of adjacent cells, and the last by taking the mean of the whole reservoir. Since we want values that do not vary to much the 16 first values was created in the following way $3000 + 2000 \cdot rand$. These permeability values are found in table 9.3. The sensitivities was calculated, and transformed using the Haar-basis transform. In table 9.4 we have given the maximum value for each of the scale elements, that is $\max_{l} \left\| (\mathbf{m})_{\psi_l^j} \right\|$ for $j = 0, 1, 2, 3, 4$. This is given for each of the different reservoirs.

Before we analyze the results we would like to make some preliminary thoughts about what results we can expect. In this numerical reservoir we do not have a perfect piston displacement, and we do not have perfectly ordered measurements. But we have tried to make the two-phase zone as narrow as possible, and we have tried to take the measurements in an ordered way. This means that we would expect results that resemble the results from the analysis of a narrow two-phase zone. In the case of a constant permeability field, with

Table 9.4: Sensitivity values for weakly heterogeneous reservoir, flow measurements

	I	II	III	IV
max $\|\mathbf{m}_\phi\|$	3824.7	3976.6	3652.2	3660.8
max $\|\mathbf{m}_{\psi^0}\|$	619.2	636.3	574.1	707.5
max $\|\mathbf{m}_{\psi^1}\|$	243.4	252.5	251.6	352.4
max $\|\mathbf{m}_{\psi^2}\|$	387.2	372.7	96.1	87.9
max $\|\mathbf{m}_{\psi^3}\|$	274.7	48.6	45.0	50.4
max $\|\mathbf{m}_{\psi^4}\|$	60.7	56.4	49.9	55.2

$i = 0, 1, 2, \ldots, 2^L$ measurements, our analysis told us to expect a drop in sensitivity, $S_{\psi_l^j}$, when $j = L$. But we could not expect the sensitivity to become zero before $j = K$, where K was some scale index larger then L. With this in mind and remembering that we have $T = 4 = 2^2$ measurements, we expect a drop in the value from S_{ψ^1} to S_{ψ^2}, and we can not expect the value to become zero, but continue to decrease.

We can also make some preliminary thoughts about the effect of a non-constant permeability field. The analysis in chapter 8 told us that a non-constant permeability field would effect the results when the frequency of the permeability field equaled the frequency of the basis element. For basis elements ψ^0 and ψ_l^1 we do not expect the integrals to become zero because $T = 4$. But we could expect an effect for S_{ψ^2}, S_{ψ^3}, and S_{ψ^4} if the permeability has a frequency that matches that of ψ_l^2, ψ_l^3, and ψ_l^4. Since the measurements are not made in an ordered fashion we do not expect the sensitivity values to become zero for any of the experiments. We instead hope that the mentioned effects are so dominating that they can be observed.

We first look at the case with a constant permeability field, that is, reservoir IV in our results. We observe that there is a drop in sensitivity values between max $\|\mathbf{m}_{\psi^1}\|$ and max $\|\mathbf{m}_{\psi^2}\|$, but the value is not zero for max $\|\mathbf{m}_{\psi^1}\|$ or the finer basis elements. This result is exactly what was expected.

Reservoir III has four different permeability zones. The basis element with corresponding frequency is ψ^1. Our preliminary thought say that there will be no effect for this case. From table 9.4 we see that this is in fact what we observe.

Reservoir II has eight different permeability zones. Following the same argument we expect to see an impact in direction of ψ^2. From table 9.4 we observe that for reservoir II, max $\|m_{\psi^2}\|$ is significantly larger than the corresponding max $\|m_{\psi^2}\|$ for reservoir III, and IV. This can be contributed to the non-constant permeability field.

Table 9.5: Permeability values for strongly heterogeneous reservoir

	I	II	III	IV
K_1(mD)	6.35	26.01	22.13	29.28
K_2(mD)	45.67			
K_3(mD)	31.62	18.25		
K_4(mD)	4.88			
K_5(mD)	13.92	20.63	34.35	
K_6(mD)	27.39			
K_7(mD)	47.88	48.06		
K_8(mD)	48.24			
K_9(mD)	7.88	28.21	32.13	
K_{10}(mD)	48.53			
K_{11}(mD)	47.86	36.06		
K_{12}(mD)	24.27			
K_{13}(mD)	40.01	23.55	28.50	
K_{14}(mD)	7.09			
K_{15}(mD)	21.09	33.44		
K_{16}(mD)	45.79			

For reservoir I, we have sixteen different permeability zones. We would here expect to see a impact in direction of ψ^3, which is quite clear when looking at table 9.4. Here we also observe a large value in direction of ψ^2, which is not expected form our preliminary toughts. One explanation could be the narrow two-phase zone. When we analysed the effects of a non-constant permeability field the only place where we could observe a high effect for high frequencys was in the case of a narrow two-phase zone. For $\max \|\mathbf{m}_{\psi^2}\|$ the frequency of the permeability is twice as high as the frequency of the basis element.

9.4.2 Strongly heterogeneous reservoir

For the strongly heterogeneous reservoir we created the four different permeability fields in the same manner as in the weakly heterogeneous reservoir. But since we wanted a larger degree of variation we created the first 16 values by $50 \cdot rand$. The permeability values for the four different reservoirs are found in table 9.5. We calculated the sensitivity in the same manner as for the weakly heterogeneous reservoir, and the results of this is given in table 9.6.

For a strongly heterogenous reservoir we expect to see similar behaviour of the sensitivity values as for the weakly heterogenous. We comment on these results

Table 9.6: Sensitivity values for strongly heterogeneous reservoir, flow measurements

	I	II	III	IV
max $\|\mathbf{m}_\phi\|$	21.583	58.778	12.036	50.456
max $\|\mathbf{m}_{\psi^0}\|$	6.6529	16.209	4.2223	9.6729
max $\|\mathbf{m}_{\psi^1}\|$	9.8616	10.956	4.1132	4.8072
max $\|\mathbf{m}_{\psi^2}\|$	3.8969	12.949	0.41674	1.2052
max $\|\mathbf{m}_{\psi^3}\|$	12.002	0.78709	0.90677	0.72383
max $\|\mathbf{m}_{\psi^4}\|$	1.1918	0.88508	1.26	0.93081

in similar fashion as for the weakly heterogeneous reservoir. With the results from chapter 8 in mind, we would expect to see an even higher effect from the non-constant permeability field for this case.

We start by looking at reservoir IV. As expected we see a clear drop in value for max $\|\mathbf{m}_{\psi^1}\|$ and max $\|\mathbf{m}_{\psi^2}\|$. As for the weakly heterogeneous reservoir we observe that the sensitivity value does not drop to zero.

For reservoir III we obseve the same behavior as for reservoir IV. This is exactly like the weakly heterogeneous reservoir.

Reservoir II has eight different permeability regions, and we hence expect to see larger value for max $\|\mathbf{m}_{\psi^2}\|$. From table 9.6 we observe that this is the case for this reservoir.

Reservoir I has sixteen different permeability zones, and as for the weakly heterogeneous reservoir we see the effect on max $\|\mathbf{m}_{\psi^3}\|$. For this case we also see a higher value for max $\|\mathbf{m}_{\psi^2}\|$ than we would expect. We contribute this effect to the narrow two-phase zone as for weakly heterogeneous reservoir.

The results from chapter 8 told us to expect a bigger effect from the strongly heterogenous reservoir, then from the weakly heterogenous reservoir. This effect is hard to observe from the values in table 9.4 and 9.6. As we will see this effect is also present for sensitivity of pressure measurements, they will hence be analyzed together later in this chapter.

9.5   Sensitivity of pressure measurements

In [33] the interrelation between sensitivity, non-linearity and scale associated with the inverse problem of permeability identification from fluid pressure observations was investigated. In this work the SNS relationship was proved to

exist, but there was not done any numerical experiments. In this section we calculate the sensitivity for some numerical experiments. We conduct the same experiments as for the case with flow measurements. The sensitivities in [33] was calculated using the Haar-basis, so the procedure to transform from local basis to Haar basis is the same. The difference is the expression for m_i.

In [33]

$$m_i(\mathbf{c}) = P(t_{i+1}; \mathbf{c}) - P(t_i; \mathbf{c}), \tag{9.5.1}$$

where

$$P(t; \mathbf{c}) = p(1, t; \mathbf{c}) - p(0, t; \mathbf{c}). \tag{9.5.2}$$

Since Eclipse gives

$$\frac{\partial (WBP)_i}{\partial (permX)_j}, \tag{9.5.3}$$

where $i = 0, \ldots$ is the different time steps, $j = 1, \ldots$ is the different regions, and WBP is the 1-point pressure average as defined in [21]. To represent the correct m_i we denote $WBP(I)$ as the pressure measurements at the injector, and $WBP(P)$ as the pressure measurements at the producer, corresponding to $p(0, t; \mathbf{c})$ and $p(1, t; \mathbf{c})$. We then write

$$\frac{\partial m_i}{\partial permX_j} = \left(\frac{\partial WBP(P)}{\partial permX} - \frac{\partial WBP(I)}{\partial permX} \right)_j^{i+1}$$
$$- \left(\frac{\partial WBP(P)}{\partial permX} - \frac{\partial WBP(I)}{\partial permX} \right)_j^{i}. \tag{9.5.4}$$

Using this expression we get the same matrix type as for the case with flow measurements. After transformation we get the sensitivities for the data in direction of each of the basis elements of the Haar basis.

In [33] the case with non-constant permeability was analyzed for the case of one-phase flow. The conclusions suggested that a non-constant permeability field would result in a gradual decrease in sensitivity. Not the abrupt scale dependent drop we see for constant permeability. These conclusions were based on analysis of the integral

$$\int_0^1 k^{-2}(x; \mathbf{c}) k(x; \mathbf{h}) \, dx. \tag{9.5.5}$$

This integral appears in the equations for flow as well, and the effects of a non-constant permeability field was investigated in chapter 8. In [33] there was no discussion about what effects different non-constant permeability field would have on the result. It is therefore of interest to see if the results obtained in chapter 8 is also valid for the case with pressure measurements.

For the following tests we use the same eight reservoirs that where described in table 9.3, and table 9.5. That is four reservoirs with weakly heterogeneity

Table 9.7: Weakly heterogeneous reservoir, press measurements

	I	II	III	IV
max $\|\mathbf{m}_\phi\|$	12.0276	12.8946	11.6904	12.5854
max $\|\mathbf{m}_{\psi^0}\|$	2.7393	2.7595	2.6941	2.8410
max $\|\mathbf{m}_{\psi^1}\|$	3.5140	3.5281	3.5246	3.6771
max $\|\mathbf{m}_{\psi^2}\|$	1.2837	1.2567	0.4440	0.4182
max $\|\mathbf{m}_{\psi^3}\|$	0.8380	0.4985	0.4957	0.5406
max $\|\mathbf{m}_{\psi^4}\|$	0.6586	0.6926	0.6954	0.7581

and different frequencies, and four reservoirs with strongly heterogeneity and different frequencies.

Since we can not get a piston like displacement we let the viscosity have the same values as for the flow measurements, and let the capillary pressure still be zero. In this way the two-phase zone is as narrow as possible. We have found the measurement points by looking at the front in FloViz, and we have said that the front is the point where $S_o = 0.9$. For the same reasons as earlier, it is reasonable to assume that this approach does not give exactly equidistant measurement points. In [33] the cases of non-ordered measurement points, and non-piston displacement where analyzed. Both lead to a more gradual decrease in sensitivity.

9.5.1   Weakly heterogeneous reservoir

In table 9.7 we see the sensitivity measurements, in direction of different basis-function elements. As for the case with the flow measurements, we are interested in what happens as the scale of basis-elements decreases. We therefore take the maximum value of all the basis-elements that are on the same scale.

For reservoir IV and reservoir III we expect to see a significant drop in the values when from direction ψ^1 to direction ψ^2. We observe that this is the case, and the values for reservoir IV, and reservoir III are almost similar as we expected.

For reservoir II we observe the effects of a non-constant permeability field can be seen in direction of ψ^2. The effect is not as prominent as we saw in the case of flow measurements, but it is clear that the sensitivity values in direction of ψ^2 is higher for reservoir II then for reservoir III, and IV.

In reservoir I we would expect a deviation to occur in direction of ψ^3. From table 9.7 we do observe a higher value then for reservoir $II - IV$. But the difference is not as clear as we saw in the case with flow measurements.

Table 9.8: Strongly heterogeneous reservoir, press measurements

	I	II	III	IV
$\max \|\mathbf{m}_\phi\|$	0.1297	0.2177	0.1991	0.2105
$\max \|\mathbf{m}_{\psi^0}\|$	0.0335	0.0557	0.0503	0.0462
$\max \|\mathbf{m}_{\psi^1}\|$	0.0546	0.0630	0.0713	0.0610
$\max \|\mathbf{m}_{\psi^2}\|$	0.0262	0.0481	0.0060	0.0063
$\max \|\mathbf{m}_{\psi^3}\|$	0.0654	0.0094	0.0086	0.0082
$\max \|\mathbf{m}_{\psi^4}\|$	0.0164	0.0150	0.0133	0.0122

9.5.2   Strongly heterogeneous reservoir

The sensitivity values for the case with strongly heterogeneous reservoirs are shown in table 9.8.

Reservoir III and IV has, as expected, similar values for this case as well. For reservoir II we expect the value in direction of ψ^2 to be higher than for reservoir III and IV. We observe that this is the case. In reservoir I the same pattern is recognized, but in direction of ψ^3. This is what was expected and we see that in direction of ψ^4 the value are of the same magnitude as for the other reservoirs.

9.6   Comparison of sensitivity data

When we look at the equation for the first order directional derivative in parameter space for two-phase flow, (7.1.43), we see that there are many factors that scale the result. In [33] the following expression was presented for the first order directional derivative in parameter space for two-phase flow

$$
\begin{aligned}
m_i(\mathbf{c}) = & u k^{-2}(\mathbf{c}) \left\{ (\mu_w - \mu_o) \int_{z_{o,i}}^{z_{o,i+1}} k(x; \mathbf{h}) \, dx \right. \\
& \left. + \left(\lambda^{-1} - \mu_w \right) \left(\int_{z_{w,i+1}}^{z_{o,i+1}} k(x; \mathbf{h}) \, dx - \int_{z_{w,i}}^{z_{o,i}} k(x; \mathbf{h}) \, dx \right) \right\}.
\end{aligned}
\tag{9.6.1}
$$

We see that we also here have many factors that scale the result. Because of this it does not provide much information to just compare the different data-types, and it is hard to observe the different effect of weakly and strongly heterogenous reservoirs. It may also be difficult to observe how the sensitivity values decrease with scale. We now introduce a method for analyzing the data that eliminates some of these effects.

Table 9.9: Comparison of data

	I	II	III	IV
Weakly heterogeneous, flow	6.4867	10.1851	23.4445	24.3964
Strongly heterogeneous, flow	2.2291	5.8780	7.8852	22.7062
Weakly heterogeneous, press	6.5752	7.8365	10.9529	11.1267
Strongly heterogeneous, press	2.0167	4.6400	11.4946	11.8989

In order to highlight the difference between the case with constant, and non-constant permeability more clearly we compare the different data. Since we chose $T = 4 = 2^2$ for all the test, our analytical work, and that of [33] suggest that there should be a considerable drop in value for $\max \|\mathbf{m}_{\psi^2}\|$, $\max \|\mathbf{m}_{\psi^3}\|$, and $\max \|\mathbf{m}_{\psi^3}\|$.

One way to investigate this is to look at the fraction

$$\frac{\max \|\mathbf{m}_\phi\| + \sum_{i=0}^{i=1} \max \|\mathbf{m}_{\psi^i}\|}{\sum_{i=2}^{i=4} \max \|\mathbf{m}_{\psi^i}\|}. \tag{9.6.2}$$

When the fraction is big the sensitivity values in direction of ϕ, ψ^0, and ψ^1 are larger that sensitivity in direction ψ^2, ψ^3, and ψ^4. This is in line with what we expect for constant permeability fields. Similarly when the fraction goes toward unity, the sensitivity values in direction ψ^2, ψ^3, and ψ^4 are not small. This is what we would expect for the cases with non-constant permeability. We have calculated the fraction for the different cases, the results are displayed in table 9.9.

From table 9.9 we observe that the fraction is largest for the case with constant permeability. We also observe almost similar values for the slowly varying field. We also observe that the fraction becomes smaller as we get permeability fields with a higher frequency, and the smallest value is for the fastest varying permeability field.

In chapter 8 we concluded that the sensitivity values would be mostly affected in strongly heterogeneous reservoirs. From table 9.9 we can see that both for flow and pressure measurements, the fraction is closer to unity for strongly heterogeneous reservoirs. This means that sensitivity values in direction ψ^2, ψ^3, and ψ^4 are more dominant for strongly than weakly heterogeneous reservoirs.

From table 9.9 it is easy to see that both pressure, and flow data act similar to a non-constant permeability field. That is the sensitivity data in direction of ψ^2, and ψ^3 is affected by non-constant permeability fields that vary with similar frequency as the basis functions.

Chapter 10

SNS for 2-D two-phase flow

So far we have only considered 1-D cases. This simplification was important so that we could perform a rigorous analysis of the SNS structure. Unfortunately the approach taken in the 1-D case is not easily extended to 2-D. In this chapter we investigate to which degree the results obtained for 1-D flow can be extended to 2-D flow.

In [33] the SNS structure for 2-D, two-phase flow with sparsely distributed times series of pressure data was discussed. Estimations performed in [24] gave indications that there was a SNS relationship for 2-D estimation of permeability, based on pressure measurements. The analytical base for this was discussed in [33] by use of streamlines. By sacrificing some rigor, the approach developed for the 1-D setting was adopted to the 2-D case. By this approach, it was indicated that there was small sensitivity values and large non-linearity associated with fine scale perturbations, and large sensitivity and small non-linearity associated with coarse scale perturbations along each streamline.

We do not adopt this method. Instead we simulate some different 2-D flooding experiments with the Eclipse simulator. We then transform the calculated sensitivities by performing a 2-D Haar transform. This gives us information about the sensitivities for the different scales. We also perform this test with pressure measurement, and then test the SNS relationship that was indicated in [33].

10.1   Multidimensional wavelet bases

In this section we give a short introduction to multidimensional wavelet bases. Most of the theory presented here is adopted from [15]. For simplicity we only consider the two-dimensional case.

There exists two ways of constructing an orthonormal basis for $L^2(\mathbb{R}^2)$. The trivial way is to start from an orthonormal wavelet basis for $L^2(\mathbb{R})$

$$\psi_{j,k}(x) = 2^{-j/2}\psi(2^{-j}x - k), \qquad (10.1.1)$$

we then take the tensor product of two of the one-dimensional bases:

$$\Psi_{j_1,k_1;j_2,k_2}(x_1, x_2) = \psi_{j_1,k_1}(x_1)\psi_{j_2,k_2}(x_2). \qquad (10.1.2)$$

The resulting functions is wavelets, and $\{\Psi_{j_1,k_1;j_2,k_2}; j_1, j_2, k_1, k_2 \in \mathbb{Z}\}$ is an orthonormal basis for $L^2(\mathbb{R}^2)$. In this basis the two variables x_1 and x_2 are dilated separately.

The other way to construct a multidimensional wavelet basis results in a orthonormal wavelet basis in which the dilation's control both variables simultaneously. The way to construct this is to consider the tensor product of two one-dimensional multiresolution analysis rather than the corresponding wavelet bases. More precisely, we define spaces $\boldsymbol{\mathcal{V}}_j$, $j \in \mathbb{Z}$ by

$$\boldsymbol{\mathcal{V}}_0 = \mathcal{V}_0 \oplus \mathcal{V}_0 = \overline{Span\{F(x,y) = f(x)g(y); f, g \in \mathcal{V}_0\}}, \qquad (10.1.3)$$

$$F \in \boldsymbol{\mathcal{V}}_j \Leftrightarrow F(2^j\cdot, 2^j\cdot) \in \boldsymbol{\mathcal{V}}_0. \qquad (10.1.4)$$

Similar to the one-dimensional case the $\boldsymbol{\mathcal{V}}_j$ form a multiresolution ladder in $L^2(\mathbb{R}^2)$ satisfying

$$\cdots \boldsymbol{\mathcal{V}}_2 \subset \boldsymbol{\mathcal{V}}_1 \subset \boldsymbol{\mathcal{V}}_0 \subset \boldsymbol{\mathcal{V}}_{-1} \subset \boldsymbol{\mathcal{V}}_{-2} \cdots, \qquad (10.1.5)$$

$$\bigcap_{j \in \mathbb{Z}} \boldsymbol{\mathcal{V}}_j = \{0\}, \quad \overline{\bigcup_{j \in \mathbb{Z}} \boldsymbol{\mathcal{V}}_j} = L^2(\mathbb{R}^2). \qquad (10.1.6)$$

Remembering that $\phi(\cdot - n)$, $n \in \mathbb{Z}$, constitute an orthonormal basis for $\mathcal{V}_0$, the product functions

$$\Phi_{0;n_1,n_2}(x,y) = \phi(x - n_1)\phi(y - n_2), \quad n_1, n_2 \in \mathbb{Z}, \qquad (10.1.7)$$

also constitute an orthonormal basis for $\boldsymbol{\mathcal{V}}_0$. Similar to before we use this to construct a basis for $\boldsymbol{\mathcal{V}}_j$. This is written as

$$\Phi_{j;n_1,n_2}(x,y) = \phi_{j,n_1}(x)\phi_{j,n_2}(y), \qquad (10.1.8)$$

$$\begin{aligned}
\Phi_{j;n_1,n_2}(x,y) &= \phi_{j,n_1}(x)\phi_{j,n_2}(y) \\
&= 2^{-j}\Phi(2^{-j}x - n_1, 2^{-j}y - n_2), \quad n_1, n_2 \in \mathbb{Z},
\end{aligned} \qquad (10.1.9)$$

Still following the one-dimensional case, we define for each $j \in \mathbb{Z}$ the complement space $\boldsymbol{\mathcal{W}}_j$ to be the orthonormal complement in $\boldsymbol{\mathcal{V}}_{j-1}$ of $\boldsymbol{\mathcal{V}}_j$. We then have

$$\begin{aligned}
\boldsymbol{\mathcal{V}}_{j-1} &= \mathcal{V}_{j-1} \oplus \mathcal{V}_{j-1} = (\mathcal{V}_j \oplus \mathcal{W}_j) \oplus (\mathcal{V}_j \oplus \mathcal{W}_j) \\
&= \mathcal{V}_j \oplus \mathcal{V}_j \oplus [(\mathcal{W}_j \oplus \mathcal{V}_j) \oplus (\mathcal{V}_j \oplus \mathcal{W}_j) \oplus (\mathcal{W}_j \oplus \mathcal{W}_j)] \qquad (10.1.10) \\
&= \boldsymbol{\mathcal{V}}_j \oplus \boldsymbol{\mathcal{W}}_j.
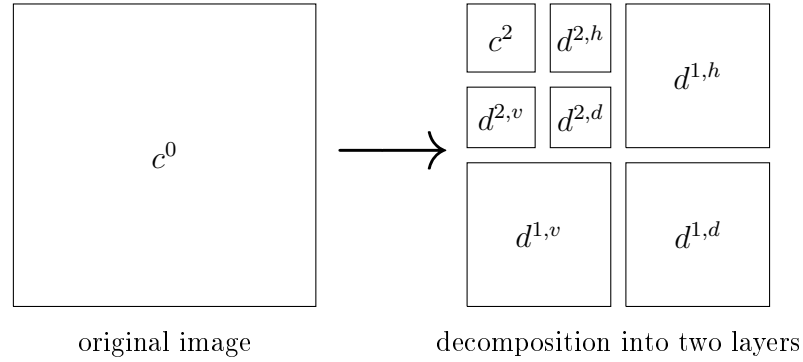\end{aligned}$$

Figure 10.1.1: Schematic visualization of the two-dimensional wavelet transform. Adopted from [15]

We see that $\boldsymbol{\mathcal{W}}_j$ consist of three pieces with orthonormal bases given by $\psi_{j,n_1}(x)\phi_{j,n_2}(y)$ for $\mathcal{W}_j \oplus \mathcal{V}_j$, $\phi_{j,n_1}(x)\psi_{j,n_2}(y)$ for $\mathcal{V}_j \oplus \mathcal{W}_j$, and $\psi_{j,n_1}(x)\psi_{j,n_2}(y)$ for $\mathcal{W}_j \oplus \mathcal{W}_j$. This leads us to define *three* wavelets,

$$\begin{aligned}
\Psi^h(x,y) &= \phi(x)\psi(y) \\
\Psi^v(x,y) &= \psi(x)\phi(y) \\
\Psi^d(x,y) &= \psi(x)\psi(y)
\end{aligned} \tag{10.1.11}$$

where h,v, and d stand for "horizontal", "vertical", and "diagonal", respectively. We can then define

$$\left\{ \Psi^\lambda_{j;n_1,n_2}; n_1, n_2 \in \mathbb{Z}, \lambda = h, v, \text{ or } d \right\} \tag{10.1.12}$$

as an orthonormal basis for $\boldsymbol{\mathcal{W}}_j$, and

$$\left\{ \Psi^\lambda_{j;\mathbf{n}}; j \in \mathbb{Z}, \mathbf{n} \in \mathbb{Z}^2, \lambda = h, v, \text{ or } d \right\} \tag{10.1.13}$$

is an orthonormal basis for $\overline{\bigoplus_{j\in\mathbb{Z}} \boldsymbol{\mathcal{W}}_j} = L^2(\mathbb{R}^2)$.

A multidimensional wavelet basis can be used to analyze two-dimensional images. For this we use a two-dimensional basis, corresponding to an image. Using a method called sub-band filtering (for more on this see e.g. [15, 42, 12]) we can express a image by the two-dimensional wavelet basis. This is done by operating on the rows, and columns in a image. Now the original image c^0, consisting of an $N \times N$ array, is divided into four arrays consisting of $(N/2) \times (N/2)$ elements. This is illustrated in figure 10.1.1. The array $d^{1,v}$ gives information about the vertical edges of the original image, $d^{1,h}$ gives the horizontal edges, and $d^{1,d}$ gives the diagonal edges. In figure 10.1.1 c^1 has been decomposed further, and one can of course decompose c^2 even further if more multiresolution layers are wanted.

10.2   2-D Haar basis transform

As for the 1-D case we want to utilize the numerical sensitivity values given by the reservoir simulator Eclipse. Unfortunately we face the same problem for the 2-D as in the 1-D case. Eclipse calculates the sensitivities by a local basis, which are not suited for scale analysis. We now adopt the method used for images. Since we have a 2-D reservoir the sensitivity values for each user defined zone corresponds to one element in the sensitivity matrix. This matrix can be transformed to a multidimensional basis in the same manner as an image.

In order to perform this transformation we look at the 2-D Haar basis transform. This transform decomposes the signal into two components, one called the average and the other called the difference. If we have a signal of length N, i.e. $f = (f_1, f_2, \ldots, f_N)$ we find the averages $a^1 = (a_1, a_2, \ldots, a_{N/2})$ by

$$a_n = \frac{f_{2n-1} + f_{2n}}{\sqrt{2}}, \ n = 1, 2, 3, \ldots, N/2, \qquad (10.2.1)$$

and the difference $d^1 = \left(d_1, d_2, \ldots, d_{N/2}\right)$ by

$$d_n = \frac{f_{2n-1} - f_{2n}}{\sqrt{2}} \ n = 1, 2, 3, \ldots, N/2. \qquad (10.2.2)$$

To see how this works on an matrix we consider a simple example. We apply the 2-D Haar transform to the following matrix, with $N = 4$.

$$A = \begin{pmatrix} 6 & 2 & 3 & 5 \\ 7 & 7 & 2 & 1 \\ 2 & 4 & 6 & 9 \\ 5 & 8 & 7 & 0 \end{pmatrix}. \qquad (10.2.3)$$

We first calculate the averages, a_n, and the differences, d_n, of the rows of A, for $n = 1, 2$. We write the averages on the left side and the differences on the right side of the stippled line.

$$\sqrt{2} \begin{pmatrix} 8 & 8 & \vdots & 4 & -2 \\ 14 & 3 & \vdots & 0 & 1 \\ 6 & 15 & \vdots & -2 & -3 \\ 13 & 7 & \vdots & -3 & 7 \end{pmatrix} \qquad (10.2.4)$$

Next we calculate the averages, a_n, and the differences, d_n, to the columns for of the resultant matrix for $n = 1, 2$. Now the averages is on top and the

difference below the horizontal stippled line.

$$\frac{1}{2}\begin{pmatrix} 22 & 11 & \vdots & 4 & -1 \\ 19 & 22 & \vdots & -5 & 4 \\ \cdots & \cdots & \vdots & \cdots & \cdots \\ -6 & 5 & \vdots & 4 & -3 \\ -7 & 8 & \vdots & 1 & -10 \end{pmatrix} = \begin{pmatrix} 11 & 5.5 & \vdots & 2 & -0.5 \\ 9.5 & 11 & \vdots & -2.5 & 2 \\ \cdots & \cdots & \vdots & \cdots & \cdots \\ -3 & 2.5 & \vdots & 2 & -1.5 \\ -3.5 & 4 & \vdots & 0.5 & -5 \end{pmatrix}. \quad (10.2.5)$$

We see that the transformed matrix is divided into four part. This corresponds to the four parts illustrated in figure 10.1.1. The sub-matix c^1 resulted from taking the averages of the rows, and then of the columns. It is clear that it contains information about the global properties of the analyzed image. The sub-matrix $d^{1,v}$ was calculated by first taking the average of the rows and then the difference of the columns. This means that horizontal lines is emphasized in this matrix. The sub-matrix $d^{1,h}$ resulted from the difference of the rows, and average of the columns. This matrix thus contains information about the vertical lines of the original image. The last sub-matrix $d^{1,d}$ was calculated by taking the difference of the rows, and then the difference of the columns. This is why $d^{1,d}$ gives information about diagonal details. Values from the next multiresolution level is easily obtained by performing the 2-D Haar transform to the c^1 matrix.

10.3 Numerical experiments

In chapter 9 we used the Eclipse simulator to analyze the sensitivity of the two-phase problem. This was done by letting Eclipse calculate the sensitivity values for the parameter in each user defined region, and then transform these values by the 1-D Haar transform. For the 2-D experiments we have a similar work flow. We let Eclipse calculate the sensitivity values for the parameter in each region, then we transform the value by using the 2-D Haar basis. In this way we can analyze the sensitivity values at different scales. Similar to the 1-D case we do not investigate the non-linearity of the problem. We start by introducing the numerical experiments, then we look at results from flow data, to the end we look at results from pressure data.

In the numerical experiments we use a 32×32 grid block square reservoir, with an injection well in the north-west corner, and a production well in the south-east corner. We divide the reservoir into 1024 parameter regions. The reservoir is illustrated in figure 10.3.1. In chapter 8 we observed differences in the SNS structure for a constant, and a non-constant permeability field. Under the suspicion that some of the 1-D properties carries over to 2-D we want to test three different types of reservoirs
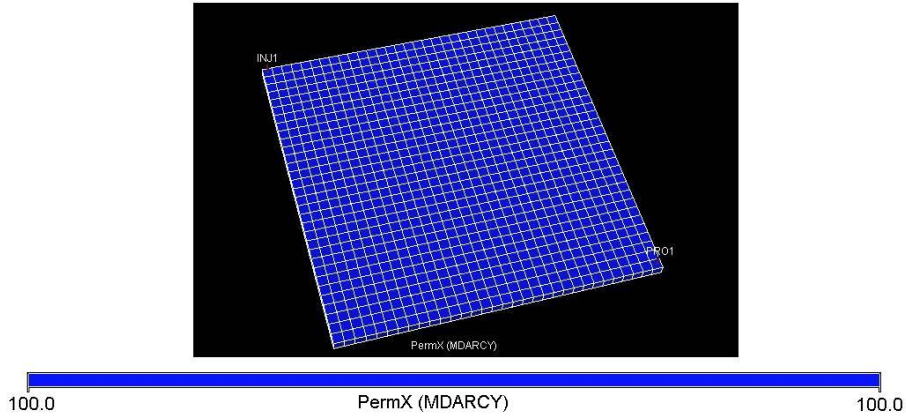
Figure 10.3.1: Permeability field for homogeneous reservoir in X-direction, Y-direction is equal.

1. homogeneous reservoir,

2. heterogeneous reservoir,

3. reservoir with channel structures.

The properties of these reservoirs are summarized in table 10.1.

The work flow are equal for all three reservoirs, and can be summarized in the following way. First we run the simulation, and choose four times where we want to collect our data. Then we find the sensitivity for all the 1024 regions by

$$\frac{\partial\, m_i}{\partial\, permX_j} = \frac{\partial\, WOPR_{i+1}}{\partial\, permX_j} - \frac{\partial\, WOPR_i}{\partial\, permX_j}. \tag{10.3.1}$$

with $i = 0, 1, 2, 3$ and $j = 1, 2, \ldots, 1024\,(2^{10})$ This vector is then reshaped into four 32×32, $(2^5 \times 2^5)$, matrices using the matlab function `Reshape`. This gives us C_i^0, for $i = 0, 1, 2, 3$. These four matrices are then transformed by the 2-D Haar transform. For a grid cell in Eclipse the permeablility is defined in the X, Z, and Y direction corresponding to well known cartesian coordinates. Since we consider 2-D flow, the Z direction is discarded. We have chosen to analyse the X-direction permeability multiplier. The experiments were tested for Y-direction permeability multipliers as well, and the results were similar. Hence we only present results from the X-direction.

When the original 2-D sensitivity matrix is transformed we obtain four new matrices, $C_i^1, D_i^{1,v}, D_i^{1,h}$, and $D_i^{1,d}$ (c.f. figure 10.1.1). These can be writen as

$$C_i^1 = \sum_{k=1}^{2^{5-1}} \sum_{p=1}^{2^{5-1}} c_{k,p}^i. \tag{10.3.2}$$
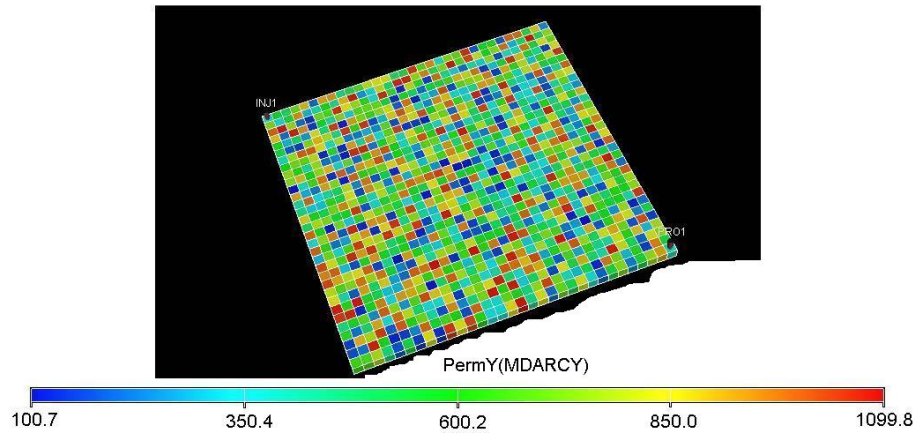
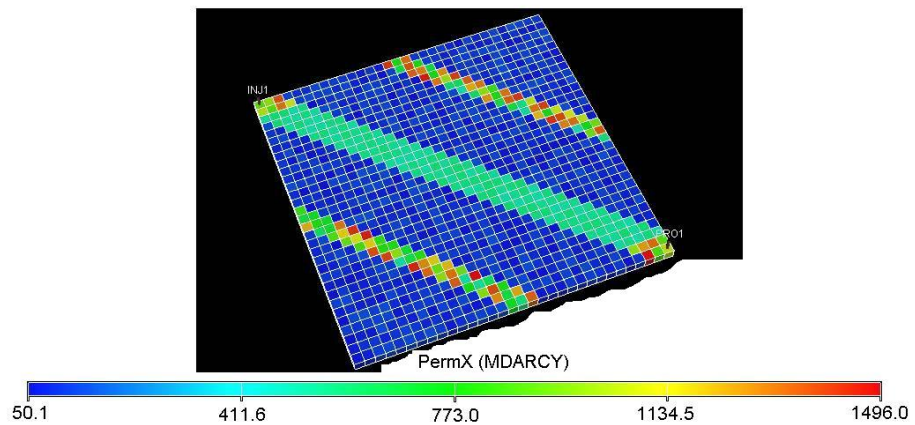Figure 10.3.2: Permeability field of heterogeneous reservoir, Y-direction. X-direction is similar.

Figure 10.3.3: Permeability field of reservoir with channel structure. X-direction shown, Y-direction is similar.

Table 10.1: Reservoir properties

	Homogenous	Heterogenous	Channel Structured	
Perm-X	100 md	$100 + 1000 \cdot$ `rand`	High perm areas: $500 + 1000 \cdot$ `rand`	
			Low perm areas: $50 + 100 \cdot$ `rand`	
Perm-Y	100 md	$100 + 1000 \cdot$ `rand`	High perm areas: $500 + 1000 \cdot$ `rand`	
			Low perm areas: $50 + 100 \cdot$ `rand`	
Porosity	0.3	0.3	0.3	
μ_w	1	1	1	
μ_o	0.5	0.5	0.5	
P_c	0	0	0	

$$D_i^{1,v} = \sum_{k=1}^{2^{5-1}} \sum_{p=1}^{2^{5-1}} d_{k,p}^{v,i}. \tag{10.3.3}$$

$$D_i^{1,h} = \sum_{k=1}^{2^{5-1}} \sum_{p=1}^{2^{5-1}} d_{k,p}^{h,i}. \tag{10.3.4}$$

$$D_i^{1,d} = \sum_{k=1}^{2^{5-1}} \sum_{p=1}^{2^{5-1}} d_{k,p}^{d,i}. \tag{10.3.5}$$

Where the time-index subscript in has been places as a super-script in order to make space for the matrix indexes. The C_i^1 matrices are then transformed to obtain the second level 2-D Haar transform (c.f. figure 10.1.1). We can write the general l level 2-D Haar transform in the following way:

$$C_i^l = \sum_{k=1}^{2^{5-l}} \sum_{p=1}^{2^{5-l}} c_{k,p}^i. \tag{10.3.6}$$

$$D_i^{l,v} = \sum_{k=1}^{2^{5-l}} \sum_{p=1}^{2^{5-l}} d_{k,p}^{v,i}. \tag{10.3.7}$$

$$D_i^{l,h} = \sum_{k=1}^{2^{5-l}} \sum_{p=1}^{2^{5-l}} d_{k,p}^{h,i}. \tag{10.3.8}$$

$$D_i^{l,d} = \sum_{k=1}^{2^{5-l}} \sum_{p=1}^{2^{5-l}} d_{k,p}^{d,i}. \tag{10.3.9}$$

From this we see that on the fith level, the matrices reduces to a scalar value. Remembering that we have $i = 0, 1, 2, 3$ it is clear that we produce many matrices. By looking at 4.1.1 we want to find a matrices over the normed element. This is obtained by using the L_2 norm om the different elements for different times. We now illustrate how this is done for the C^l matrix. The procedure is identical for the other three matrices. Denoting $\overline{C^l}$ as the matrix over the norms we have:

$$\overline{C^l} = \sum_{k=1}^{2^{5-l}} \sum_{p=1}^{2^{5-l}} \sqrt{\left\{ \left(c_{k,p}^0\right)^2 + \left(c_{k,p}^1\right)^2 + \left(c_{k,p}^2\right)^2 + \left(c_{k,p}^3\right)^2 \right\}}. \qquad (10.3.10)$$

We have now reduced the problem to representing $\overline{C^l}, \overline{D^{l,v}}, \overline{D^{l,h}}$, and $\overline{D^{l,d}}$ for $l = 1, 2, 3, 4, 5$. Hence 20 matrices. Idealy we would like to keep in line with the 1-D example, and present the maximum element of each matrix, but by looking at the actual matrices we observe that one or two elements are always much larger than the others, hence the maximum value would not present a good measure for how the general sensitivity depend on the scale. Thus we present the mean value of the matrices. Note that $l = 1$ represents the finest scale, and $l = 5$ the coarsest.

$$\text{mean}\overline{C^l}, \quad \text{for } l = 1, 2, 3, 4, 5. \qquad (10.3.11)$$

$$\text{mean}\overline{D^{l,v}}, \quad \text{for } l = 1, 2, 3, 4, 5. \qquad (10.3.12)$$

$$\text{mean}\overline{D^{l,h}}, \quad \text{for } l = 1, 2, 3, 4, 5. \qquad (10.3.13)$$

$$\text{mean}\overline{D^{l,d}}, \quad \text{for } l = 1, 2, 3, 4, 5. \qquad (10.3.14)$$

To keep the discussion simple, and highlighting information about the general structure of the SNS relationship we analyze and discuss all results in the end of this chapter. We now calculate the sensitivity values for the following four cases:

- Homogeneous reservoir, the permeability field in X-direction are shown in figure 10.3.1 , Y-direction is similar. Mean values of transformations are seen in table 10.2.

- Heterogeneous reservoir, the permeability field in Y-direction are shown in figure 10.3.2 , X-direction is similar. Mean values of transformations are seen in table 10.3.

- Reservoir with channel structures, the permeability field in X-direction are shown in figure 10.3.3, Y-direction is similar. Mean values of transformations are seen in table 10.4.

- Reservoir with channel structures, and contradiagonal well placement. Mean values of transformations are seen in figure 10.5.

Table 10.2: Sensitivity values for homogeneous reservoir, flow measurements

	mean$\left(\overline{C^l}\right)$	mean$\left(\overline{D^{l,v}}\right)$	mean$\left(\overline{D^{l,h}}\right)$	mean$\left(\overline{D^{l,d}}\right)$
$l = 5$	15.1993	4.0893	5.8757	15.9503
$l = 4$	8.4007	5.4727	4.9671	7.9550
$l = 3$	4.9367	2.8927	2.3002	2.2786
$l = 2$	2.6301	1.1039	0.7138	0.5559
$l = 1$	1.3466	0.3748	0.2311	0.1055

Table 10.3: Sensitivity values for heterogeneous reservoir, flow measurements

	mean$\left(\overline{C^l}\right)$	mean$\left(\overline{D^{l,v}}\right)$	mean$\left(\overline{D^{l,h}}\right)$	mean$\left(\overline{D^{l,d}}\right)$
$l = 5$	11.9311	5.2219	6.1297	12.8773
$l = 4$	7.3475	5.5677	5.0517	6.6283
$l = 3$	4.5239	2.8505	2.6264	2.1429
$l = 2$	2.5630	1.0565	0.7449	0.5442
$l = 1$	1.3278	0.5338	0.4603	0.3564

Table 10.4: Sensitivity values for reservoir with channel structures, flow measurements

	mean$\left(\overline{C^l}\right)$	mean$\left(\overline{D^{l,v}}\right)$	mean$\left(\overline{D^{l,h}}\right)$	mean$\left(\overline{D^{l,d}}\right)$
$l = 5$	12.0490	4.8904	6.0251	13.3732
$l = 4$	7.5204	3.3200	3.2648	6.6419
$l = 3$	4.4827	1.5756	1.2269	2.5725
$l = 2$	2.5100	0.7692	0.7692	0.8969
$l = 1$	1.3545	0.3790	0.3455	0.1695

Table 10.5: Sensitivity values for reservoir with flow across channel structures, flow measurements

	mean$\left(\overline{C^l}\right)$	mean$\left(\overline{D^{l,v}}\right)$	mean$\left(\overline{D^{l,h}}\right)$	mean$\left(\overline{D^{l,d}}\right)$
$l = 5$	9.3635	3.0349	3.4921	10.7412
$l = 4$	5.5819	3.9408	3.4638	5.2129
$l = 3$	3.1338	1.9264	1.3134	1.5206
$l = 2$	1.6258	0.8009	0.5726	0.4849
$l = 1$	0.8308	0.3081	0.1819	0.1151

Table 10.6: Sensitivity values for homogeneous reservoir, pressure measurements

	mean$\left(\overline{C^l}\right)$	mean$\left(\overline{D^{l,v}}\right)$	mean$\left(\overline{D^{l,h}}\right)$	mean$\left(\overline{D^{l,d}}\right)$
$l = 5$	0.0434	0.0276	0.0271	0.0370
$l = 4$	0.0270	0.0220	0.0190	0.0199
$l = 3$	0.0148	0.0103	0.0084	0.0077
$l = 2$	0.0082	0.0043	0.0034	0.0029
$l = 1$	0.0044	0.0020	0.0011	0.0008

10.4 Pressure measurements

We are also interested in investigating how the sensitivity behave when we look at pressure measurements. We use the same type of reservoir as for flow measurements, that is, a 32×32 cell square reservoir, and select four times where the measurements are made. Eclipse gives sensitivities for each of the used defined regions. The sensitivities for difference in pressure drop at different times are then calculated in the following way

$$
\frac{\partial \, m_i}{\partial \, permX_j} = \left(\frac{\partial \, WBP(P)}{\partial \, permX} - \frac{\partial \, WBP(I)}{\partial \, permX} \right)_j^{i+1} \\
- \left(\frac{\partial \, WBP(P)}{\partial \, permX} - \frac{\partial \, WBP(I)}{\partial \, permX} \right)_j^{i}
\tag{10.4.1}
$$

Where $WBP(P)$ is the pressure at the producer, and $WBP(I)$ is the pressure at the injector. We choose four different times i, and reshape the 1024 length vector of sensitivity values into a 32×32 matix corresponding to the original reservoir matrix. This matrix is then transformed into the Haar basis by the 2-D Haar basis transform, the results from this transformation is presented in the exact same manner as for the flow measurements. We calculated the sensitivity values for the following three cases:

- Homogeneous reservoir, with permeability field as in figure 10.3.1. Results are shown in table 10.6.

- Heterogeneous reservoir, with permeability field as in figure 10.3.2 . Results are shown in table 10.7.

- Reservoir with channel structures, with permeability field as in figure 10.3.3. Results are shown in table 10.8.

Table 10.7: Sensitivity values for heterogeneous reservoir,pressure measurements

	mean$\left(\overline{C^l}\right)$	mean$\left(\overline{D^{l,v}}\right)$	mean$\left(\overline{D^{l,h}}\right)$	mean$\left(\overline{D^{l,d}}\right)$
$l = 5$	0.0593	0.0843	0.0734	0.0676
$l = 4$	0.0554	0.0481	0.0396	0.0444
$l = 3$	0.0373	0.0267	0.0292	0.0234
$l = 2$	0.0260	0.0121	0.0079	0.0059
$l = 1$	0.0139	0.0058	0.0050	0.0040

Table 10.8: Sensitivity values for reservoir with channel structures, pressure measurements

	mean$\left(\overline{C^l}\right)$	mean$\left(\overline{D^{l,v}}\right)$	mean$\left(\overline{D^{l,h}}\right)$	mean$\left(\overline{D^{l,d}}\right)$
$l = 5$	0.1167	0.0762	0.0763	0.0972
$l = 4$	0.0701	0.0408	0.0277	0.0468
$l = 3$	0.0401	0.0163	0.0166	0.0207
$l = 2$	0.0232	0.0077	0.0071	0.0084
$l = 1$	0.0123	0.0037	0.0031	0.0013

10.5   Summary and conclusions

In this chapter we have looked at the sensitivity values for different types of permeability fields, and with respect to different data-types. We have transformed these sensitivity values by using the 2-D Haar transform. This enabled us to analyze how the value of the sensitivity changed according to scale. The properties of the 2-D Haar transform enabled us also to analyze if there was a difference in the SNS structure when we looked at the mean, horizontal, vertical or diagonal changes.

When we look at the results presented in tables 10.2-10.8 it is clear that the sensitivity goes to zero as the scale goes to 1 for all the reservoir types, considering all the different directions, at different times, and using different data-types. This is a promising result as to the existence of an SNS structure for 2-D two-phase fluid flow. In the 1-D analysis we concluded that a heterogeneous reservoir would not have as clear SNS structure as a homogeneous reservoir. Comparing the values in table 10.2 and table 10.3, we see that it is hard to draw the same conclusions for this case. The mean sensitivity value gradually decreases and is of approximately the same size for both heterogeneous and homogeneous cases. For the 1-D case we saw that the frequency of the non-constant permeability field was important. We have only investigated one frequency so we should try different frequencies before drawing any final conclusions.

For a 2-D case, we could investigate if the SNS structure would be affected by a permeability field with some strong features. We therefore chose to analyze a reservoir with channel structures. From table 10.4 we see that the sensitivity decrease as the scale go to 1.This indicated that there exists a SNS relationship for this case. We also investigated what happened when the flow was perpendicular to the strong permeability features. The results are seen in table 10.5. The sensitivity values goes to zero for this case as well. The sensitivity values are somewhat lower for the coarsest scale, but the general trend is similar as for the three other reservoirs.

When we look at pressure measurements we observe the same features as for flow measurements. In general the sensitivity values is smaller for pressure measurements, but there is a clear trend that the sensitivity go towards zero as the scale goes to 1. There is higher sensitivity values associated with the heterogeneous reservoir compared to the homogeneous. This difference is so small though, that we must say that these results does not indicate any difference between the homogeneous and heterogeneous reservoir. As we mentioned for the flow measurements, there might be a dependence on the frequency of the reservoir, and we can therefore not conclude that there is no difference between homogeneous and heterogeneous reservoirs. We have only looked at flow parallel to the strong features of the permeability field for the reservoir with channel structures, but the results are similar as for flow measurements. We see that the sensitivity values goes to zero as the scale goes to 1. This indicates that there also exists SNS structure for reservoirs with strong features, and flow parallel to these.

Chapter 11

Final summary and conclusions

The inverse problem of estimating permeability in a porous media from data observed at the wells is inherently complex. One promising way of solving this problem is through multiscale estimation techniques. We start out with a coarse representation of the permeability and gradually make the representation finer. These techniques will only work if there exist a relationship between sensitivity, non-linearity and scale for a given data type and a given parameter that we want to estimate. In [33] it was shown that this relationship does exist for estimation of permeability from time series of pressure data. Motivated by this we have shown that the same relationship does exist between permeability and time series of flow data.

The approach to this problem is to find expressions for the directional derivatives of the data-vector along different directions in parameter space. By letting the directions correspond to a multiscale basis, we were able to analyze the directional derivatives in directions corresponding to coarse or fine scale perturbations.

In chapter 6 and chapter 7 we used this approach to study the SNS structure for one-dimensional, one- and two-phase flow. We made some simplifications in order to perform the analysis. The most critical of these simplifications was that we assumed a constant permeability field. With this assumption we showed the existence of a SNS relationship for estimation of permeability from measurements of the fluid flow. This was analyzed for several different flooding scenarios, each reaching the same conclusions.

The assumption that the permeability value in a porous media is constant is never valid in any real world applications. In chapter 8 the validity of the results in chapter 6 and 7 was tested. This was done by highlighting the effect of a non-constant permeability field on the governing terms for the sensitivity expressions derived in chapter 6 and 7. The results from this analysis suggested

that if we have a non-constant permeability field, the SNS structure would still be present, but not as predictable as it was for a constant permeability field. One important case we saw here was that the SNS structure depended on the frequency of the permeability field, and the greatest deviation was observed for permeability fields with a frequency equal to the frequency of the basis element. This effect was most prominent in strongly heterogeneous reservoirs.

The results from chapter 8 only suggested that the SNS structure would not be affected by a non-constant permeability field. We did not calculate the complete equations for the sensitivity values. To this end we chose to utilize the reservoir simulator Eclipse. With Eclipse we obtained numerically calculated sensitivity values for each user defined region in a one-dimensional grid. These sensitivities were expressed using a local basis, and hence not suited for multiscale analysis. We therefore transformed the values by a one-dimensional Haar basis transform. In this way we could perform an numerical experiment to test the different results obtained in chapter 7 and 8. The results from the numerical experiments were promising with regard to existence of SNS. The structure of sensitivity that was proposed in chapter 7 were confirmed by the numerical study. The effects of a non-constant permeability field that were predicted in chapter 8 was also observed in the numerical experiments. The theoretical predictions from [33] could also be tested by numerical experiments. This test showed a clear SNS structure. The value of these experiments was to confirm the results obtained by an analytical study of the equations that govern fluid flow in a porous media.

For 2-D flow we were not able to perform any analytical analysis. In chapter 10 we performed a numerical analysis for a two-dimensional reservoir. The sensitivity values outputted by Eclipse was then transformed by a two-dimensional Haar basis transform. This enabled us to analyze if the SNS relationship carried over to two-dimensional flow. The results obtained showed that SNS relationship does also exist for a two-dimensional case. In [33] there was only done some discussions of a speculative nature regarding SNS for two-dimensional cases. By using the Eclipse simulator we were able to try experiments with pressure data as well. Results were similar to the ones for flow measurements, hence we gain more confidence in our belief that SNS carries over from one-dimension to two-dimensions.

The question posed at the start of this thesis was if there existed a relationship between sensitivity, non-linearity and scale associated with the estimation of permeability from time series measurements of flow data. By making some assumptions we were able to analyze the analytical equations governing the fluid flow in a porous media. This lead us to prove the existence of a SNS relationship. The next question was if this somewhat simplified case could be extended to a more realistic scenario. To this end we analyzed the governing terms in the sensitivity expression to see the effect of the most grave simplification, and

finally we tested by numerical experiments conducted by the reservoir simulator Eclipse, both for one- and two-dimensions. The results were conclusive, there is substantial evidence to confirm the existence of a SNS relationship associated with the estimation of permeability from time series measurements of flow data, both for one- and two-dimensional cases.

11.1   Future work

Future work related to this thesis would be to investigate different types of non-constant permeability fields for the 2-D case, and different flow patterns. By doing this analysis we might gain more information about things that could alter our SNS relationship.

To analyze how sensitivity and non-linearity depends on scale, can also be valuable for other parameters than the permeability. We can investigate how the porosity depends on different data-types. This would involve some other equations, and could lead to an interesting analysis of the scale dependence. An analysis of the sensitivity and non-linearity based on other data-types could also be of interest. This could be related to the problem of estimating fluid saturation from seismic data. For this case we have a dense grid of data points, but with long intervals between the accusation times.

Appendix A

Derivation of directional derivatives

In this appendix we present the complete calculations of directional derivatives in parameter space.

A.1   Two-phase

A.1.1   Piston displacement

Given

$$m_i(\mathbf{c}) = \frac{\Delta_x p(t_{i+1})}{\mu_w \int_0^1 k^{-1}(x; \mathbf{c})\, dx + (\mu_o - \mu_w) \int_{z(t_{i+1})}^1 k^{-1}(x; \mathbf{c})\, dx} \\ - \frac{\Delta_x p(t_i)}{\mu_w \int_0^1 k^{-1}(x; \mathbf{c})\, dx + (\mu_o - \mu_w) \int_{z(t_i)}^1 k^{-1}(x; \mathbf{c})\, dx}. \tag{A.1.1}$$

we have

$$f(\mathbf{c}) = q\left(K_1\left(I_1(g(\star, \mathbf{c})), I_2(g(\star, \mathbf{c}))\right), K_2\left(I_1(g(\star, \mathbf{c})), I_3(g(\star, \mathbf{c}))\right)\right) \tag{A.1.2}$$

where $\star$ indicates that the variable dependence is lost through integration. We have

$$q = \frac{\Delta_x p(t_{i+1})}{K_1} - \frac{\Delta_x p(t_i)}{K_2} \tag{A.1.3}$$

$$K_1 = I_1 + I_2 \tag{A.1.4}$$

$$K_2 = I_1 + I_3 \tag{A.1.5}$$

$$I_1 = \mu_w \int_0^1 g(x; \mathbf{c}) \, dx \tag{A.1.6}$$

$$I_2 = (\mu_o - \mu_w) \int_{z(t_{i+1})}^1 g(x; \mathbf{c}) \, dx \tag{A.1.7}$$

$$I_3 = (\mu_o - \mu_w) \int_{z(t_i)}^1 g(x; \mathbf{c}) \, dx \tag{A.1.8}$$

$$g(x; \mathbf{c}) = r(k(x; \mathbf{c})) \tag{A.1.9}$$

$$r(k) = k^{-1} \tag{A.1.10}$$

$$\mathcal{F}(f; t_i) = f \tag{A.1.11}$$

This gives the following expression for $f'(\mathbf{c})$:

$$
\begin{aligned}
f'(\mathbf{c}) = & \frac{\partial q}{\partial K_1} \left\{ \frac{\partial K_1}{\partial I_1} \frac{\partial I_1}{\partial g} + \frac{\partial K_1}{\partial I_2} \frac{\partial I_2}{\partial g} \right\} \\
& - \frac{\partial q}{\partial K_2} \left\{ \frac{\partial K_2}{\partial I_1} \frac{\partial I_1}{\partial g} + \frac{\partial K_2}{\partial I_3} \frac{\partial I_3}{\partial g} \right\}
\end{aligned}
\tag{A.1.12}
$$

using the definitions this gives

$$\frac{\partial q}{\partial K_1} = -\frac{\Delta_x p(t_{i+1})}{K_1^2} \tag{A.1.13}$$

$$\frac{\partial K_1}{\partial I_1} = 1 \tag{A.1.14}$$

$$\frac{\partial I_1}{\partial g} = -\mu_w \int_0^1 k^{-2}(x; \mathbf{c}) \, dx \tag{A.1.15}$$

$$\frac{\partial K_1}{\partial I_2} = 1 \tag{A.1.16}$$

$$\frac{\partial I_2}{\partial g} = -(\mu_o - \mu_w) \int_{z(t_{i+1})}^1 k^{-2}(x; \mathbf{c}) \, dx \tag{A.1.17}$$

$$\frac{\partial q}{\partial K_2} = -\frac{\Delta_x p(t_i)}{K_2^2} \tag{A.1.18}$$

$$\frac{\partial K_2}{\partial I_1} = 1 \tag{A.1.19}$$

$$\frac{\partial K_2}{\partial I_3} = 1 \tag{A.1.20}$$

$$\frac{\partial I_3}{\partial g} = -(\mu_o - \mu_w) \int_{z(t_i)}^1 k^{-2}(x; \mathbf{c}) \, dx \tag{A.1.21}$$

Now since

$$(m_i)_h = \mathcal{F}(f'(k(\mathbf{x}; \mathbf{c}))k(\mathbf{x}; \mathbf{h})), \tag{A.1.22}$$

we get

$$
\begin{aligned}
(m_i)_h = {} & \frac{\Delta_x p(t_{i+1})}{\left[\mu_w \int_0^1 k^{-1}(x; \mathbf{c})\, dx + (\mu_o - \mu_w) \int_{z(t_{i+1})}^1 k^{-1}(x; \mathbf{c})\, dx\right]^2} \\
& \times \left\{\mu_w \int_0^1 k^{-2}(x; \mathbf{c})k(x; \mathbf{h})\, dx + (\mu_w - \mu_o) \int_{z(t_{i+1})}^1 k^{-2}(x; \mathbf{c})k(x; \mathbf{h})\, dx\right\} \\
& - \frac{\Delta_x p(t_i)}{\left[\mu_w \int_0^1 k^{-1}(x; \mathbf{c})\, dx + (\mu_o - \mu_w) \int_{z(t_i)}^1 k^{-1}(x; \mathbf{c})\, dx\right]^2} \\
& \times \left\{\mu_w \int_0^1 k^{-2}(x; \mathbf{c})k(x; \mathbf{h})\, dx + (\mu_w - \mu_o) \int_{z(t_i)}^1 k^{-2}(x; \mathbf{c})k(x; \mathbf{h})\, dx\right\}
\end{aligned}
\tag{A.1.23}
$$

which can be further simplified by letting $k(x; \mathbf{c}) = k(\mathbf{c})$. This leads to

$$
\begin{aligned}
(m_i)_h = {} & \left(\frac{\Delta_x p(t_{i+1})}{[\mu_o + (\mu_w - \mu_o)z(t_{i+1})]^2} \right. \\
& \times \left\{\mu_w \int_0^1 k(x; \mathbf{h})\, dx + (\mu_w - \mu_o) \int_{z(t_{i+1})}^1 k(x; \mathbf{h})\, dx\right\} \\
& - \frac{\Delta_x p(t_i)}{[\mu_o + (\mu_w - \mu_o)z(t_i)]^2} \\
& \left. \times \left\{\mu_w \int_0^1 k(x; \mathbf{h})\, dx + (\mu_w - \mu_o) \int_{z(t_i)}^1 k(x; \mathbf{h})\, dx\right\} \right).
\end{aligned}
\tag{A.1.24}
$$

For the second derivative in parameter space we have

$$(m_i)_{hh} = \mathcal{F}(f''(k(\mathbf{x}; \mathbf{c}))k^2(\mathbf{x}; \mathbf{h}); \zeta_i). \tag{A.1.25}$$

We need an expression for

$$f''(k(\mathbf{x}; \mathbf{c})) \tag{A.1.26}$$

since we can write

$$
\begin{aligned}
f'(\mathbf{c}) = {} & \frac{\partial q}{\partial K_1} \left\{\frac{\partial I_1}{\partial g} + \frac{\partial I_2}{\partial g}\right\} \\
& - \frac{\partial q}{\partial K_2} \left\{\frac{\partial I_1}{\partial g} + \frac{\partial I_3}{\partial g}\right\}
\end{aligned}
\tag{A.1.27}
$$

we then have

$$
\begin{aligned}
f''(\mathbf{c}) = & \frac{\partial^2 q}{\partial K_1^2} \left\{ \frac{\partial I_1}{\partial g} + \frac{\partial I_2}{\partial g} \right\}^2 \\
& + \frac{\partial q}{\partial K_1} \left\{ \frac{\partial^2 I_1}{\partial g^2} + \frac{\partial^2 I_2}{\partial g^2} \right\} \\
& - \frac{\partial^2 q}{\partial K_2^2} \left\{ \frac{\partial I_1}{\partial g} + \frac{\partial I_3}{\partial g} \right\}^2 \\
& - \frac{\partial q}{\partial K_2} \left\{ \frac{\partial^2 I_1}{\partial g^2} + \frac{\partial^2 I_3}{\partial g^2} \right\}
\end{aligned}
\tag{A.1.28}
$$

with

$$
\frac{\partial^2 q}{\partial K_1^2} = 2 \frac{\Delta_x p(t_{i+1})}{K_1^3}
\tag{A.1.29}
$$

$$
\frac{\partial^2 I_1}{\partial g^2} = 2 \mu_w \int_0^1 k^{-3}(x; \mathbf{c}) \, dx
\tag{A.1.30}
$$

$$
\frac{\partial^2 I_2}{\partial g^2} = 2 \left(\mu_o - \mu_w \right) \int_{z(t_{i+1})}^1 k^{-3}(x; \mathbf{c}) \, dx
\tag{A.1.31}
$$

$$
\frac{\partial^2 q}{\partial K_2^2} = 2 \frac{\Delta_x p(t_i)}{K_2^3}
\tag{A.1.32}
$$

$$
\frac{\partial^2 I_3}{\partial g^2} = 2 \left(\mu_o - \mu_w \right) \int_{z(t_i)}^1 k^{-3}(x; \mathbf{c}) \, dx.
\tag{A.1.33}
$$

This gives

$$
\begin{aligned}
(m_i)_{hh} = & \frac{2\Delta_x p(t_{i+1})}{\left[\mu_w \int_0^1 k^{-1}(x; \mathbf{c})\, dx + (\mu_o - \mu_w) \int_{z(t_{i+1})}^1 k^{-1}(x; \mathbf{c})\, dx\right]^3} \\
& \times \left\{ \mu_w \int_0^1 k^{-2}(x; \mathbf{c}) k(x; \mathbf{h})\, dx \right. \\
& \left. + (\mu_o - \mu_w) \int_{z(t_{i+1})}^1 k^{-2}(x; \mathbf{c}) k(x; \mathbf{h})\, dx \right\}^2 \\
& - \frac{2\Delta_x p(t_{i+1})}{\left[\mu_w \int_0^1 k^{-1}(x; \mathbf{c})\, dx + (\mu_o - \mu_w) \int_{z(t_{i+1})}^1 k^{-1}(x; \mathbf{c})\, dx\right]^2} \\
& \times \left\{ \mu_w \int_0^1 k^{-3}(x; \mathbf{c}) k^2(x; \mathbf{h})\, dx \right. \\
& \left. + (\mu_o - \mu_w) \int_{z(t_{i+1})}^1 k^{-3}(x; \mathbf{c}) k^2(x; \mathbf{h})\, dx \right\} \\
& - 2 \frac{\Delta_x p(t_i)}{\left[\mu_w \int_0^1 k^{-1}(x; \mathbf{c})\, dx + (\mu_o - \mu_w) \int_{z(t_i)}^1 k^{-1}(x; \mathbf{c})\, dx\right]^3} \\
& \times \left\{ \mu_w \int_0^1 k^{-2}(x; \mathbf{c}) k(x; \mathbf{h})\, dx \right. \\
& \left. + (\mu_o - \mu_w) \int_{z(t_i)}^1 k^{-2}(x; \mathbf{c}) k(x; \mathbf{h})\, dx \right\}^2 \\
& + \frac{2\Delta_x p(t_i)}{\left[\mu_w \int_0^1 k^{-1}(x; \mathbf{c})\, dx + (\mu_o - \mu_w) \int_{z(t_i)}^1 k^{-1}(x; \mathbf{c})\, dx\right]^2} \\
& \times \left\{ \mu_w \int_0^1 k^{-3}(x; \mathbf{c}) k^2(x; \mathbf{h})\, dx \right. \\
& \left. + (\mu_o - \mu_w) \int_{z(t_i)}^1 k^{-3}(x; \mathbf{c}) k^2(x; \mathbf{h})\, dx \right\}
\end{aligned}
\tag{A.1.34}
$$

By setting $k(x; \mathbf{c}) = k(x)$ we get this expression for the second derivative in

parameter space

$$
\begin{aligned}
(m_i)_{hh} =& \frac{2k^{-1}(\mathbf{c})\Delta_x p(t_{i+1})}{[\mu_o + (\mu_w - \mu_o)z(t_{i+1})]^3} \\
& \times \left\{ \mu_w \int_0^1 k(x;\mathbf{h})\,dx + (\mu_o - \mu_w)\int_{z(t_{i+1})}^1 k(x;\mathbf{h})\,dx \right\}^2 \\
& - \frac{2k^{-1}(\mathbf{c})\Delta_x p(t_{i+1})}{[\mu_0 + (\mu_w - \mu_o)z(t_{i+1})]^2} \\
& \times \left\{ \mu_w \int_0^1 k^2(x;\mathbf{h})\,dx + (\mu_o - \mu_w)\int_{z(t_{i+1})}^1 k^2(x;\mathbf{h})\,dx \right\} \\
& - \frac{2k^{-1}(\mathbf{c})\Delta_x p(t_i)}{[\mu_o + (\mu_w - \mu_o)z(t_i)]^3} \\
& \times \left\{ \mu_w \int_0^1 k(x;\mathbf{h})\,dx + (\mu_o - \mu_w)\int_{z(t_i)}^1 k(x;\mathbf{h})\,dx \right\}^2 \\
& + \frac{2k^{-1}(\mathbf{c})\Delta_x p(t_i)}{[\mu_0 + (\mu_w - \mu_o)z(t_i)]^2} \\
& \times \left\{ \mu_w \int_0^1 k^2(x;\mathbf{h})\,dx + (\mu_o - \mu_w)\int_{z(t_i)}^1 k^2(x;\mathbf{h})\,dx \right\}
\end{aligned}
\tag{A.1.35}
$$

A.1.2   Non-piston displacement

In the case of non-piston displacement, the equation for $m_i(\mathbf{c})$ is different than for piston displacement. So given

$$
m_i(\mathbf{c}) = \frac{\Delta_x p(t_{i+1})}{I_1 + I_2 + I_3} - \frac{\Delta_x p(t_i)}{I_1 + I_4 + I_5},
\tag{A.1.36}
$$

we have

$$
\begin{aligned}
f(\mathbf{c}) = q\, & \left(K_1\left(I_1(g(\star,\mathbf{c})), I_2(g(\star,\mathbf{c})), I_3(g(\star,\mathbf{c}))\right), \right. \\
& \left. K_2\left(I_1(g(\star,\mathbf{c})), I_4(g(\star,\mathbf{c})), I_5(g(\star,\mathbf{c}))\right)\right)
\end{aligned}
\tag{A.1.37}
$$

$$
q = \frac{\Delta_x p(t_{i+1})}{K_1} - \frac{\Delta_x p(t_i)}{K_2}
\tag{A.1.38}
$$

$$
K_1 = I_1 + I_2 + I_3
\tag{A.1.39}
$$

$$
K_2 = I_1 + I_4 + I_5
\tag{A.1.40}
$$

$$
I_1 = \mu_w \int_0^1 g(x;\mathbf{c})\,dx
\tag{A.1.41}
$$

$$
I_2 = (\mu_o - \mu_w)\int_{z_{o,i+1}}^1 g(x;\mathbf{c})\,dx
\tag{A.1.42}
$$

$$I_3 = \int_{z_{w,i+1}}^{z_{o,i+1}} \left(\lambda^{-1}(S(x,t)) - \mu_w \right) g(x; \mathbf{c}) \, dx \tag{A.1.43}$$

$$I_4 = (\mu_o - \mu_w) \int_{z_{o,1}}^{1} g(x; \mathbf{c}) \, dx \tag{A.1.44}$$

$$I_5 = \int_{z_{w,i}}^{z_{o,i}} \left(\lambda^{-1}(S(x,t)) - \mu_w \right) g(x; \mathbf{c}) \, dx \tag{A.1.45}$$

$$g(x; \mathbf{c}) = r(k(x; \mathbf{c})) \tag{A.1.46}$$

$$r(k) = k^{-1} \tag{A.1.47}$$

$$\mathcal{F}(f; t_i) = f. \tag{A.1.48}$$

We then find an expression for $f'(\mathbf{c})$:

$$\begin{aligned}
f'(\mathbf{c}) =& \frac{\partial q}{\partial K_1} \left\{ \frac{\partial K_1}{\partial I_1} \frac{\partial I_1}{\partial g} + \frac{\partial K_1}{\partial I_2} \frac{\partial I_2}{\partial g} + \frac{\partial K_1}{\partial I_3} \frac{\partial I_3}{\partial g} \right\} \\
&- \frac{\partial q}{\partial K_2} \left\{ \frac{\partial K_2}{\partial I_1} \frac{\partial I_1}{\partial g} + \frac{\partial K_2}{\partial I_4} \frac{\partial I_4}{\partial g} + \frac{\partial K_2}{\partial I_5} \frac{\partial I_5}{\partial g} \right\}.
\end{aligned} \tag{A.1.49}$$

With the definitions above we get:

$$\frac{\partial q}{\partial K_1} = -\frac{\Delta_x p(t_{i+1})}{K_1^2} \tag{A.1.50}$$

$$\frac{\partial K_1}{\partial I_1} = 1 \tag{A.1.51}$$

$$\frac{\partial I_1}{\partial g} = -\mu_w \int_0^1 k^{-2}(x; \mathbf{c}) \, dx \tag{A.1.52}$$

$$\frac{\partial K_1}{\partial I_2} = 1 \tag{A.1.53}$$

$$\frac{\partial I_2}{\partial g} = -(\mu_o - \mu_w) \int_{z_{o,i+1}}^1 k^{-2}(x; \mathbf{c}) \, dx \tag{A.1.54}$$

$$\frac{\partial K_1}{\partial I_3} = 1 \tag{A.1.55}$$

$$\frac{\partial I_3}{\partial g} = -\int_{z_{w,i+1}}^{z_{o,i+1}} \left(\lambda^{-1}(S(x,t)) - \mu_w \right) k^{-2}(x; \mathbf{c}) \, dx \tag{A.1.56}$$

$$\frac{\partial q}{\partial K_2} = -\frac{\Delta_x p(t_i)}{K_2^2} \tag{A.1.57}$$

$$\frac{\partial K_2}{\partial I_1} = 1 \tag{A.1.58}$$

$$\frac{\partial K_2}{\partial I_4} = 1 \tag{A.1.59}$$

$$\frac{\partial I_4}{\partial g} = -\left(\mu_o - \mu_w\right) \int_{z_{o,i}}^{1} k^{-2}(x; \mathbf{c})\, dx \tag{A.1.60}$$

$$\frac{\partial K_2}{\partial I_5} = 1 \tag{A.1.61}$$

$$\frac{\partial I_5}{\partial g} = -\int_{z_{w,i}}^{z_{o,i}} \left(\lambda^{-1}(S(x,t)) - \mu_w\right) k^{-2}(x; \mathbf{c})\, dx \tag{A.1.62}$$

This leads to the following equation for $(m_i)_h$:

$$
\begin{aligned}
(m_i)_h =& \frac{\Delta_x p(t_{i+1})}{[I_1 + I_2 + I_3]^2} \\
& \times \left\{ \mu_w \int_0^1 k^{-2}(x; \mathbf{c})k(x; \mathbf{h})\, dx + (\mu_o - \mu_w) \int_{z_{o,i+1}}^1 k^{-2}(x; \mathbf{c})k(x; \mathbf{h})\, dx \right. \\
& \left. + \int_{z_{w,i+1}}^{z_{o,i+1}} \left(\lambda^{-1}(S(x,t)) - \mu_w\right) k^{-2}(x; \mathbf{c})k(x; \mathbf{h})\, dx \right\} \\
& - \frac{\Delta_x p(t_i)}{[I_1 + I_4 + I_5]^2} \\
& \times \left\{ \mu_w \int_0^1 k^{-2}(x; \mathbf{c})k(x; \mathbf{h})\, dx + (\mu_o - \mu_w) \int_{z_{o,i}}^1 k^{-2}(x; \mathbf{c})k(x; \mathbf{h})\, dx \right. \\
& \left. + \int_{z_{w,i}}^{z_{o,i}} \left(\lambda^{-1}(S(x,t)) - \mu_w\right) k^{-2}(x; \mathbf{c})k(x; \mathbf{h})\, dx \right\}
\end{aligned}
\tag{A.1.63}
$$

Inside the two-phase zone we assume that the saturation decreases monotonically, and we also assume that the mobility varies slowly with the saturation. If these two assumptions holds, we replace $\lambda^{-1}(S(x,t))$ with an average value λ^{-1}, that does not vary with time. If we in addition assume that $k(x; \mathbf{c})$ is

constant in space we get:

$$
\begin{aligned}
(m_i)_h = & \frac{\Delta_x p(t_{i+1})}{\left[\mu_o + (\mu_w - \mu_o)\, z_{o,i+1} + (\lambda^{-1} - \mu_w)\, \delta_{i+1}\right]^2} \\
& \times \left\{ \mu_w \int_0^1 k(x; \mathbf{h})\, dx + (\mu_o - \mu_w) \int_{z_{o,i+1}}^1 k(x; \mathbf{h})\, dx \right. \\
& \left. + \left(\lambda^{-1} - \mu_w\right) \int_{z_{w,i+1}}^{z_{o,i+1}} k(x; \mathbf{h})\, dx \right\} \\
& - \frac{\Delta_x p(t_i)}{\left[\mu_o + (\mu_w - \mu_o)\, z_{o,i} + (\lambda^{-1} - \mu_w)\, \delta_i\right]^2} \\
& \times \left\{ \mu_w \int_0^1 k(x; \mathbf{h})\, dx + (\mu_o - \mu_w) \int_{z_{o,i}}^1 k(x; \mathbf{h})\, dx \right. \\
& \left. + \left(\lambda^{-1} - \mu_w\right) \int_{z_{w,i}}^{z_{o,i}} k(x; \mathbf{h})\, dx \right\}
\end{aligned}
\tag{A.1.64}
$$

where $\delta_{i+1} = z_{o,i+1} - z_{w,i+1}$, and $\delta_i = z_{o,i} - z_{w,i}$.

For the second derivative in parameter space we still want to find the expression

$$
(m_i)_{hh} = \mathcal{F}(f''(k(\mathbf{x}; \mathbf{c}))k^2(\mathbf{x}; \mathbf{h}); \zeta_i).
\tag{A.1.65}
$$

This means that we need to find $f''(k(\mathbf{x}; \mathbf{c}))$, using the same approach as for piston displacement. We observe that $f'(k(\mathbf{x}; \mathbf{c}))$ can be written as

$$
\begin{aligned}
f'(\mathbf{c}) = & \frac{\partial q}{\partial K_1} \left\{ \frac{\partial I_1}{\partial g} + \frac{\partial I_2}{\partial g} + \frac{\partial I_3}{\partial g} \right\} \\
& - \frac{\partial q}{\partial K_2} \left\{ \frac{\partial I_1}{\partial g} + \frac{\partial I_4}{\partial g} + \frac{\partial I_5}{\partial g} \right\}.
\end{aligned}
\tag{A.1.66}
$$

This gives the following expression for $f''(\mathbf{c})$

$$
\begin{aligned}
f''(\mathbf{c}) = & \frac{\partial^2 q}{\partial K_1^2} \left\{ \frac{\partial I_1}{\partial g} + \frac{\partial I_2}{\partial g} + \frac{\partial I_3}{\partial g} \right\}^2 \\
& + \frac{\partial q}{\partial K_1} \left\{ \frac{\partial^2 I_1}{\partial g^2} + \frac{\partial^2 I_2}{\partial g^2} + \frac{\partial^2 I_3}{\partial g^2} \right\} \\
& - \frac{\partial^2 q}{\partial K_2^2} \left\{ \frac{\partial I_1}{\partial g} + \frac{\partial I_4}{\partial g} + \frac{\partial I_5}{\partial g} \right\}^2 \\
& - \frac{\partial q}{\partial K_2} \left\{ \frac{\partial^2 I_1}{\partial g^2} + \frac{\partial^2 I_4}{\partial g^2} + \frac{\partial^2 I_5}{\partial g^2} \right\}.
\end{aligned}
\tag{A.1.67}
$$

With

$$
\frac{\partial^2 q}{\partial K_1^2} = \frac{2\Delta_x p(t_{i+1})}{K_1^3},
\tag{A.1.68}
$$

$$\frac{\partial^2 I_1}{\partial g^2} = 2\mu_w \int_0^1 k^{-3}\left(\mathbf{x}; \mathbf{c}\right) dx, \qquad (A.1.69)$$

$$\frac{\partial^2 I_2}{\partial g^2} = 2\left(\mu_o - \mu_w\right) \int_{z_{o,i+1}}^1 k^{-3}(\mathbf{x}; \mathbf{c}) \, dx, \qquad (A.1.70)$$

$$\frac{\partial^2 I_3}{\partial g^2} = 2 \int_{z_{w,i+1}}^{z_{o,i+1}} \left(\lambda^{-1}\left(S\left(\mathbf{x}, t\right)\right) - \mu_w\right) k^{-3}(\mathbf{x}; \mathbf{c}) \, dx, \qquad (A.1.71)$$

$$\frac{\partial^2 q}{\partial K_2^2} = -2\frac{\Delta_x p(t_i)}{K_2^3}, \qquad (A.1.72)$$

$$\frac{\partial^2 I_4}{\partial g^2} = 2\left(\mu_o - \mu_w\right) \int_{z_{o,i}}^1 k^{-3}(\mathbf{x}; \mathbf{c}) \, dx, \qquad (A.1.73)$$

$$\frac{\partial^2 I_5}{\partial g^2} = 2 \int_{z_{w,i}}^{z_{o,i}} \left(\lambda^{-1}\left(S\left(\mathbf{x}, t\right)\right) - \mu_w\right) k^{-3}(\mathbf{x}; \mathbf{c}) \, dx. \qquad (A.1.74)$$

We can now write

$$
\begin{aligned}
(m_i)_{hh} =& 2\frac{\Delta_x p(t_{i+1})}{[I_1 + I_2 + I_3]^3} \\
& \times \left\{ \mu_w \int_0^1 k^{-2}(x; \mathbf{c})k(x; \mathbf{h})\, dx + (\mu_o - \mu_w)\int_{z_{o,i+1}}^1 k^{-2}(x; \mathbf{c})k(x; \mathbf{h})\, dx \right. \\
& \left. + \int_{z_{w,i+1}}^{z_{o,i+1}} \left(\lambda^{-1}(S(x,t)) - \mu_w \right) k^{-2}(x; \mathbf{c})k(x; \mathbf{h})\, dx \right\}^2 \\
& - \frac{\Delta_x p(t_{i+1})}{[I_1 + I_2 + I_3]^2} \\
& \times \left\{ 2\mu_w \int_0^1 k^{-3}(x; \mathbf{c})k^2(x; \mathbf{h})\, dx + 2(\mu_o - \mu_w)\int_{z_{o,i+1}}^1 k^{-3}(x; \mathbf{c})k^2(x; \mathbf{h})\, dx \right. \\
& \left. + 2\int_{z_{w,i+1}}^{z_{o,i+1}} \left(\lambda^{-1}(S(x,t)) - \mu_w \right) k^{-3}(x; \mathbf{c})k^2(x; \mathbf{h})\, dx \right\} \\
& + - 2\frac{\Delta_x p(t_i)}{[I_1 + I_4 + I_5]^3} \\
& \times \left\{ \mu_w \int_0^1 k^{-2}(x; \mathbf{c})k(x; \mathbf{h})\, dx + (\mu_o - \mu_w)\int_{z_{o,i}}^1 k^{-2}(x; \mathbf{c})k(x; \mathbf{h})\, dx \right. \\
& \left. + \int_{z_{w,i}}^{z_{o,i}} \left(\lambda^{-1}(S(x,t)) - \mu_w \right) k^{-2}(x; \mathbf{c})k(x; \mathbf{h})\, dx \right\}^2 \\
& + \frac{\Delta_x p(t_i)}{[I_1 + I_4 + I_5]^2} \\
& \times \left\{ 2\mu_w \int_0^1 k^{-3}(x; \mathbf{c})k^2(x; \mathbf{h})\, dx + 2(\mu_o - \mu_w)\int_{z_{o,i}}^1 k^{-3}(x; \mathbf{c})k^2(x; \mathbf{h})\, dx \right. \\
& \left. + 2\int_{z_{w,i}}^{z_{o,i}} \left(\lambda^{-1}(S(x,t)) - \mu_w \right) k^{-3}(x; \mathbf{c})k^2(x; \mathbf{h})\, dx \right\}.
\end{aligned}
$$

$$(A.1.75)$$

Using the same assumptions as for $(m_i)_h$ we get the following:

$$
\begin{aligned}
(m_i)_{hh} =\; & 2k^{-1}(\mathbf{c}) \frac{\Delta_x p(t_{i+1})}{\left[\mu_o + (\mu_w - \mu_o)\, z_{o,i+1} + (\lambda^{-1} - \mu_w)\, f_{i+1}\right]^3} \\
& \times \left\{ \mu_w \int_0^1 k(x;\mathbf{h})\, dx + (\mu_o - \mu_w) \int_{z_{o,i+1}}^1 k(x;\mathbf{h})\, dx \right. \\
& \left. + \left(\lambda^{-1} - \mu_w\right) \int_{z_{w,i+1}}^{z_{o,i+1}} k(x;\mathbf{h})\, dx \right\}^2 \\
& -2k^{-1}(\mathbf{c}) \frac{\Delta_x p(t_{i+1})}{\left[\mu_o + (\mu_w - \mu_o)\, z_{o,i+1} + (\lambda^{-1} - \mu_w)\, f_{i+1}\right]^2} \\
& \times \left\{ \mu_w \int_0^1 k^2(x;\mathbf{h})\, dx + (\mu_o - \mu_w) \int_{z_{o,i+1}}^1 k^2(x;\mathbf{h})\, dx \right. \\
& \left. + \left(\lambda^{-1} - \mu_w\right) \int_{z_{w,i+1}}^{z_{o,i+1}} k^2(x;\mathbf{h})\, dx \right\} \\
& -2k^{-1}(\mathbf{c}) \frac{\Delta_x p(t_i)}{\left[\mu_o + (\mu_w - \mu_o)\, z_{o,i} + (\lambda^{-1} - \mu_w)\, f_i\right]^3} \\
& \times \left\{ \mu_w \int_0^1 k(x;\mathbf{h})\, dx + (\mu_o - \mu_w) \int_{z_{o,i}}^1 k(x;\mathbf{h})\, dx \right. \\
& \left. + \left(\lambda^{-1} - \mu_w\right) \int_{z_{w,i}}^{z_{o,i}} k(x;\mathbf{h})\, dx \right\}^2 \\
& +2k^{-1}(\mathbf{c}) \frac{\Delta_x p(t_i)}{\left[\mu_o + (\mu_w - \mu_o)\, z_{o,i} + (\lambda^{-1} - \mu_w)\, f_i\right]^2} \\
& \times \left\{ \mu_w \int_0^1 k^2(x;\mathbf{h})\, dx + (\mu_o - \mu_w) \int_{z_{o,i}}^1 k^2(x;\mathbf{h})\, dx \right. \\
& \left. + \left(\lambda^{-1} - \mu_w\right) \int_{z_{w,i}}^{z_{o,i}} k^2(x;\mathbf{h})\, dx \right\}
\end{aligned}
\tag{A.1.76}
$$

Bibliography

[1] S. AANONSEN AND D. EYDINOV, *A multiscale method for distributed parameter estimation with application to reservoir history matching*, Computational Geosciences, 10 (2006), pp. 97–117.

[2] S. AANONSEN, G. NÆVDAL, D. OLIVER, A. REYNOLDS, AND B. VALLÈS, *The Ensemble Kalman Filter in Reservoir Engineering–a Review*, SPE Journal, 14 (2009), pp. 393–412.

[3] H. AMEUR, G. CHAVENT, AND J. JAFFRÉ, *Refinement and coarsening indicators for adaptive parametrization: application to the estimation of hydraulic transmissivities*, Inverse Problems, 18 (2002), p. 775.

[4] F. ANTERION, R. EYMARD, AND B. KARCHER, *Use of parameter gradients for reservoir history matching*, in SPE Symposium on Reservoir Simulation, 1989.

[5] R. ASTER, C. THURBER, AND B. BORCHERS, *Parameter estimation and inverse problems*, Academic Press, 2005.

[6] K. AZIZ AND A. SETTARI, *Petroleum reservoir simulation*, Elsevier Applied Science Publisher, 1985.

[7] D. M. BATES AND D. G. WATTS, *Relative curvature measures of nonlinearity*, Journal of the Royal Statistical Society. Series B (Methodological), 42 (1980), pp. 1–25.

[8] J. BEAR, *Dynamics of fluid in porous media*, American Elsevier, New York, 1972.

[9] J. BENEDETTO AND M. FRAZIER, *Wavelets: mathematics and applications*, CRC, 1994.

[10] I. BERRE, M. LIEN, AND T. MANNSETH, *A level-set corrector to an adaptive multiscale permeability prediction*, Computational Geosciences, 11 (2007), pp. 27–42.

[11] Å. BJÖRCK, *Numerical methods for least squares problems*, Society for Industrial Mathematics, 1996.

129

[12] C. Burrus, R. Gopinath, H. Guo, J. Odegard, and I. Selesnick, *Introduction to wavelets and wavelet transforms: a primer*, vol. 55, Prentice hall Upper Saddle River NJ, 1998.

[13] G. Chavent and J. Liu, *Multiscale parametrization for the estimation of a diffusion coefficient in elliptic and parabolic problems*, (1989), pp. 315–324.

[14] H. Darcy, *Les fontaines publiques de la ville de Dijon, 1856*, Victor Dalmont, Paris.

[15] I. Daubechies, *Ten lectures on wavelets*, Society for Industrial and Applied Mathematics, Philadelphia, PA, USA, 1992.

[16] O. Dorn and D. Lesselier, *Level set methods for inverse scattering*, Inverse Problems, 22 (2006), p. R67.

[17] M. Ehrendorfer, *A review of issues in ensemble-based Kalman filtering*, Meteorologische Zeitschrift, 16 (2007), pp. 795–818.

[18] G. Evensen, *Sequential data assimilation with a nonlinear quasi-geostrophic model using Monte Carlo methods to forecast error statistics*, J. Geophys. Res, 99 (1994), pp. 143–10.

[19] ——, *Application of ensemble integrations for predictability studies and data assimilation*, in Monte Carlo Simulations in Oceanography Proceedings' Aha Huliko'a Hawaiian Winter Workshop, University of Hawaii at Manoa, Citeseer, 1997, pp. 14–17.

[20] R. Freeze and J. Cherry, *Groundwater, 604 pp*, PrenticeHall, Englewood Cliffs, NJ, (1979).

[21] S. Geoquest, *ECLIPSE 100 Reference Manual*, Schlumberger Geoquest, (2007).

[22] W. G. Gray, *Introduction to Conservation Principles for Environmental Analysis*, Department of Environmental Sciences and Engineering, University og North Carolina at Chapel Hill, 2009. Lecture notes.

[23] A. Grimstad and T. Mannseth, *Nonlinearity, scale, and sensitivity for parameter estimation problems*, SIAM Journal on Scientific Computing, 21 (2000), pp. 2096–2113.

[24] A. Grimstad, T. Mannseth, G. Nævdal, and H. Urkedal, *Adaptive multiscale permeability estimation*, Computational Geosciences, 7 (2003), pp. 1–25.

[25] A. Haar, *Zur theorie der orthogonalen funktionensysteme*, Mathematische Annalen, 71 (1911), pp. 38–53. 10.1007/BF01456927.

[26] M. HAYEK, F. LEHMANN, AND P. ACKERER, *Adaptive multi-scale parameterization for one-dimensional flow in unsaturated porous media*, Advances in Water Resources, 31 (2008), pp. 28–43.

[27] P. JACQUARD AND C. JAIN, *Permeability distribution from field pressure data*, Old SPE Journal, 5 (1965), pp. 281–294.

[28] R. KALMAN ET AL., *A new approach to linear filtering and prediction problems*, Journal of basic Engineering, 82 (1960), pp. 35–45.

[29] J. R. LIEN, *Reservoarteknikk I*, Department of physics and technology, University of Bergen, 2007. Lecture notes in Norwegian.

[30] M. LIEN, I. BERRE, AND T. MANNSETH, *Combined adaptive multiscale and level-set parameter estimation*, Multiscale Modeling and Simulation, 4 (2006), pp. 1349–1374.

[31] J. LIU, *A multiresolution method for distributed parameter estimations*, SIAM Journal on Scientific Computing, 14.

[32] S. G. MALLAT, *Multiresolution approximations and wavelet orthonormal bases of l2(r)*, Transactions of the American Mathematical Society, 315 (1989), pp. pp. 69–87.

[33] T. MANNSETH, *Permeability identification from pressure observations: Some foundations for multiscale regularization*, Multiscale Modeling & Simulation, 5 (2006), pp. 21–44.

[34] C. MARLE, *Multiphase flow in porous media*, Éditions technip, 1981.

[35] Y. MEYER, *Ondelettes, fonctions splines et analyses gradu ees*, Lectures given at the University of Torino, Italy, (1986).

[36] E. MOORE, *On the reciprocal of the general algebraic matrix*, Bull. Amer. Math. Soc, 26 (1920), pp. 394–395.

[37] J. MORE, *The Levenberg-Marquardt algorithm: implementation and theory*, Numerical analysis, (1978), pp. 105–116.

[38] S. NASH AND A. SOFER, *Linear and nonlinear programming*, vol. 692, McGraw-Hill, 1996.

[39] J. NOCEDAL AND S. WRIGHT, *Numerical optimization*, Springer verlag, 1999.

[40] R. PENROSE, *A generalized inverse for matrices*, in Mathematical proceedings of the Cambridge philosophical society, vol. 51, Cambridge Univ Press, 1955, pp. 406–413.

[41] D. RADUNOVIĆ, *Wavelets: from math to practice*, Springer, 2009.

[42] H. RESNIKOFF AND R. WELLS, *Wavelet analysis: the scalable structure of information*, Springer Verlag, 1998.

[43] L. SHAMPINE, *Vectorized adaptive quadrature in MATLAB*, Journal of Computational and Applied Mathematics, 211 (2008), pp. 131–140.

[44] D. SIVIA AND J. SKILLING, *Data analysis: a Bayesian tutorial*, Oxford University Press, USA, 2006.

[45] A. TARANTOLA, *Inverse problem theory and methods for model parameter estimation*, Society for Industrial and Applied Mathematics, 2005.

[46] R. WANG, *Introduction to Orthogonal Transforms*, Cambridge University Press, 2011.

[47] A. ZOLOTUKHIN AND J. URSIN, *Introduction to Petroleum Reservoir Engineering*, Høyskoleforlaget, Norwegian Academic Press, 2000.